Review



# Delving into the Inception of BODIPY Dyes: Paradigms of In Vivo Bioimaging, Chemosensing, and Photodynamic/Photothermal Therapy

Olivia Agnes Basant , Edgardo Lobo , Gyliann Pena , Maged Henary *

Posted Date: 24 November 2025

doi: 10.20944/preprints202511.1766.v1

Keywords: boron dipyrrin; aza-BODIPY; photosensitizer; stoke's shift; bioconjugate; chemosensor; near-infrared dyes; fluorescent dyes; tumor imaging; theranostics

 doi:10.20944/preprints202511.1766.v1



*Review*

# Delving into the Inception of BODIPY Dyes: Paradigms of *In Vivo* Bioimaging, Chemosensing, and Photodynamic/Photothermal Therapy

**Olivia Basant [1,2], Edgardo Lobo [1], Gyliann Peña [1] and Maged Henary [1,2,*]**

[1] Department of Chemistry, Petit Science Center, Georgia State University, 100 Piedmont Avenue SE, Atlanta, GA 30303, USA

[2] Center for Diagnostics and Therapeutics, Georgia State University, 100 Piedmont Avenue SE, Atlanta, GA 30303, USA

* Correspondence: mhenary1@gsu.edu (M.H); Tel.: +1-404-413-5566

**Abstract**

Boron-dipyrromethene (BODIPY) dyes belong to a class of organoboron compounds that have become ubiquitous for researchers in areas of fluorescence imaging, photodynamic therapy, and optoelectronics. The intrinsic qualities of BODIPY dyes and their meso-modified structural analogs, Aza-BODIPY dyes, have propelled their recent increase in use in biomedical applications. The two scaffolds have high quantum yields, narrow absorption and emission bandwidths with large Stokes' shifts, and high photo- and thermal stability. Because their properties are independent of solvent polarity and dye functionality, they can be tuned to promote novel analytical methods, resulting in the adaptation of the physicochemical and spectral properties of the dyes. In this review of BODIPY and Aza-BODIPY scaffolds, we will summarize their spectral properties, synthetic methods of preparation, and applications reported between 2014 and 2025. This review aims to summarize the advances in chemosensing, especially pH sensor development, and the advances in NIR-II window bioimaging probes. We hope that this succinct overview of Aza-BODIPY scaffolds will highlight their untapped potential, elucidating insights that may catalyze novel ideas in the physical organic realm of BODIPY.

**Keywords:** boron dipyrrin; aza-BODIPY; photosensitizer; stoke's shift; bioconjugate; chemosensor; near-infrared dyes; fluorescent dyes; tumor imaging; theranostics

## 1. Introduction

During the last few decades, novel dye chemistry has conferred significant advancements in cell imaging modalities using fluorescent probes. However, despite these significant strides in optical imaging, light emitted by fluorescent probes exhibits the tendency to be absorbed by blood cells and proximal cells, resulting in a suppressed contrast and low signal-to-noise ratio [1]; a high signal-to-noise (SNR) ratio is desired to ensure a clear bioimage is generated. A few probes emit around 800 nm, such as 4,4-difluoro-4-bora-3a,4a-diaza-s-indacene (BODIPY), which are dyes that have strong ultraviolet (UV) absorbing molecules that can emit sharp fluorescence peaks with high quantum yields. BODIPY-centered $\pi$–$\pi^*$ transitions have been reported to display absorption peaks within the range of 570-640 nm and emission peaks around 615- 664 nm with quantum yields of up to 25% [2]. Developing fluorophores with a larger Stokes shift affords a larger window for greater spectral acquisition in quantity of scans with higher resolutions at *multiple* wavelengths, supporting the propensity of imaging into the NIR-II window (1,000-1,700 nm) [3]. One differentiating characteristic of BODIPY dyes that distinguishes them from other classes of small molecular organic dyes is the central complexation of two fluorine atoms to a boron atom that is connected to a dipyrromethene ligand; the dipyrromethene ligand is formed from two pyrrole rings connected by a polymethine

 doi:10.20944/preprints202511.1766.v1



bridge. The dipyrromethene ligand forms the core scaffold that binds to the boron atom, which is essential to the dye's fluorescent properties [4]. These components synergize to give BODIPY dyes their photophysical characteristics. The employment of NIR BODIPY dyes seeks to accomplish absorbance and fluorescence in the near-infrared region (NIR). This region encompasses the NIR-I and NIR-II classes, which exist between the 650-900 nm and 900-1700 nm range, respectively, rendering them optimal for biomedical applications [5]. Optical imaging is extensively employed *in vivo* for research purposes, offering tissue contrast that hinge upon the interplay between photons and cellular structures, especially by other classes of dyes such as donor- π- acceptor fluorophores [6] and squarine fluorophores [7].

The mechanism by which fluorophores are responsible for causing fluorescence occurs through the absorption of photons in the ground singlet state, leading to vibrational relaxation in the first singlet excited state. As a result, the electron reverts to its ground state, emitting a photon during this relaxation process, known as fluorescence [8]. Fluorescence imaging has become an essential mechanism for monitoring *in vivo* biological targets due to its noninvasive, real-time imaging abilities and no radiation associated. Fluorescence imaging is a non-invasive technique that allows for the infiltration of animal tissues due to its ability to generate longer wavelengths and low energy with negligible scattering, and no interference with the innate autofluorescence of biological tissues, making NIR dyes an exemplary contender for bioimaging applications [9, 10]. As displayed in Figure 1, the notable classes of NIR-I fluorophores are squaric acid, pentamethine cyanine, and heptamethine cyanine fluorophores. At the same time, the BODIPY core exists at the lowest wavelength and penetration depth among the displayed fluorophore classes, warranting the need for future development of BODIPY probes [11].

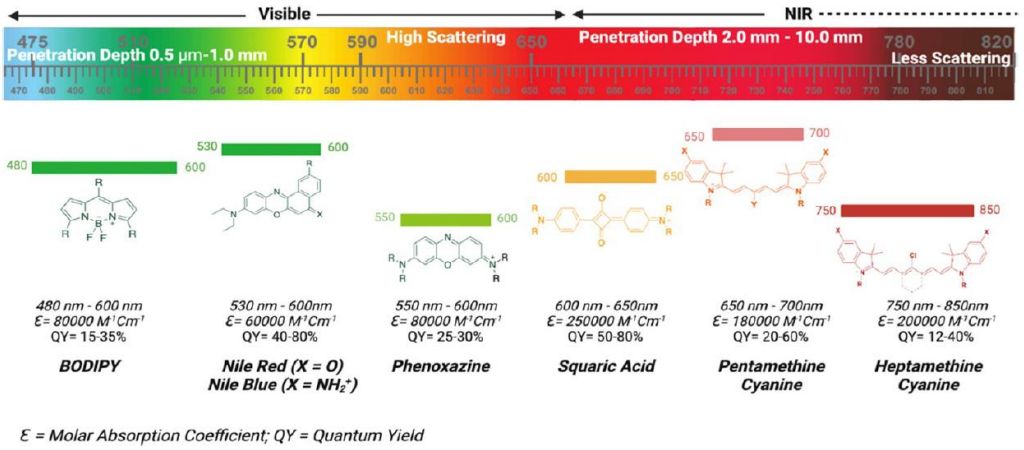


**Figure 1.** Prominent structures used with numerous classes of NIR fluorophores with their absorption/emission profiles meeting the candidacy for potential agents for *in vivo* imaging. This figure was reproduced with permission from Cao *et al*., 2020, copyright 2020 [11].

In the last decade, BODIPY dyes have been integral in their employment in two prominent imaging modalities: optoacoustic imaging and fluorescence imaging for photodynamic therapy. Exogenous contrast agents play an integral role in optical imaging due to their highly modifiable structures and ability to improve pre-existing physicochemical and optical properties to constitute bright fluorophores that provide detailed, high-resolution images in image-guided surgery [12]. First, optoacoustic imaging, also known as photoacoustic imaging (PAI) is a non-invasive medical modality that entails laser pulses directed at biological tissues to induce expansion of tissues to generate ultrasound waves and is reliant contingent on the absorption of a light to elicit a signal response to subsequently propagate ultrasound waves for signal acquisition [13]. As photons propagate through the tissue, light is absorbed by the exogenous contrast agent (dye), and the tissues are locally heated and subjected to expansion. This increase in pressure from the expansion of the

 doi:10.20944/preprints202511.1766.v1



tissue results in ultrasound waves, which are detected by an ultrasound transducer to reconstruct an image, as shown in Figure 2 [13].

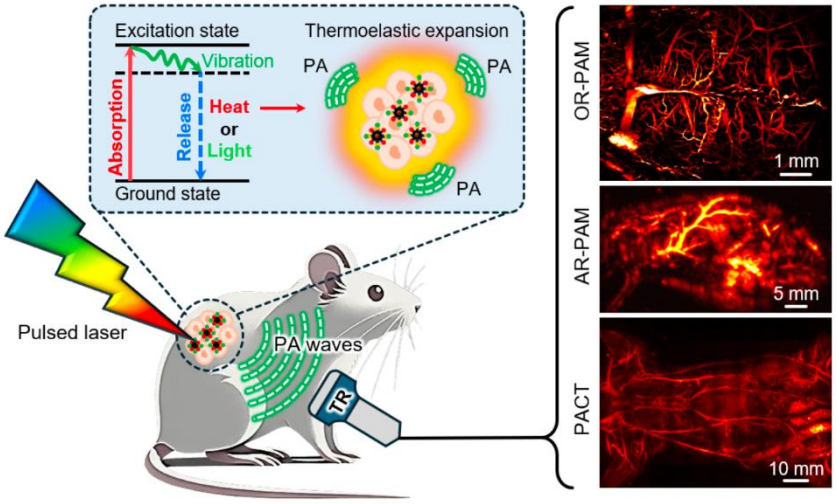


**Figure 2.** Visual depiction of the principles that govern photoacoustic imaging and its variations. Abbreviations denoted: **PA**, photoacoustic; **TR**, ultrasound transducer; OR-PAM, optical resolution photoacoustic microscopy; **AR-PAM**, acoustic resolution photoacoustic microscopy; **PACT**, photoacoustic computed tomography. This figure was reproduced with permission from Kye *et al*., 2024, copyright 2024 [14].

In photodynamic therapy, the transition of fluorophores from the excited to the ground state *via* the absorption of light in the near-infrared (NIR) region is succeeded by the emission of light, known as fluorescence. Absorbed energy, scattered and dissipated as non-radiative energy, assumes the form of thermal heat because of the vibronic relaxations occurring within the excited state of the fluorophore [15]. When this heat dissipation exceeds the rate of absorption, tissue temperatures begin to rise gradually above 40 degrees Celsius, at which cellular tumor cytotoxicity typically occurs. As displayed in Figure 3, in the NIR I and II region, at imaging wavelengths of 700-1700 nm, there is less scattering and absorption of light by hemoglobin and water are relatively low, leading to deeper penetration [16].

Henceforth, this review investigates the current paradigms of BODIPY dyes in their synthetic methodologies, reported applications, and optical properties. The review summarizes the applications of notable BODIPY and Aza-BODIPY dyes synthesized in the last 10 years due to the strides in the development of BODIPY fluorophores that have successfully served as chemo sensors for detrimental analytes such as reactive oxygen species (ROS) and/or simultaneously expanded their clinical potential promoting selective cancer cell uptake, plasma membrane (PM) targeting, and inducing pyroptosis, - with the ultimate goal of this class of NIR dyes to be leveraged as efficient theranostic agents.

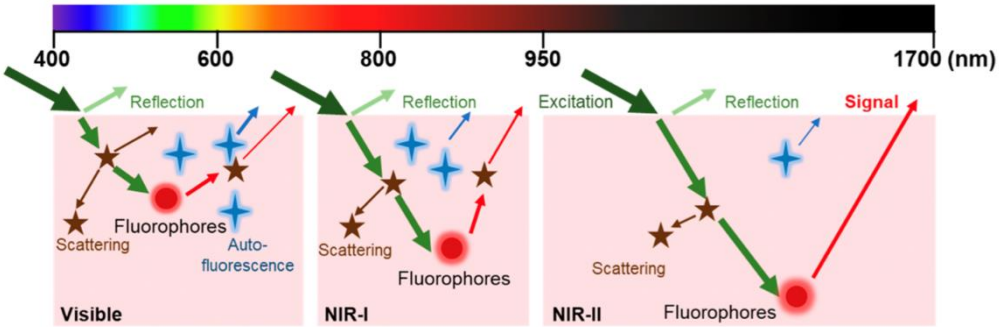

 doi:10.20944/preprints202511.1766.v1



**Figure 3.** Comparison of fluorescence imaging in different biological regions, such as the visible region (400-700 nm), the NIR-I region (700-900 nm), and the NIR-II region (950-1700 nm). This figure was reproduced with permission from Zhang *et al*., 2023, copyright 2023 [16].

## 2. Synthesis of BODIPY Dyes

The first BODIPY dye was discovered in 1968 by Triebs and Kreuzer, and the dyes have since been investigated for their propensity to behave as bimodal imaging agents. Strategies to modify the substituents attached to the core have been directed towards ligand tuning with electron-donating groups and halogenation to promote intersystem crossing [17]. Strategies for synthesizing functional BODIPY fluorophores have encompassed multicomponent reactions (MCRs), metal-catalyzed C-H activation, cycloadditions, and biomolecule-based methods, such as the inclusion of tyramine amino acid units [18, 19], as shown in Figure 4. The various strategies that have been adopted to synthesize the NIR BODIPYs aza-BODIPYs include: 1) Establishment of π-conjugated systems like aryl, vinyl or styryl groups at the 2nd, 3rd, 5th and 6th position of the BODIPY core [20]; 2)Replacement of the meso position carbon with nitrogen atom to form aza-BODIPYs; 3) Functionalizing the boron center by replacing fluorine with different atoms or group of atoms, in place of borylation; 4) Further functionalizing at the meso position through meso modifications such as C-C cross couplings, and 5) Extension of π-conjugation by fusing (alpha fusion or beta fusion) different aromatic rings to enhance the rigidity in the system due to the supplemented π-conjugation and improve π-π stacking [20].

BODIPY dyes are impervious to most pH and polarity changes within their environment and can withstand physiological conditions [21, 22]. By making small modifications to their structures, it is possible to tune their fluorescence characteristics. BODIPY fluorophore dyes feature a chromophore that enables the design of tailor-made molecules for specific biological and technological purposes [23, 24]. They have tunable properties that are famous for their chemical versatility and flexible photophysical and electrochemical properties, such as electrochemiluminescence (ECL), that can aid their abilities to be used in chemo sensing and serve as labels for bioimaging [18, 25]. Last, BODIPY dyes undergo degradation mechanisms in both acidic and basic media and displayed no decomposition after three days in deuterated chloroform ($CDCl_3$) or pure chloroform ($CH_2Cl_2$) solutions [26, 27].

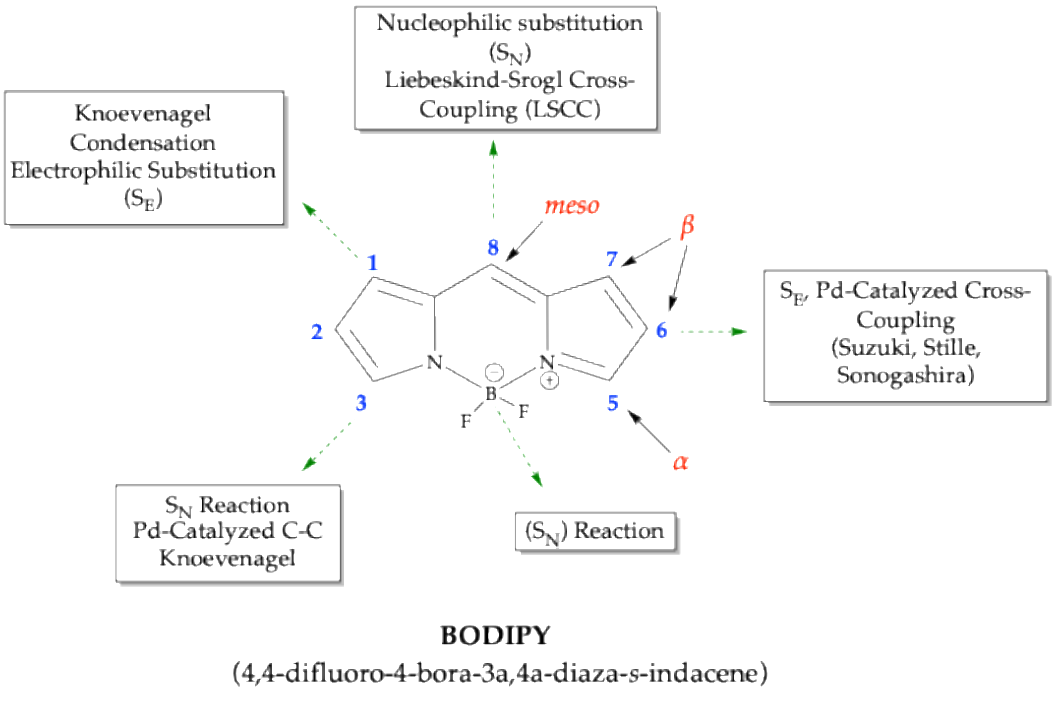


**BODIPY**
(4,4-difluoro-4-bora-3a,4a-diaza-*s*-indacene)

 doi:10.20944/preprints202511.1766.v1



**Figure 4.** Overlay of approaches used to adopt different moieties into the core of the BODIPY scaffold and increase the absorption wavelength ($\lambda_{max}$).

*2.1. General Synthetic Strategies for BODIPY Dyes*

Dye chemistry has gained traction in organic chemistry since the first BODIPY dye was discovered in 1968; its popularity allowed for the new development of molecular structures that deck the chromophore's backbone. Since advanced techniques of synthesizing unique functional fluorophores have been made possible, exploration of chemotypes that were not accessible in the past due to limitations of conventional approaches is now possible. Classical synthetic methods, such as amide formations, Knoevenagel reactions, and Suzuki couplings [28, 29] enable the ability to increase the quantum yield by designing compounds that will dominate in radiative photon emission processes rather than losing energy from rotatable bonds to non-radiative decay pathways, ultimately increasing the molecular brightness of the fluorophores, as displayed in Figure 4 .

There are two commonly distinct synthetic approaches to obtain BODIPY dyes for use in porphyrin research, one of which is the condensation of aldehydes **2** with pyrrole **1** that yields a dipyrromethene as shown in Scheme 1, below [30, 31]. To prevent polymerization, these reactions must be carried out in a solvent of pyrrole. For the best yields, dipyrromethenes are used immediately after preparation, as they are unstable in solution and are sensitive to light. Dipyrromethene **3** or dipyrrin **4** can undergo oxidation by DDQ or p-chloranil, which yields dipyrromethene. Then the addition of base to dipyrrin and boron trifluoride etherate leads to the creation of boron difluoride complex **5**. Using this synthetic approach, two equivalents of a substituted pyrrole undergo reaction with one equivalent of an acyl chloride, yielding an unstable dipyrromethene intermediate. This intermediate is then subjected to a strong base like triethylamine (TEA) along with a boron source to generate the BODIPY dye.

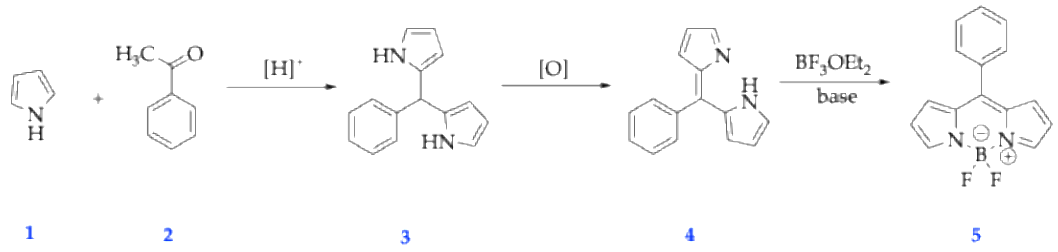


**Scheme 1.** Schematic depiction of the acid-catalyzed condensation of example aromatic aldehydes with pyrrole *en route* to the formation of BODIPY fluorophores.

However, a different synthetic route uses condensation with another pyrrole and an acylium **6**. An acylium is an acyl group, such as a carboxylic acid, that can be derivatized into other functional groups. The acylium may be an acid chloride, anhydride, or orthoester [32, 33]; the intermediate acylpyrrole **7** is not usually isolated and is committed to further reaction under acidic conditions with excess pyrrole **1** to yield dipyrrin **8**; this technique has been used to develop *meso*-substituted 3-pyrrolyl BODIPY fluorophores as precursor substrates to prepare a series of BODIPY-metal dipyrrin conjugates using palladium (Pd), ruthenium (Ru), and rhenium (Re) [33]. After the condensation, the addition of excess base and boron trifluoride etherate can also yield fluorescent BODIPY dyes **(9)** as shown in Scheme 2**.**

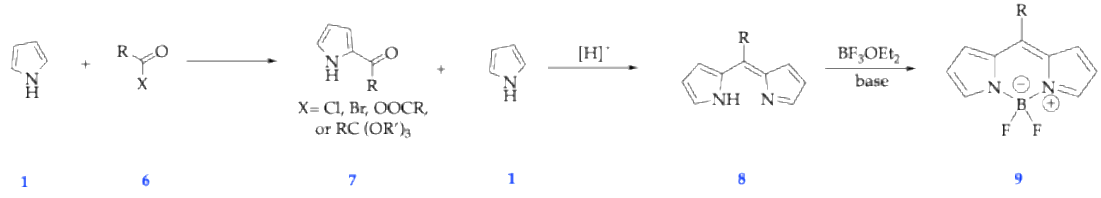

 doi:10.20944/preprints202511.1766.v1



**Scheme 2.** Schematic depiction of the acid-catalyzed condensation example reaction of acylpyrrole with an additional pyrrole *en route* to the formation of BODIPY fluorophores.

## 3. Synthesis of Aza-BODIPY Dyes

Currently, there are three prominent routes for the synthesis of Aza-BODIPY dyes: 1) O'Shea's, 2) Carreira's, and 3) Lukyanets' method, which were all discovered in the early 2000s, specifically between 2002-2008, and are displayed in Table 1. O'Shea *et al.* (2002) developed a novel method to create symmetrical and asymmetrical aza-BODIPY dyes *via* cyclization of 1,3-diaryl-4-nitrobutan-1-one and subsequently reported that the replacement of the methine carbon at the *meso*-position with a nitrogen results in a red shift without lowering the extinction coefficients and fluorescence intensities of the non-*meso* substituted parent dyes [32, 34]. Carriera *et al.* (2005) constructed symmetrical and asymmetrical aza-BODIPY structures from 2,4-diaryl-pyrroles and $NaNO_2$. Finally, Lukyanets *et al.* (2008) leveraged the ubiquity of Grignard chemistry to prepare aza-BODIPYs from a reaction between phthalonitrile and aryl Grignard reagents [34]. In addition to the three previously mentioned synthetic routes, Aza-BODIPY units have also been employed as linker and acceptor groups, due to the conjugated and photochemically stable BODIPY core to be leveraged as a scaffold for D-π-A fluorophores [6, 34]. The inherent electron-withdrawing ability of the $BF_2$ group enables the BODIPY structure to be leveraged as an acceptor unit for several donor groups to be attached to it.

**Table 1.** Summary of reported yields and representative compounds for the three synthetic methods of Aza-BODIPY fluorophores [34].

| Method | Reported Yield | Representative Compounds | Forms: Asymmetrical or Symmetrical Fluorophores? |
|---|---|---|---|
| O'Shea's | 20-50% [34] | Tetraphenyl Aza-BODIPY<br>Dimethylamino Aza-BODIPY | Both |
| Carriera's | 60-90% [34] | Cyclized 2,4-diaryl pyrroles complexed with $BF_3OEt_2$ | Both |
| Lukyanet's | 10-30% [34] | Phthalonitrile and aryl Grignard reagents complexed with $BF_3OEt_2$ | Symmetrical Only |

### *3.1. O'Shea's Route*

As presented in Scheme 3, the chalcone can be used to form a nitro chalcone or a 2,4-disubstituted pyrrole, to then undergo intramolecular cyclization to form the UV-active fluorophore and establish the conjugated polymethine backbone chain of the fluorophore. In chalcone 12, aryl ring 1 ($Ar_1$) denotes the substituent contributed from the benzaldehyde 10, and aryl ring 2 ($Ar_2$) denotes the substituent contributed from the acetophenone 11. The mechanistic overview of O' Shea's route involves 3 steps: 1) Michael Addition, 2) Intramolecular Cyclization, and 3) Boron complexation. Chalcone 12 is subjected to Michael Addition under reflux with diethylamine and nitromethane to add a nitro ($-NO_2$) group to the β (beta) position of the diketone, forming a nitro-substituted intermediate- aptly named "nitro chalcone" 13.

When forming *symmetrical* Aza-BODIPYs, the two units of the nitro chalcone 13 react in a 2:1 ratio with excess ammonium acetate in the presence of a high-boiling solvent, such as butanol (BuOH) or acetic anhydride ($Ac_2O$), where the nitro group is reduced to a pyrrolic amine, in the presence of ammonium acetate ($NH_4OAc$). Typically, the pyrrolic amine 14 is not isolated and used *in situ* as the reaction is allowed to proceed to completion. Herein, the 1st pyrrolic amine unit is reduced 15 and reacts with another equivalent of the nitro chalcone diketone to form a transient diamino ketone

 doi:10.20944/preprints202511.1766.v1



intermediate. This ephemeral structure is not isolated and undergoes intramolecular cyclization, leading to the formation of the Aza-dipyrromethene core 17. When forming *asymmetrical* Aza-BODIPYs, two unique nitro chalcones bearing four different aryl (Arx) substituents are reacted in a 2:1 ratio to form two units of pyrrolic amines, which will react in the same fashion as the symmetrical route, to form the asymmetrical aza-dipyrromethene core 16. Finally, in both the symmetrical and asymmetrical case, the aza-dipyrromethene intermediate is deprotonated in the presence of a base such as triethylamine (TEA) or *N*, *N*-diisopropylamine (Hünig's base) where the nucleophilic attack by the Lewis acid $BF_3$ from the source of boron trifluoride yields the final $BF_2$ complexed fluorophores 18 and 19 as outlined in Scheme 3.

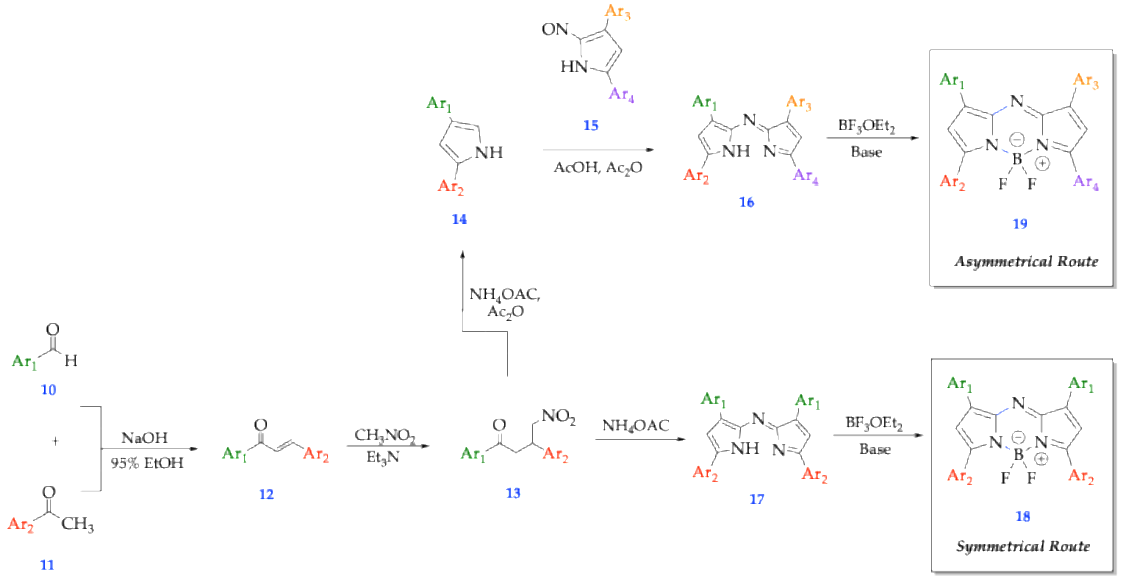


**Scheme 3.** Symmetrical and Asymmetrical Aza-BODIPY fluorophore synthetic route through O'Shea's method [34].

### *3.2. Carriera's Route*

In Carriera's Route, the synthesis of the Aza-BODIPY fluorophores is characterized by the direct cyclization of 2,4-diaryl pyrroles 20 to form the BODIPY core, or the BODIPY core is formed through Schiff Base formation from a lactam (i.e., phthalimide) and a heteroaromatic amine to form a Schiff base intermediate 21, characterized by a C=N double bond [34]. The Schiff base undergoes intramolecular cyclization under acidic conditions, forming a dihydro-azadipyrromethene intermediate. The dihydro-azadipyrromethene is treated with boron trifluoride diethyl etherate in the presence of a base such as triethylamine to form the final fluorophore 22 as outlined in Scheme 4.

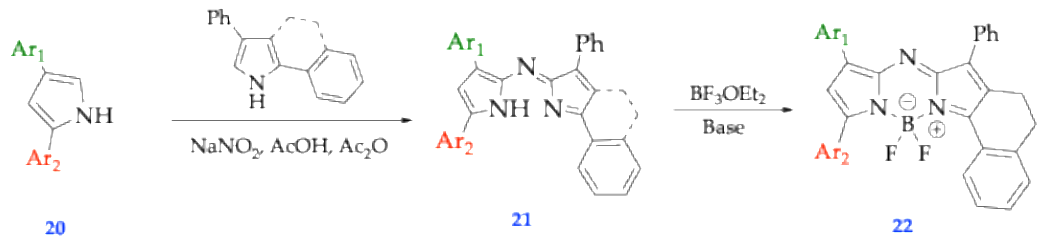


**Scheme 4.** Asymmetrical Aza-BODIPY fluorophore synthetic route through Carriera's method of Schiff Base formation [34].

 doi:10.20944/preprints202511.1766.v1



*3.3. Lukyanet's Route*

In 2008, the third method for synthesizing Aza-BODIPY fluorophores was pioneered by Lukyanets *et.al* (2008) [35], who developed this novel route to establish a phthalocyanine analog Aza-BODIPY, through the reaction of phthalonitrile (1,2-dicyanobenzene), as seen in Scheme 5 , compound 23 reacts with aryl magnesium bromide in dry benzene at room temperature for 1 hr [35] First, a nucleophilic addition of the Grignard reagent, aryl magnesium bromide, adds to the nitrile carbon of the phthalonitrile, resulting in an unstable, short lived intermediate diimine (Ar-C=N-Ar'), which undergoes intramolecular condensation *via* acid-catalyzed or thermally driven reaction to lead to the aza-dipyrromethene, as shown in structure 24, containing the central nitrogen in the six-membered ring, flanked by two pyrrole-like aromatic rings. Finally, the synthesis is completed by the chelation of boron to the two basic site pyrrolic nitrogen atoms, resulting in the planar, rigid aza-BODIPY dye, as seen in structure 25. The structure of compound 25 was revealed through single crystal X-ray analysis and revealed that the fluorophore adopts a near $C_{2v}$ symmetric conformation, in which the isoindole substituents are fixed in a coplanar manner, and the coordination geometry around the boron atom is similar to Aza-BODIPY dyes synthesized through O'Shea's and Carriera's method, as evidenced by B–N distances of 1.573 Å and 1.579 Å and by two fluorine atoms with B–F distances of 1.372 Å and 1.380 Å, respectively [35, 36].

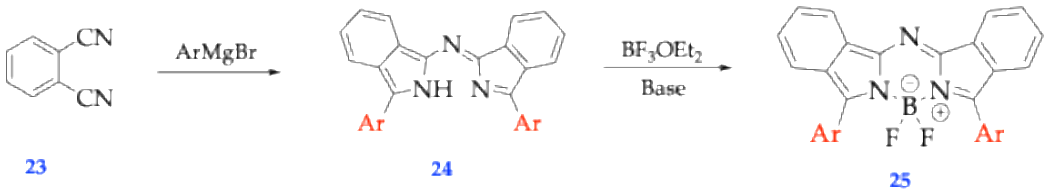


**Scheme 5.** Symmetrical Aza-BODIPY fluorophore synthetic route through Lukyanet's method of using Grignard reagents [34, 35].

*3.4. Strategies to Achieve Bathochromic Shift*

Prominent strategies to red shift the wavelength are highlighted in Figure 5, which include 1) extending the conjugation of the dye system and 2) increasing the rigidity of the BODIPY core. The absorption and emission of a compound are directly influenced by electronic conjugation. Therefore, the most common design strategy for shifting BODIPY molecules towards red wavelengths is extending conjugation. Increasing the extent of conjugation reduces the energy gap between the frontier orbitals- the highest occupied molecular orbital (HOMO) and the lowest unoccupied molecular orbital (LUMO)-, resulting in more energy being conserved to convert into longer absorbance wavelengths. There are various approaches to designing an expanded delocalized π system, including extending π conjugation and increasing rigidity. 1,3,5, and 7 positions of the BODIPY core incorporating aryl, styryl, or similar functionality can effectively extend π conjugation. For simplicity in synthesis, conjugation is frequently extended only at the 3- and 5-positions of the BODIPY core, demonstrating the spacer effects of donor-π spacer-acceptor sensitizers [37]. Expanding conjugation involves adding more π electrons to a delocalized system, thereby increasing the number of molecular orbitals and consequently narrowing the HOMO-LUMO gap. Similarly, by virtue of increasing the system's planarity *via* increased conjugation, restricting the degree of rotatable bonds increases the rigidity of the BODIPY core. Unrestricted rotation along the bonds connecting the BODIPY and an attached π spacer can result in misalignment of the π orbitals, thereby diminishing the impact of π conjugation. Additionally, bulky alkyl groups that are sterically constrained can be added to the core to enhance steric hindrance, thereby fixing or restraining the degree of rotation inherent to the π spacer (or linker). Torsion angles can be reduced by either fusing aromatic rings or by incorporating five-membered heterocycles instead of aryl functionality [22, 37].

 doi:10.20944/preprints202511.1766.v1



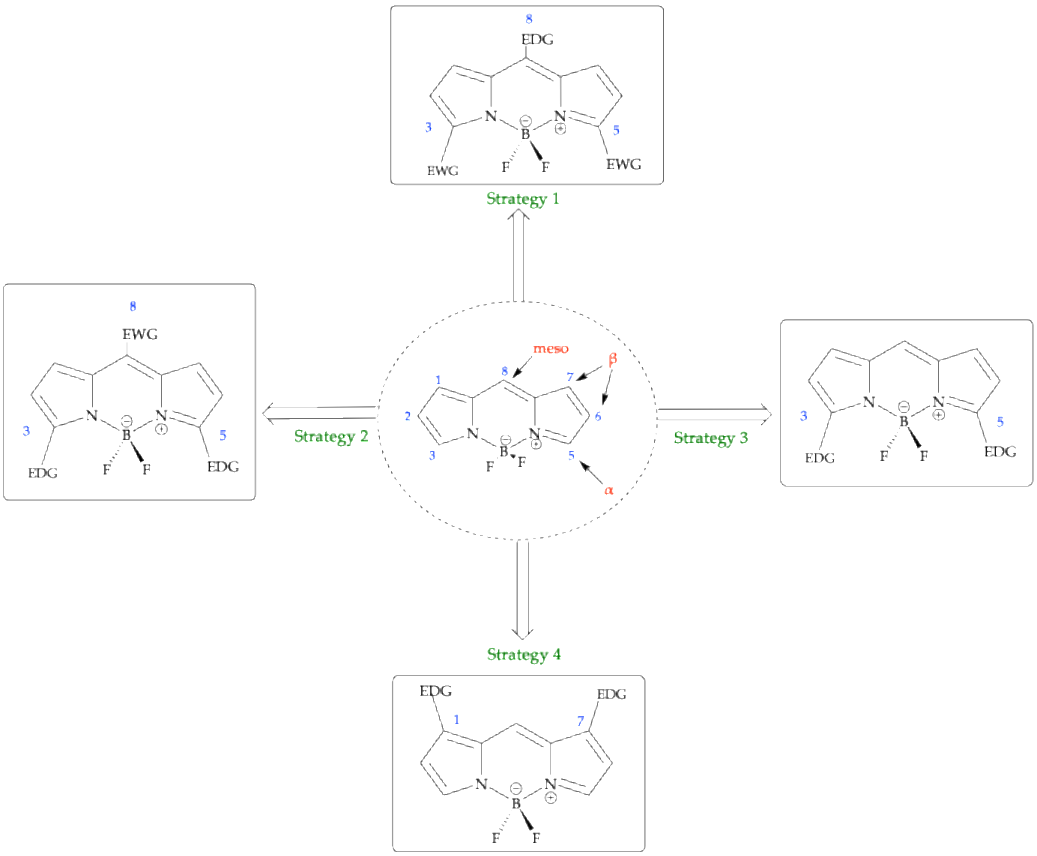


**Figure 5.** 4 types of synthetic modifications to favor a further push into the NIR region (red shift) [30].

*3.5. Synthetic Modifications Favoring Bathochromic Shift*

The creation of a narrow band-gap chromophore is possible by incorporating intramolecular charge transfer (ICT) properties into the molecule. An ICT molecule undergoes a transfer of electron density of an electron (rich) donor group (EDG) through a π -conjugated linker to an electron (poor) withdrawing group (EWG) [30]. π linker, depending on the type, acts as an insulator or conductor and undergoes the charge transfer process. The introduction of charge transfer is an effective way to modulate the excited state by altering the emission geometry. This procedure stabilizes the lowest unoccupied molecular orbital (LUMO), thereby influencing the emission wavelength [25, 29]. Figure 5 entails various for synthetically modifying the BODIPY core to achieve a bathochromic shift. Strategy 1 entails placing an EDG group at 8 position (aza) and 2 EWG on positions 3 and 5 on the core, results in large MO coefficients in both the LUMO and HOMO. Strategy 2 entails placing an EWG group at 8 position (aza) and 2 EDG groups on positions 3 and 5 on the core results, which should narrow the HOMO-LUMO gap, making for a red-shifted dye. Strategy 3 entails incorporating an EDG at 3 and 5 positions should raise HOMO energy level, causing longer wavelength. In 2009, the first reported effect of chalcogens bathochromically shifting BODIPY absorbance maximums was reported, described as the periodic trend that descends a group of chalcogens (from O, Se, S, Te, onwards…) employed at 3 and 5 positions increases longer wavelength absorption [38]. Furthermore, recent advances in functionalization at the 3 and 5 positions to shift the excitation/emission bands were created by targeting the 3 and 5 positions to install phenyl boronic acid (PBA) as a means of also tethering glycan domains to streptavidin monoclonal antibody, to also address the bottleneck of versatility among the BODIPY dyes [39]. Likewise, it is a known trend that the higher the strength of the electron-donating species (EDG), the greater the energy of the highest occupied molecular orbital (HOMO) [25,29, 30]. Finally, strategy 4 entails an EDG being placed at 1, 7 positions because there are no nodal planes in the HOMO near these positions- generally, it can be inferred that electron-donating groups (EDGs) exert a stabilizing influence on the highest occupied molecular orbital

 doi:10.20944/preprints202511.1766.v1



(HOMO) by elevating its energy when appropriately attached to the BODIPY core. Here, there are nodes; a region of no electronic density exists. Thus, the more nodes are present, the higher the energy of the system [30].

## 4. BODIPY Dyes as Fluorescent Sensors

The works of Bardon *et.al* (2018) developed a variety of adaptable reactive systems, which are readily substitutable. One prominent application of these systems is their utilization in fabricating fluorescent sensors. Given the high sensitivity of fluorescence response measurement, this method can be employed for detecting biologically significant substrates. Significantly, the potential to incorporate nitrogen nucleophiles at the 3,5-positions could be intriguing, as substitution at these positions directly impacts the spectral characteristics of the dye [40]. Moreover, the spectroscopic properties of transition metal-catalyzed benzofuran formation BODIPYs **26, 27,** and **28,** as outlined in Figure 6, demonstrate one of the earliest reported instances of the rigidification of the BODIPY structure *via* annulation, an efficient strategy to confer higher molar extinction coefficients and fluorescence quantum yields (ϕf) values [41]. The progressive enhancement in the planarity of the chromophore within the series **26** → **27** → **28** explains the rising bathochromic shifts observed in both $\lambda_{abs}$ (max) and $\lambda_{em}$ (max). By increasing the stiffness of systems **27** and **28** through benzofuran formation and by increasing the planarity of the chromophore, the degrees of vibrational freedom decrease.

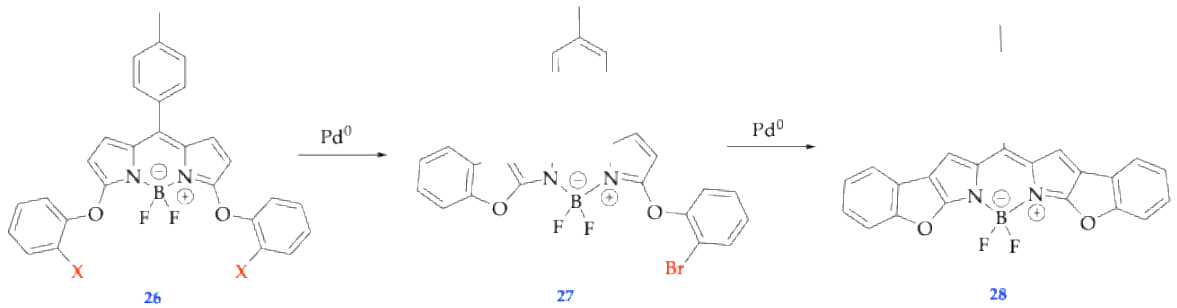


**Figure 6.** Structural depictions of benzofuran BODIPY derivatives probed for spectral properties [41].

Recent advances in BODIPYs as fluorescent sensors have been achieved through combining spectral properties and synthetic reactive systems from 2014-2025. One new advent has been the employment of BODIPYs as explosive sensors for the tracing of picric acid (PA), hexahydro-1,3,5-trinitro-1,3,5-triazine (RDX), and peroxides through a fluorescence turn-on mechanism. Compounds **29** and **30,** as shown in Figure 7, were developed to detect picric acid and showed fluorescence emission at 473 nm, but fluorescence was quenched in the presence of picric acid. Their respective limit of detection (LOD) was at 0.038 and 0.017 μM, respectively [42].

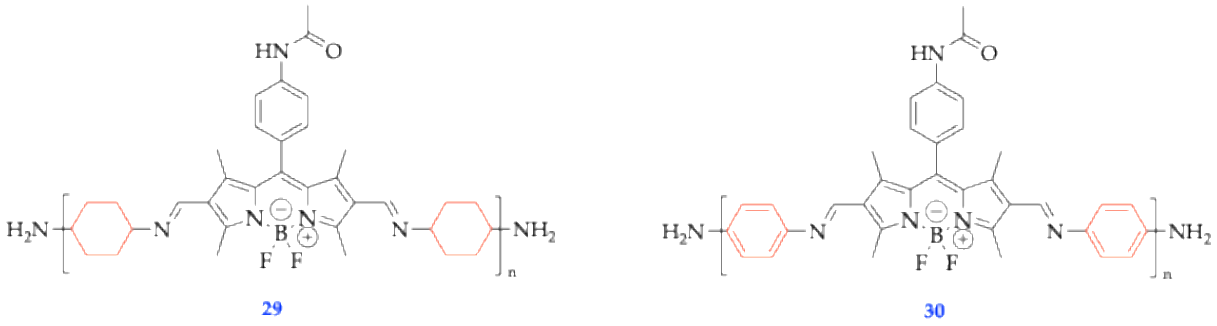


**Figure 7.** Fluorophores **29** and **30**, which have been used as fluorescent sensors in the detection of explosives and picric acid [42].

 doi:10.20944/preprints202511.1766.v1



Another advance in the development of BODIPY fluorescent sensors is the concept of a "fluoroionophore" that is highly selective for sodium cations ($Na^+$). BODIPY-equipped benzo-crown-ethers were employed as fluorescent sensors for the independent detection of sodium and potassium ions [43], equipped with different-sized macrocycles to facilitate binding to and subsequent fluorometric detection of biological $Na^+$ and $K^+$ levels, as depicted in Figure 8. BODIPY ionophore 34 displayed significant fluorescent enhancement (FE) within the pH range from 3 to 5, due to the protonation of the anilino nitrogen donor. As a result, the protonation of the anilino nitrogen blocks the fluorescence quenching process and triggers the FE. Compared against BODIPY ionophores 31, 32, and 33, which exhibited a highly stable fluorescence signal across pH ranges 3.5 to 9.5, they were subjected to fluorescence titration experiments with alkali metal ions ($Na^+$, $K^+$, and $Li^+$) at different pH values. Compounds 32 displayed a higher affinity for $Na^+$, and compound 33 formed a more stable complex with $K^+$ than with $Na^+$, as indicated by dissociation constants their dissociation constants displayed in Table 2.

**Table 2.** Tabulated photophysical properties for compounds 31, 32, and 33 in $H_2O$/DMSO mixtures (v/v 999/1) at pH 4.7 (10 mM acetic acid/acetate buffer): [a] Fluorescence quantum yield (±15)%; [b] Fluorescence enhancement factor (FEF = $I/I_0$], (± 0.2); [c] Dissociation constants $K_d$; [d] $K_d$ value for these cations' complexes could not be calculated due to low cation induced intensity changes [43].

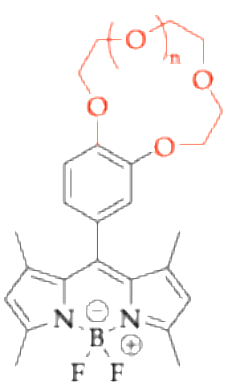

**31** $n = 1$
**32** $n = 2$
**33** $n = 3$

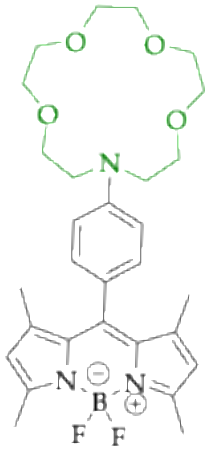

**34**

| Compound | $\lambda_{abs}$ [nm] | $\lambda_{em}$ [nm] | Φf [a] | FEF [b] | $K_d$ [c] [mM] |
|---|---|---|---|---|---|
| **31** | 498 | 506 | 0.072 | ------- | ------- |
| **31**+ 100 mM $Na^+$ | 498 | 507 | 0.073 | 1.0 | ---- [d] |
| **31**+ 100 mM $K^+$ | 498 | 507 | 0.072 | 1.0 | ---- [d] |
| **31**+ 100 mM $Li^+$ | 498 | 507 | 0.072 | 1.0 | ---- [d] |
| **32** | 498 | 507 | 0.008 | ------- | ------- |
| **32** + 1000 mM $Na^+$ | 498 | 507 | 0.056 | 7.3 | 276 |
| **32** + 1000 mM $K^+$ | 498 | 507 | 0.023 | 2.8 | 342 |
| **33** | 498 | 507 | 0.008 | ------- | ------- |
| **33** + 250 mM $Na^+$ | 498 | 507 | 0.013 | 1.8 | 65 |
| **33** + 250 mM $K^+$ | 498 | 508 | 0.035 | 4.7 | 18 |

 doi:10.20944/preprints202511.1766.v1



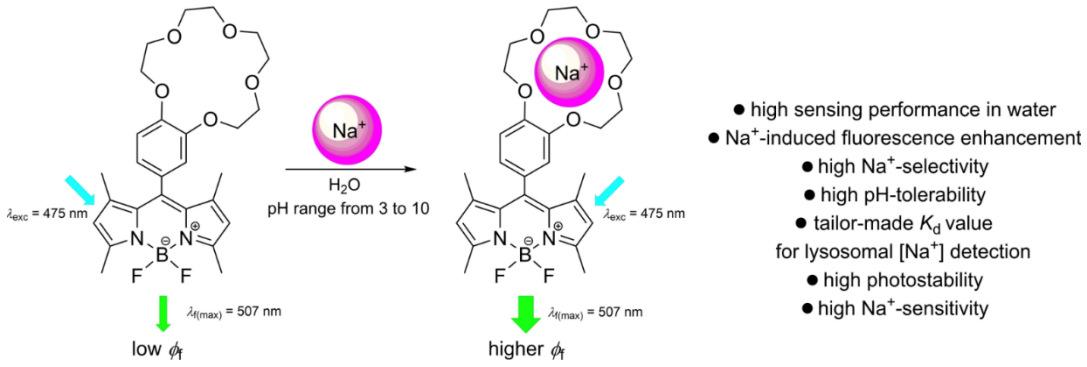


**Figure 8.** Schematic depicting the mechanism of action of compound **32,** which quenches fluorescence through protonation because the excited fluorophore experiences contact with an atom or molecule that can facilitate non-radiative transitions to the ground state. This figure was reproduced with permission from Sprenger *et al*., 2022, copyright 2022 [43].

Finally, a Seleno-BODIPY fluorescent sensor for differential and highly selective detection of bio thiols, cysteine (Cys), and glutathione (GSH) was developed by Cugnasca *et.al.* (2025) [44]. Compound **37** displayed colorimetric and turn-on fluorometric responses to Cys and GSH, exhibiting low detection limits of 61.18 nM and 1.66 μM, respectively, as shown in Figure 9. Compound **37** was screened against 26 analytes including amino acids, reactive sulfur species (RSS), and anions, where was possible to verify selectivity and expressive responses for bio thiols like Cys, N-acetylcysteine (NAC), GSH, Homocysteine (Hcy), and sodium sulfide ($Na_2S$) *via* absorbance, exhibiting a color change from blue to orange (Cys) and pink (NAC and GSH) [44]. After obtaining emission spectra, $\lambda_{ex}$ = 488 nm was employed to detect Cys, and $\lambda_{ex}$ = 553 nm was employed to detect GSH. Through a titration with increasing amounts of Cys (0-50 equivalents), decrease at $\lambda_{max}$ = 594 nm and an increase at $\lambda_{max}$ = 496 nm in a radiometric colorimetric response, with the presence of an isosbestic point, as shown in Figure 10, indicating the conversion of Se-BODIPY in another product (**Cys-BODIPY**) was observed, as shown in Figure 8.

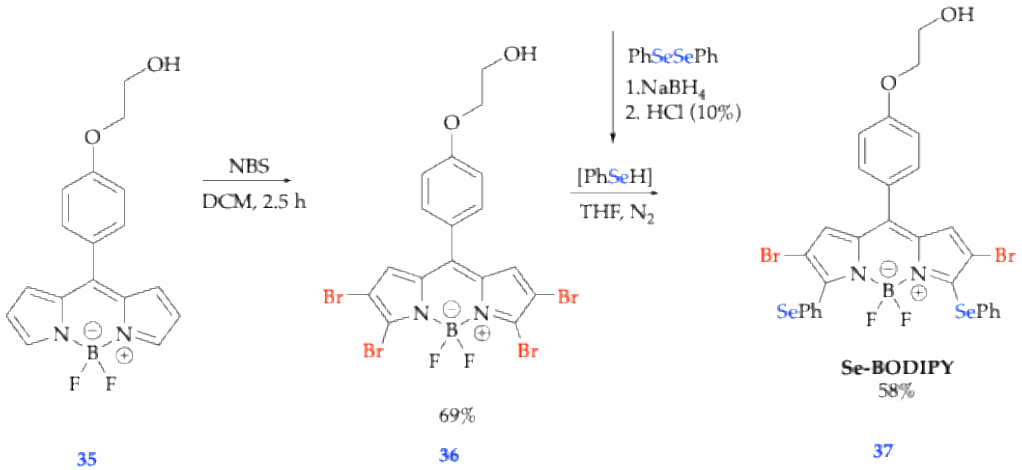

 doi:10.20944/preprints202511.1766.v1



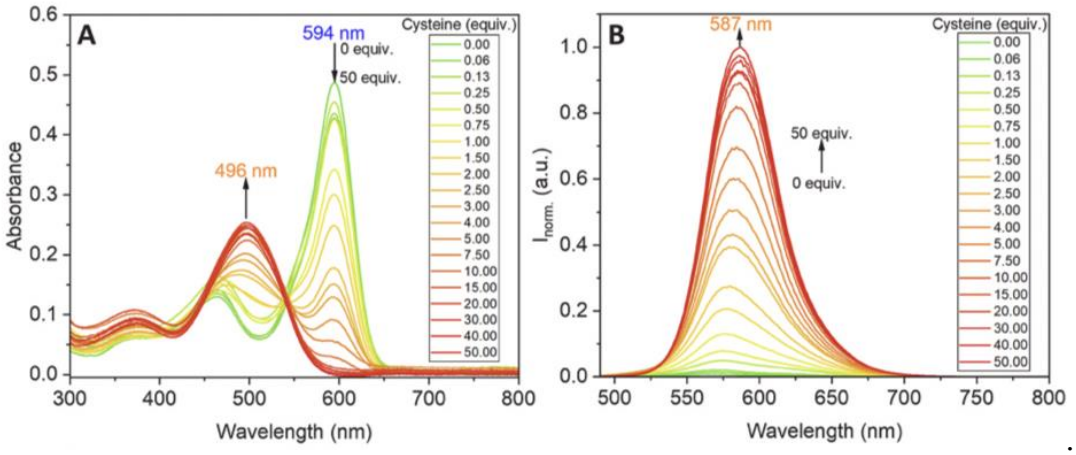


**Figure 9.** A) Absorption and B) emission spectra profiles of Se-BODIPY (7.6 μmol/L) in THF/$H_2O$ 50% v/v pH 7.0, upon addition of increasing concentration of Cys (0–380 μmol/L; 0–50 equiv.), after 30 min of reaction. $\lambda_{ex}$ = 480 nm, slits 3.0/3.0 nm This figure was reproduced with permission from Cugnasca *et al*., 2025, copyright 2022 [44].

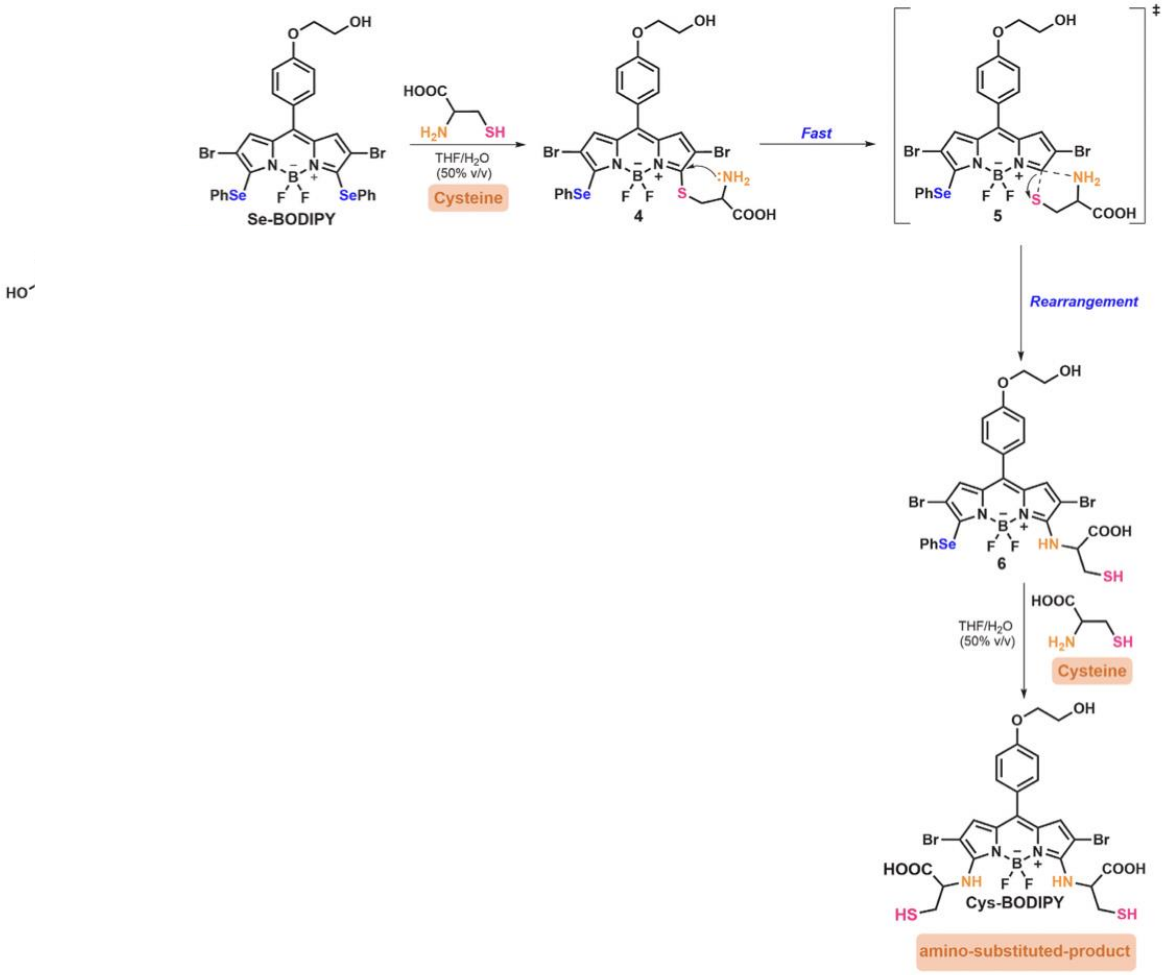


**Figure 10.** Proposed reaction mechanism of Se-BODIPY, compound 37, with Cys and GSH. This figure was reproduced with permission from Cugnasca *et al*., 2025, copyright 2022 [44].

 doi:10.20944/preprints202511.1766.v1



## 5. Optical Properties of Selected Compounds

### *5.1. Two-Photon Absorption*

Karatay *et al.* (2015) synthesized new Aza-BODIPY fluorophores containing bromine atoms at various positions to enhance the triplet state populations as a means of improving two photon absorption properties for two photon photodynamic therapy; the researchers studied the effects of the photoinduced electron transfer mechanism because of the introduction of the heavy-atom, bromine, using ultrafast pump probe spectroscopy experiments and density-functional theory (DFT) calculations. Ultrafast pump-probe experimental results explained observed fluorescence quenching by portraying evidence of the intersystem crossing (ISC) mechanism, where the lifetime of the signals shows great differences whether including Br atoms at the 2 and 6 positions of aza-BODIPY core or not [45]. To further investigate why compound 39, with bromines added to the peripheral positions of the BODIPY core, exhibited stronger intersystem crossing (lower fluorescence) than compound 38, DFT studies were conducted by optimizing the ground state geometries of the compounds, as shown in Figures 11 and 12. Compared to the measured energy value from the first singlet excited state to the first triplet state, it is shown in Figure 12, that compound 39 has a higher energy value of 0.98 eV, compared to compound 38, than at 0.90 eV for compound 38. The DFT studies were imperative to explaining this interaction as the DFT calculations supported the preliminary results that revealed the singlet and triplet energy levels become closer and more concomitant with each other when the Bromine (Br) atoms are at the 2,6 positions of the aza-BODIPY core. The authors implore that their experimental and theoretical investigations, through the introduction of Br onto the peripheral positions of aza-BODIPY compounds, do not affect the triplet state populations [45].

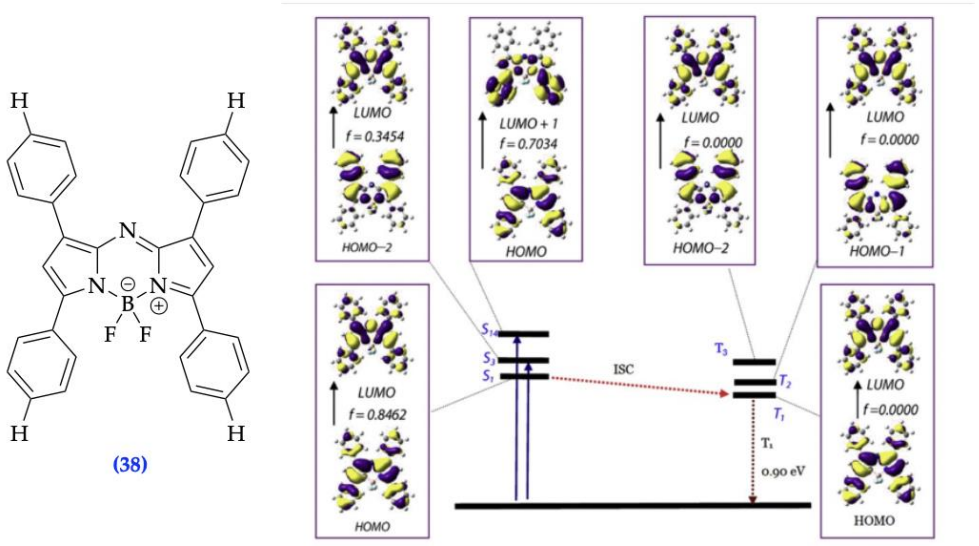


**Figure 11.** Electronic density map showing the frontier molecular orbitals (highest occupied and lowest occupied) of compound 38. Computed and analyzed at the B3LYP/6-31G(d)/LanL2DZ level with Gaussian modeling software. This figure was reproduced with permission from Karatay *et al.* (2015), copyright 2015 [45].

 doi:10.20944/preprints202511.1766.v1



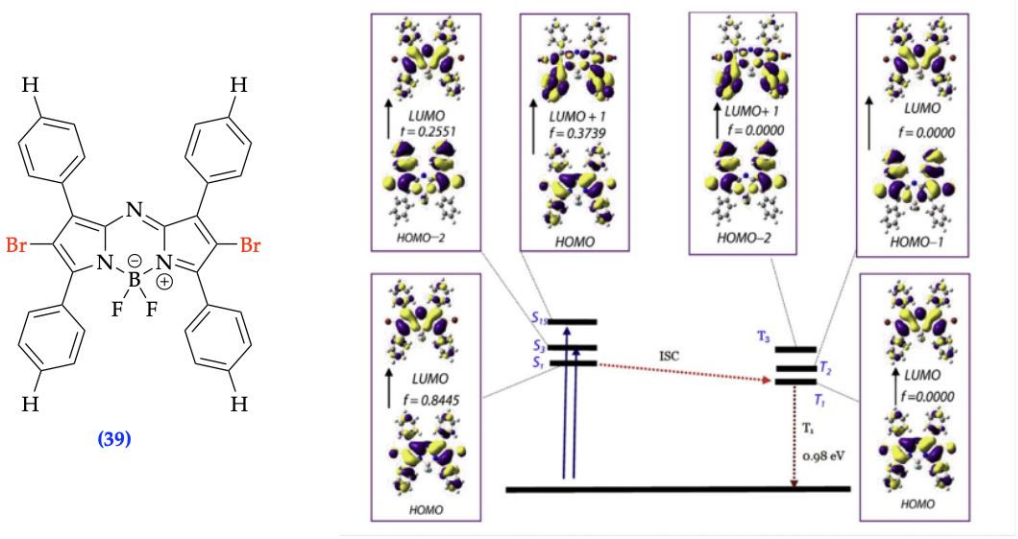


**Figure 12.** Electronic density map showing the frontier molecular orbitals (highest occupied and lowest occupied) of compound 39. Computed and analyzed at the B3LYP/6-31G(d)/LanL2DZ level with Gaussian modeling software. This figure was reproduced with permission from Karatay *et al*. (2015), copyright 2015 [45].

*5.2. Aggregation-Induced Emission*

Given that aggregation of molecules confers a facile way to selectively tune and rationally modify the optical profiles of dyes, a significant challenge still exists in how to control the molecular organization of dye monomers to adopt certain aggregate formations to maximize the efficiency of PDT. Herein, Liu *et. al* (2023) devised a novel supramolecular strategy to formulate nano-photosensitizers from heavy-atom free Aza-BODIPYs (BDP-1 and BDP-2), shown as compounds 50 and 51, as shown in Scheme 6, bearing a pyridine unit, on the benzaldehyde and acetophenone sides of the aza-BODIPY, respectively *via* O'Shea's synthetic route [46]. The general synthetic route for compounds 50 and 51 is displayed in Scheme 6. To further support this tenet, these photosensitizers (PSs) readily form aggregates predominantly in aqueous media because of synergistic π–π stacking and hydrophobic interactions. BDP-1 (50) and BDP-2 (51) were encapsulated in Pluronic F127 (F127) nanoparticles to serve as an amphiphilic copolymer form nanoparticles, termed BDP-1 NPs and BDP-2 NPs, respectively. However, these niche aggregate formations especially hinder the abundance of reactive oxygen species (ROSs) formation due to the innate self-quenching tendency of the excited state, often resulting in limited clinical utility. It was reported that BDP-1 NPs formed J-aggregates, whereas BDP-2 NPs formed H-aggregates.

J-aggregates are aggregates that arise and form because of the transition dipole moments of individual dye monomers undergoing a "slip-stack" alignment, which manifests as an optical tendency to red-shift absorption maximums [23,24], as shown in Figure 13. Furthermore, the HOMO and LUMO frontier orbitals for dyes forming J-aggregates can be segregated efficiently due to the electron transfer to lower split energy levels, conferring an advantageous point to boost the quantum yield (ΦΔ) by decreasing the frontier orbital band gap (ΔEST). Conversely, in H-aggregates, the molecular alignments result from the equilibrium generated from the strong overlapping "face-to-face" contacts. Thereby, by deduction, perfectly aligned H-aggregates are nonfluorescent, as their lowest energy level is forbidden. All in all, it is of keen interest within the arena of dye chemistry to exploit the formation of H-type aggregates of fluorophores, which may emanate energy in other nonradiative forms.

 doi:10.20944/preprints202511.1766.v1



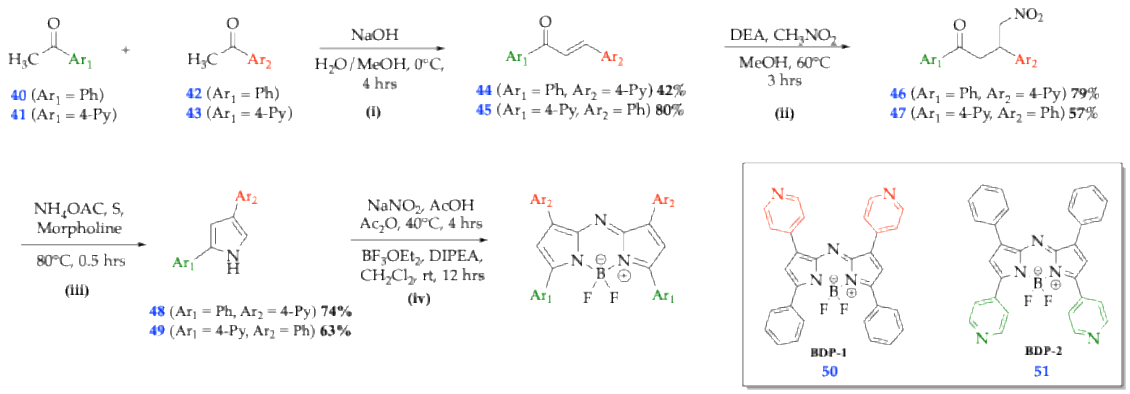


**Scheme 6.** General scheme displaying stepwise synthetic procedure and structures of newly synthesized BDP-1 50 and BDP-2 51 [46].

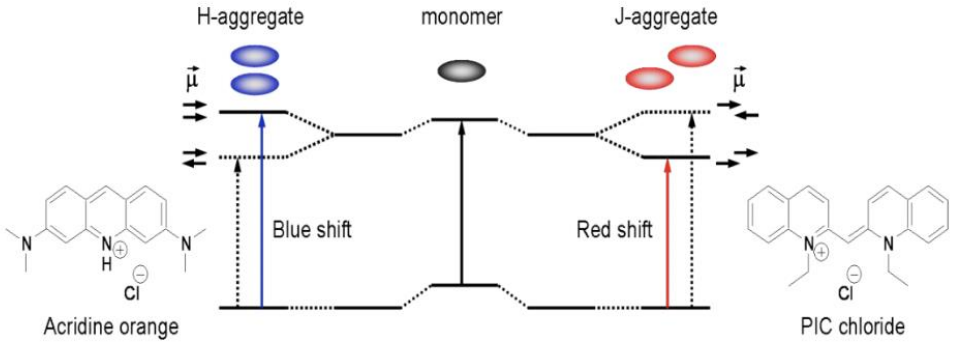


**Figure 13.** Energy diagram portraying examples of H- and J-aggregates in examples of dyes forming these aggregates, respectively. This figure was reproduced with permission from Klymchenko *et al*. (2013), copyright 2013 [47].

Moreover, through the introduction of pyridine rings into O'Shea's synthetic routes of compounds 50 and 51, it was discovered that their absorption maxima were contingent upon the nature of the substituents installed at the 3,5- and 1,7-positions of the dipyrrin core. As depicted in Figure 14b, the effect of shifting from the phenyl aryl ring (BDP-3) to the pyridyl (BDP-1) at the 1,7-positions resulted in a 11 nm redshift in the pyridyl (BDP-1) optical profile, whereas there is an 18 nm blueshift in the phenyl (BDP-3) optical profile as 3,5-substituents. Likewise, the fluorescence properties of BDP-1 (50) and BDP-2 (51) were investigated and exhibited a similar pattern as displayed in the absorption spectra, as shown in Figure 14c. These results demonstrated the optical benefit of employing the higher conjugation effect of the switching one of the phenyl heterocycles with a pyridyl group in the 1 and 7 position of the fluorophore core. As a result, the aggregation trends of BDP-1, BDP-2, and BDP-3 were further evaluated by employing a mixed solvent system of water and THF [46, 47].

 doi:10.20944/preprints202511.1766.v1



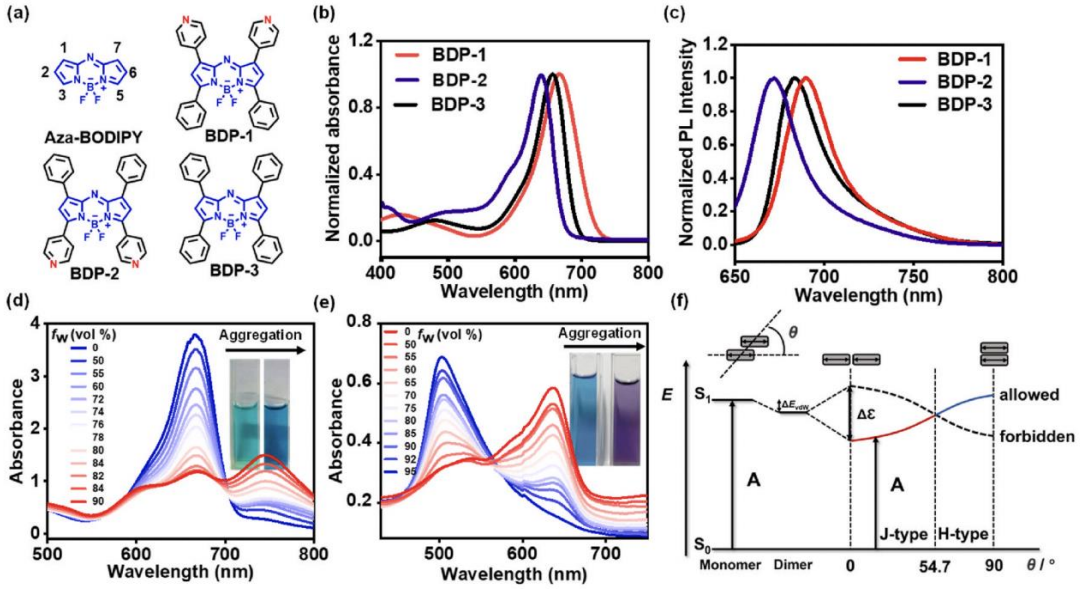


**Figure 14.** a) Chemical structures BDP-1, BDP-2, and BDP-3; b) normalized absorbance; c) Normalized fluorescence intensity; d) BDP-1 and e) BDP-2 in THF/water mixtures with different water fractions (*fw*); f) schematic illustration for energy diagram of aggregated dimers. This figure was reproduced with permission from Liu *et al*. (2023), copyright 2023 [46].

### *5.3. Spectroscopic Properties of Dicationic and Dianionic BODIPY Dyes*

Bardon *et.al* (2018) investigated the synthesis of two water-soluble BODIPY dyes, compounds 52 and 53, as shown in Figure 15, bearing dicationic or dianionic groups, which aided in imparting water solubility and preventing the translocation of the dye through plasma membranes, facilitating their use in aqueous media and minimizing the cytotoxicity issues commonly encountered when organic solvents are used to dissolve and/or load the dyes for bioanalysis and bioimaging applications [40, 47]. To prepare photostable, NIR fluorescent water-soluble membrane probes, compounds 52 and 53 were strategically prepared with combinations of dications and solubilizing agents. Compound 52 employed the use of the triazabicyclo [2.2.2] octane (DABCO) moiety due to its high hydrophilicity across the biological pH range, whereas compound 53 employed the installation of itaconic acid for solubilizing purposes. The parent BODIPY core possessed butyl groups on the amino phenylene unit as a measure of balancing the oleophilic nature of the core. The synthetic strategy conferred the ability of compounds 52 and 53 to be able to partially into micelles or membranes while the hydrophilic end allows the compound to be anchored outside of the membrane to interact with the extracellular environment [40]. Previous efforts of Choi *et al*. (2014) aided in the development of targeted zwitterionic near-infrared fluorophores that exhibited low background, by balancing the total net surface charge distribution of the fluorophore to be 0; this was accomplished by balancing the sulfonate and quaternary ammonium salt substituents to improve tumor targetability [48, 49], which is a common modality governing the scope of amphiphilic BODIPY fluorophore synthesis.

**Table 3.** Photophysical properties of compounds 52 and 53 in $CHCl_3$. [a] Oxazine standard using ethanol as a solvent [40].

| Compound | $\lambda_{abs}$ [nm] | log [ε] | $\lambda_{em}$ [nm] | Φf% % [a] |
|---|---|---|---|---|
| **52** | 630 | 4.80 | 690 | 55.4 |
| **53** | 625 | 4.80 | 678 | 51.0 |

 doi:10.20944/preprints202511.1766.v1



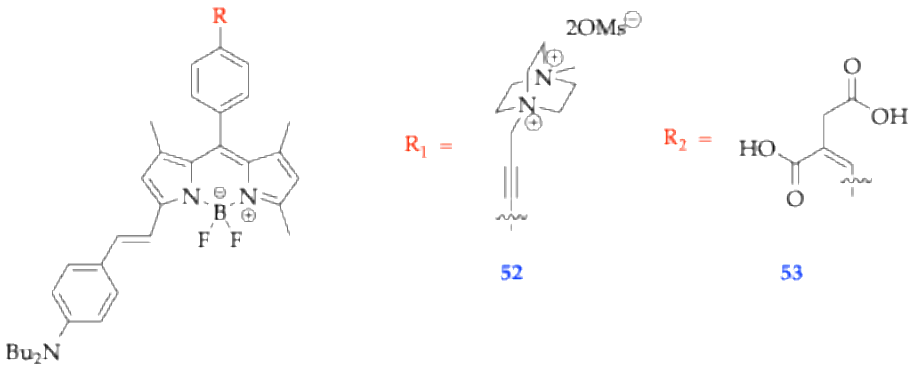


**Figure 15.** Newly designed BODIPY amphiphilic derivatives 52 and 53 with dibutylaminophenylene vinylene group attached to the 3-position to extend conjugation of chromophore [40].

## 6. Biomedical Applications

Aza-BODIPY fluorophores find applications in C-H activation reactions, organic solar voltaic cells [10, 18], anti-cancer photodynamic and photothermal activity [14,15,16], bioimaging [16,19], and chemo sensors [44, 46]. Moreover, Aza-BODIPY dyes possess a similar BODIPY core structure except that the nitrogen replaces the carbon atom at the *meso*-position. These dyes demonstrate high NIR extinction coefficients and high quantum yields. Aza-BODIPY dyes may be manipulated with hydrophilic groups to facilitate the compound to be leveraged in aqueous environments- an ode to its propensity for *in vivo* applications. A few examples that can improve the solubility and still retain the fluorescence properties are adding quaternary ammonium, sulfonate, or oligo-ethylene glycol moieties to the BODIPY core. The modifications of the aza-BODIPY dye to become water-soluble allow for the applications of chemo sensors, fluorescence labeling and imaging, pH indicators, and photodynamic therapy [50, 51].

### *6.1. Metal-Catalyzed C-H Activation Reactions*

Metal-catalyzed couplings, such as, the Suzuki–Miyaura reactions, are the most common approach to prepare biaryl compounds because there is a need for two functionalized substrates, which include boronic acid and aryl halide. However, a few limitations continue to restrict the availability of substituted boronic acid derivatives. As a result, the limited availability of substituted boronic acid by-products may be overcome with C-H activation processes that directly connect aryl halides to (hetero) arenes by metal-promoted activation of a C-H bond in the latter compound [52, 53]. Henceforth, Verbelen *et.al* (2012) developed a general method for preparing brightly fluorescent 3,5-arylated BODIPY dyes with red-shifted electronic spectra, by utilizing C-H functionalization to avoid the cumbersome synthesis of substituted pyrroles to form the BODIPY core. This work was integral to advancing the development of functionalized BODIPY fluorophores for multicomponent reactions from 2014-2025. Scheme 7 displays the synthesis of diaryl BODIPY fluorophores 54 and 55, whereas Table 4 outlines the scope of the direct C-H arylation presented in Scheme 7. Table 4 presents the various C-H arylations and their comparisons of traditional synthesis denoted superscript “a” to install different aryl rings, compared to the microwave irradiated protocols denoted with superscript “b.” As evidenced by selected examples for installing phenyl ring substituents at reaction times of 24 and 28 h in entries 1 and 9, the utility of microwave irradiation to accelerate the reaction is shown in entries 13 and 15. Another example is shown in the installation of 3-thienyl, which improved the reaction time from 27 h to 3 hrs in entries 4 and 14, respectively.

 doi:10.20944/preprints202511.1766.v1



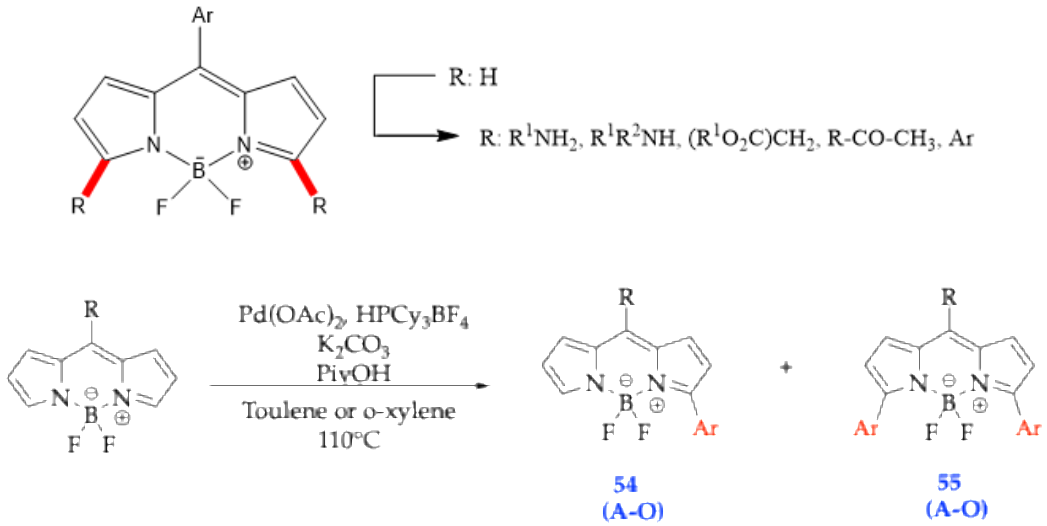


**Scheme 7.** Scheme of C-H arylation of *meso*-substituted BODIPY with different bromoarenes [53].

**Table 4.** Comparison of reaction times and yields across varying aryl rings [53]. a) Denotes reaction conducted under traditional conventional synthesis; b) Denotes reaction conducted in microwave-assisted synthesis.

| Entry | Compound | Ar | Reaction Time | Yield (%) of 54 | Yield (%) of 55 |
|---|---|---|---|---|---|
| **1** | A | Phenyl [a] | 24 h | 44 | 17 |
| **2** | B | 4-Anisyl | 43 h | 42 | 10 |
| **3** | C | 4-(Dimethylamino)-phenyl | 48 h | --- | --- |
| **4** | D | 3-Thienyl [a] | 27 h | 55 | 10 |
| **5** | E | Mesityl | 43 h | 35 | 0 |
| **6** | F | 1-Naphthyl | 24 h | 20 | 16 |
| **7** | G | 4-Cyanophenyl | 48 h | --- | --- |
| **8** | H | 3-Nitrophenyl | 48 h | --- | --- |
| **9** | I | Phenyl [a] | 28 h | 31 | 32 |
| **10** | J | Phenyl | 46 h | 28 | 18 |
| **11** | K | Phenyl | 4 days | 13 | 43 |
| **12** | L | Phenyl | 4 days | --- | 39 |
| **13** | M | Phenyl [b] | 3 h | 39 | 40 |
| **14** | N | 3-Thienyl [b] | 3 h | 26 | --- |
| **15** | O | Phenyl [b] | 3.5 h | 28 | 46 |

Synthesis of fluorogenic tryptophan (Trp) serves as a critical building block for the preparation of peptide-based fluorophores [54,55]. These peptide-based fluorophores are synthesized in single-step reactions that result in good yields. These reactions are coupled using meta iodophenyl-substituted BODIPY 57 and Fmoc-Trp-OH in the company of $Pd(OAc)_2$ by microwave irradiation, as shown in compound 58, as shown in Scheme 8. Subsequently, the Trp–BODIPY amino acid was combined with antimicrobial peptides to label the fungal pathogen *Aspergillus fumigatus* in *ex vivo* human tissue [56]. Notably, their activity and selectivity were not deterred by peptides, and this created several chances for the development of novel peptide-based imaging probes. Compound 58's interaction with the phospholipid bilayer membranes was studied concerning its co-culture with human lung epithelial cells, where it was established that the use of Tryptophan as a fluorogenic surrogate caused increased hydrogen bonding to peptides within the lipid bilayer, promoting the increased fluorescence intensity, as shown in Figure 16. The use of the Fmoc protection was due to mitigating degradation during the solid-phase peptide synthesis. [56].

 doi:10.20944/preprints202511.1766.v1



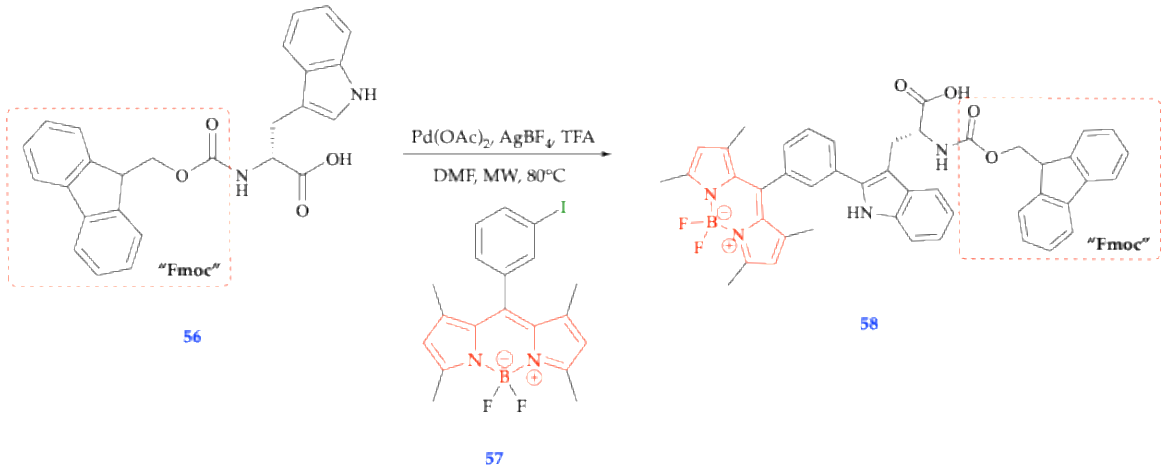


56 57 58

**Scheme 8.** Synthetic scheme of Trp-BODIPY fluorogenic amino acid 58 [56].

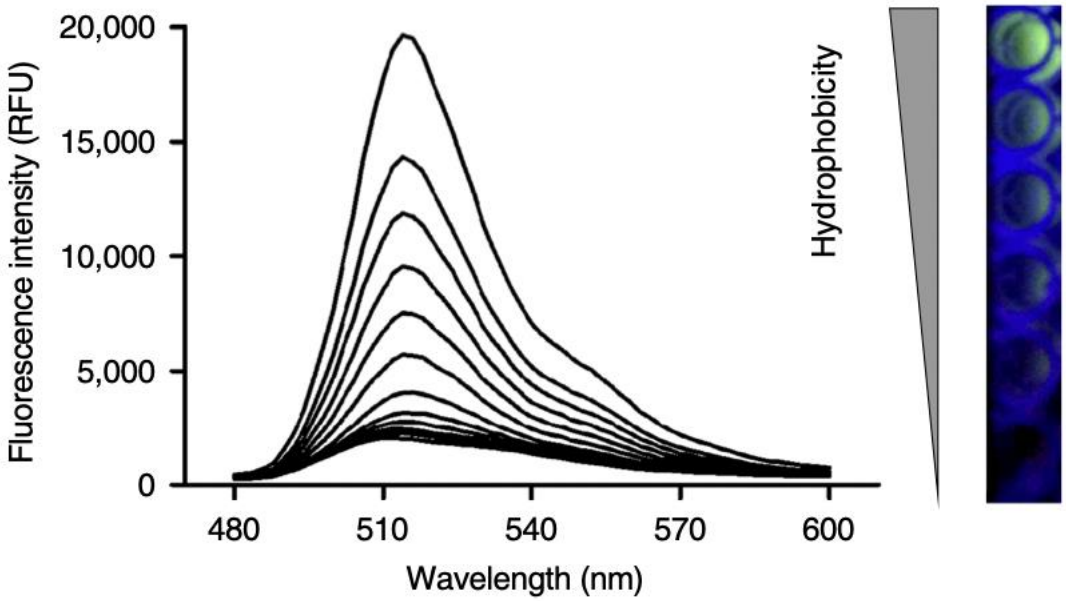


**Figure 16.** Spectral properties of compound 58 at 10 μM were obtained after incubation with phosphatidylcholine (PC) and cholesterol (7:1) liposome suspensions in PBS. This figure was reproduced with permission from Mendive-Tapia *et al*. (2016), copyright 2016 [56].

*6.2. Functionalized BODIPY Fluorophores for Multicomponent Reactions (MCRs)*

Multicomponent reactions (MCRs) are precursors colored to differentiate the multicomponent nature of the syntheses. MCRs are derived from their convergent character, modular features, and access to novel chemotypes, such as those. Based on FRET principles, to create water-soluble chitosan BODIPY derivatives that present good photostability, as successfully achieved by Zhu *et al*. (2018) [50]. Moliner de, Fabio, and colleagues explored the applicability of Ugi 4-CRs, which is a four-component reaction to functionalize fluorophores for optical imaging [57]. Biological analysis has acknowledged PhagoGreen, 59, as a pH-sensitive fluorophore for imaging phagocytic macrophages *in vivo* as well as green-fluorescent mesoionic BODIPY 60 conjugated to natamycin for live fungal cell imaging, shown in Figure 17. Antimycotic activation is seen through the mesoionic BODIPY compounds [57].

 doi:10.20944/preprints202511.1766.v1



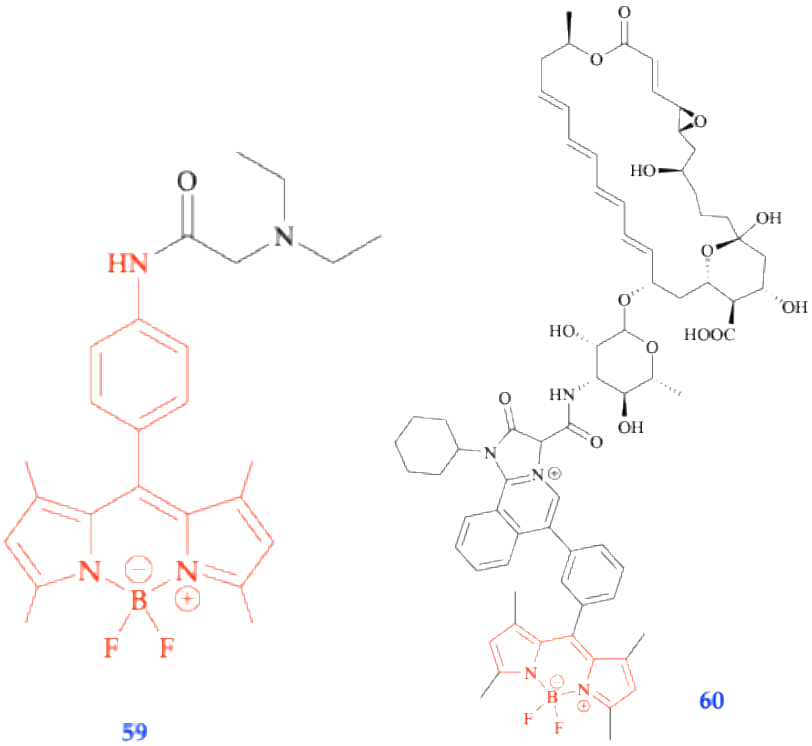


**Figure 17.** Functional fluorophore obtained by MCR, PhagoGreen as a pH-sensitive BODIPY fluorophore for *in vivo* imaging of phagocytic macrophages. Used without permission from de Moliner *et al*, 2017 [57]. MCR's synthetic approach has been used to isoquinoline-substituted BODIPY structures with labels of bioactive amines and fluorescent analogues. [52,57]. .

*6.3. Activatable Photosensitizer Design Considerations*

Activatable photosensitizers (aPS) are imaging probes for their nonspecific phototoxicity outside activation or target sites and serve as molecular activation, which differentiates between target cells from healthy cells. Photodynamic therapy (PDT) is a minimally invasive treatment that eliminates target cells in the presence of oxygen by irradiating a photosensitizer with light, producing highly reactive singlet oxygen [58]. Singlet oxygen then attacks cellular targets, which damage cells, resulting in the shutdown of vascular cells and activation of the immune response. When a molecule produces a chemical change in another molecule through a photochemical process, this is known as a photosensitizer. Photosensitizers are used in reactions involving polymer chemistry; examples are photo-polymerization, photo-crosslinking, and photo-degradation.

PDT has many advantages over traditional therapies. Some to mention are the noninvasive, very selective, capable of giving recurring doses without building resistance or going above total doses [58]. PDTs have small to no scarring, fast healing, an outpatient setting, and no associated side effects, unlike radiotherapy, where patients develop resistance to the dose limitations. Photosensitizers are not only for the therapeutic production of singlet oxygen. They are bright fluorophores and can emit in the NIR part of the spectrum, which is very useful for *in vivo* imaging. Another way to modulate activation is by using controllable quenching instead of making the photosensitizer singlet oxygen through solvents or pH. Correctly, quenching through photoinduced electron transfer (PET) can be used to control a PS. In pH-activated photosensitizers, they have been shown to successfully kill cells through attaching photoinduced electron transfer-based quenchers that have specific pKa; they are active in the protonated form, like iodinated BODIPY derivative, such as seen by the unprotonated amino fluorophore 61, and the protonated amino fluorophore 62, where fluorescence quenching occurs through the PET process, shown in Figure 18.

 doi:10.20944/preprints202511.1766.v1



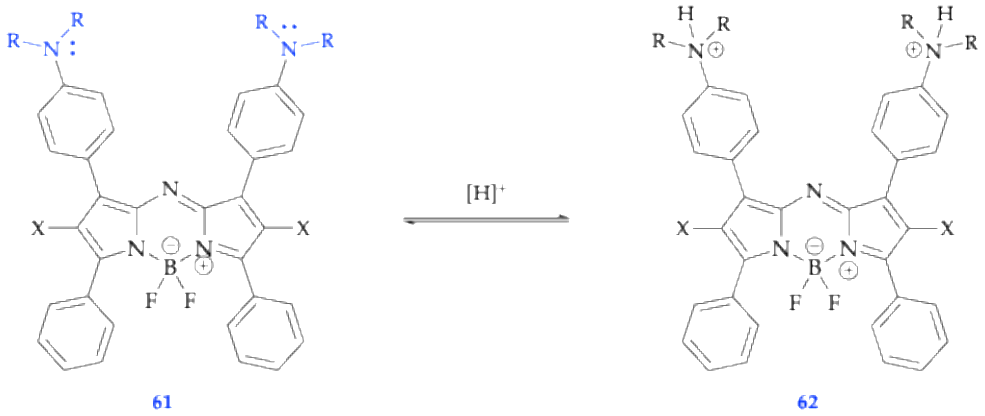


**Figure 18.** The pH-activatable photosensitizer based on electron transfer: compounds 61 and 62 [57, 58].

The next approach mentioned was developed using photoinduced electron transfer quenchers, which are activated in hydrophobic solvents that have low dielectric constants [59]. As shown in Figure 19, compound 63 is an iodinated BODIPY photosensitizer, serving dually as a photoinduced electron transfer (PET) quencher and as a protein-targeting ligand to navigate a desired photosensitizer to the Inositol 1,4,5-trisphosphate (IP3) receptors within the endoplasmic reticulum of eukaryotic cells to mediate the release of $Ca^{2+}$. The photoinduced electron transfer quencher turns out to be wasteful upon binding to the hydrophobic pockets of cellular proteins. To display this phenomenon, iodinated BODIPY photosensitizer (orange) was attached to a photoinduced electron transfer quencher (blue) whose quenching ability was contingent upon solvent hydrophobicity. This led to the inositol 1,4,5-triphosphate ligand (green) to be able to direct the photosensitizer to its protein target, where it was activated by binding in the hydrophobic pocket. This result is indicative of the fluorophore 63's ability to be able to be activated to specifically site-selectively damage the desired protein through singlet oxygen generation [59], revealing the inactivation mechanism of certain proteins within live cells.

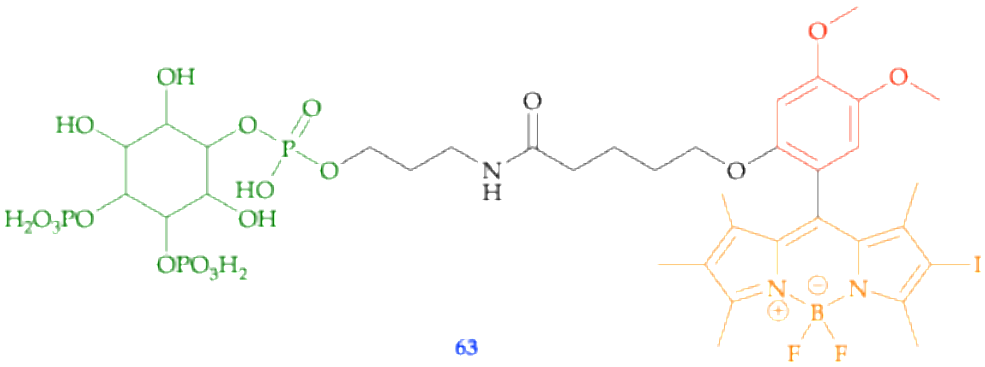


**Figure 19.** The hydrophobically activatable photosensitizer with protein targeting moiety for chromophore-assisted light inactivation 63 [59].

*6.4. Biocompatible Aza-BODIPY Biotin Conjugates and Nanoparticles for PDT*

Dutta *et al*. (2023) synthesized the first novel biotin-conjugated Aza-BODIPY dye to be used for PDT, incorporating a three-component framework comprised of 1) Aza-BODIPY, 2) PEG-3, and 3) Biotin alongside an iodinated BODIPY core to promote intersystem crossing [60,61]. When compared against DPR2a and DPR2b cell lines, the aza-biotin conjugate was found to exhibit significant photocytotoxicity when activated by light, even though they are neither cytotoxic nor toxic in the dark, as compared to Photofrin, the currently most widely used commercial photosensitizer [60, 62-63]. As shown in Scheme 9, using click chemistry, fluorophore derivatives 64 and 65 were joined to

 doi:10.20944/preprints202511.1766.v1



the azide containing AzBiotin unit through 1,3-dipolar cycloaddition to yield fluorophore derivatives 66 and 67. In total, 4 new biotin-based Aza-BODIPY fluorophores were developed and studied spectroscopically.

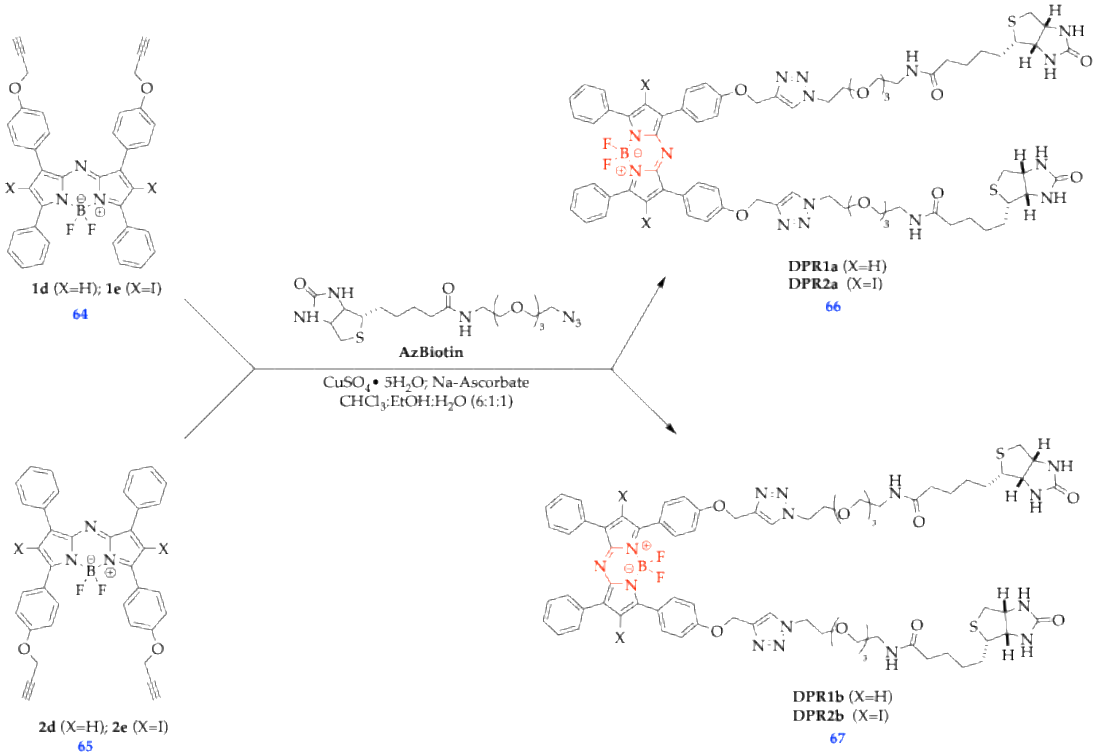


**Scheme 9.** Synthetic pathway developed to form novel fluorophores 66 and 67 with terminal alkyne and copper catalysis to click with AzBiotin conjugate [60].

As shown in Table 5, the fluorophore DPR1b, represented by fluorophore scaffold 67, exhibited the highest absorption and emission maxima, as well as the highest fluorescence quantum yield. However, a triplet quantum yield, or the proportion of singlet oxygen yield, could be used to quantify photodynamic activity. In comparison, the fluorophore DPR2b, also shown as fluorophore scaffold 67, exhibited the highest potential therapeutic capacity, boasting the highest triplet and singlet oxygen generation quantum yields.

**Table 5.** Tabulated optical properties (absorbance and fluorescence) for four new Aza-Biotin conjugate fluorophores [60].

| Sensitizer | $\lambda_{abs}$ nm ( ε, $M^{-1}$ $cm^{-1}$) | $\lambda_{em}$ nm | Fluorescence QY, $\Phi_f$ | Triplet QY $\Phi_T$ | Singlet Oxygen Generation QY $\Phi$ ($^1O_2$) |
|---|---|---|---|---|---|
| **DPR1a** [60] | 660 (106,500) | 698 | 0.200 | ND | ND |
| **DPR1b** [60] | 684 (80,000) | 721 | 0.300 | ND | ND |
| **DPR2a** [60] | 648 (67,000) | 703 | 0.027 | 0.75 | 0.72 |
| **DPR2b** [60] | 670 (63,500) | 706 | 0.065 | 0.79 | 0.75 |
| **Photofrin** [60] | 628 (3000) | 630 | 0.10 | 0.61 | 0.30 |
| **Aza-BODIPY 5a** [60] | 660 (83,000) | 706 | ------- | 0.68 | 0.65 |

*6.5. Development of NIR-II Aza-BODIPY Fluorophores*

Bian *et al*, 2023 developed pyrrolopyrrole aza-BODIPY-based NIR-II fluorophores with donor-acceptor-donor (D-A-D) structures by using tetraphenylethylene (TPE) derivatives as electron donors (D) and pyrrolopyrrole aza-BODIPY (PPAB) as electron acceptors (A). As shown in Scheme 10, the

 doi:10.20944/preprints202511.1766.v1



three phenyl groups in the TPE derivatives acted as molecular rotors to endow the fluorophores with aggregation-induced emission (AIE) [64,65,66], properties that could be retained when assembled into amphiphilic polymer nanoparticles (PTPE$_3$ NPs). PTPE$_3$ fluorophores displayed high brightness ($\epsilon_{max}$ Φf > 1000 nm ≈ 180.05 $M^{-1}$ $cm^{-1}$) after encapsulation with amphiphilic polymers and provided long fluorescence emission extending beyond 1300 nm. In Figure 20, it is shown how compound 70 was distributed along the entire circulatory system, with primary accumulation in the mesentery and liver, but Figure 20d, shows the nanoparticle-encapsulated fluorophore 20 with a half-life of 86.5 min, which is much longer than the reported half-life of FDA approved ICG, at 6.1 min, indicating high-spatial temporal resolution and prolonged systemic circulation time, establish a promising fluorophore for real-time vasculature monitoring of thrombosis formation, vessel occlusion, hemorrhage, and vasculature collapse *in vivo.* [64].

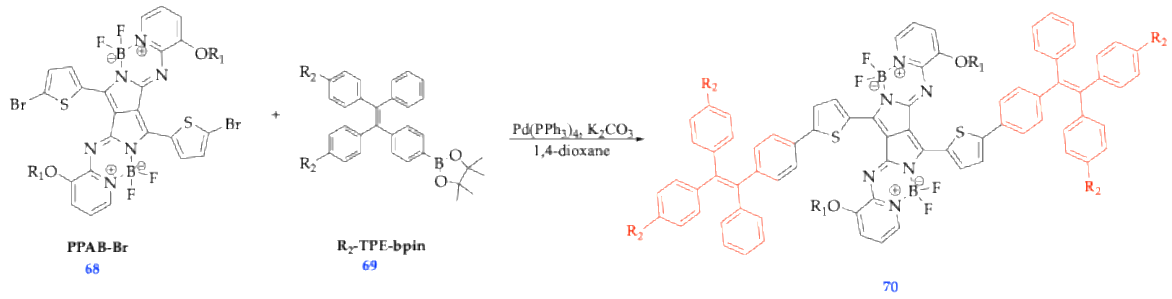


**Scheme 10.** Newly developed tetraphenylethylene (TPE) derivative scaffold that has erred into the NIR-II region (beyond 1200 nm) [64].

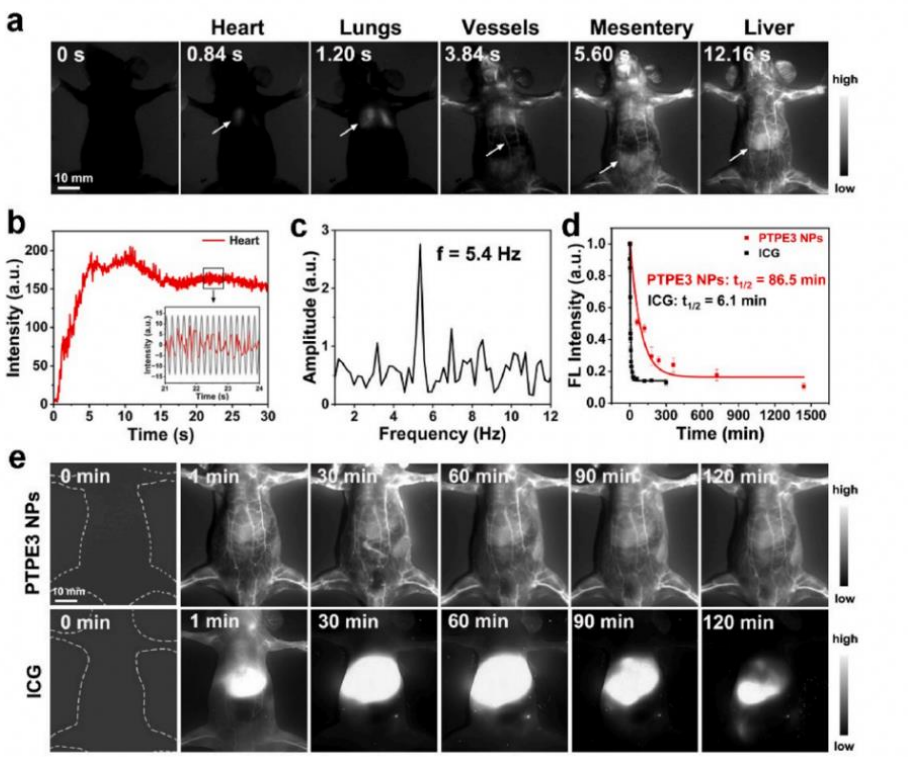


**Figure 20.** Still-shot images captured during real-life vasculature imaging of vasculature dysfunction processes. This figure was reproduced with permission from Bian *et al*. (2023), copyright 2023 [64].

*6.6. Self-Assembly of Polymeric BODIPY Micelles for Fluorescence Imaging*

To demonstrate the utility of BODIPY as potential NIR photosensitizers (PS) for photodynamic therapy (PDT), Liu *et.al* (2021) formed a neutral Ir (III) complex with a distyryl boron dipyrromethene

 doi:10.20944/preprints202511.1766.v1



(BODIPY-Ir), which was found to be effective in instigating the production of reactive oxygen species and onset of hyperthermia to potentiate *in vivo* tumor suppression. As depicted in Figure 21, through the micellization of BODIPY-IR to form "Micelle-Ir", BODIPY-Ir (compound 74), forms J-aggregates within Micelle-Ir, to boost both singlet oxygen generation and photothermal effect to induce severe cell apoptosis; this results in a disruption of the cell cycle and spontaneously generates programmed cell suicide, in which cell degradation is aided by lysosomes [67, 68]. When dye molecules aggregate in a parallel fashion with plane-to-plane stacking to form a sandwich-type arrangement, this is known as H aggregate and causes a blue shifted absorption- a hallmark example of dye quenching at high concentrations; conversely, when dye molecules orient in a head-to-toe arrangement (end-to-end stacking), a lower transition energy is exhibited compared to the free dye, resulting in a red shifted absorption. As shown in Scheme 11, compound 71 was subjected to Suzuki coupling with a benzo[*d*] imidazole moiety to obtain compound 72. Then compound 72 was subjected to methylation in the presence of tetrahydrofuran and excess iodomethane to obtain compound 73. Finally, compound 73 was heated to reflux under inert nitrogen atmosphere and treated with $Ag_2O$ and [Ir(benzo[*h*]quinoline)2($\mu$-Cl)]$_2$ to obtain the cyclometalated ligand-enable Aza-BODIPY fluorophore 74 [67]. As depicted in Figure 21, fluorophore 74 was then subjected to ultrasonication with poly(ethylene glycol)114-poly ($\varepsilon$-caprolactone)$_{60}$ (PEG-PCL) to form Micelle-Ir. Upon nanoencapsulation, it was found that Micelle-Ir exhibited both further amplified light-to-ROS and heat conversion, promoting both photothermal and photodynamic processes. Due to the addition of the Ir (III) complex, the Micelle-Ir displayed a 0.15 quantum yield and 29% photothermal conversion efficiency (PCE), promoted by the clathrin-mediated energy-dependent endocytosis with the lysosome that promoted negligible dark cytotoxicity [67].

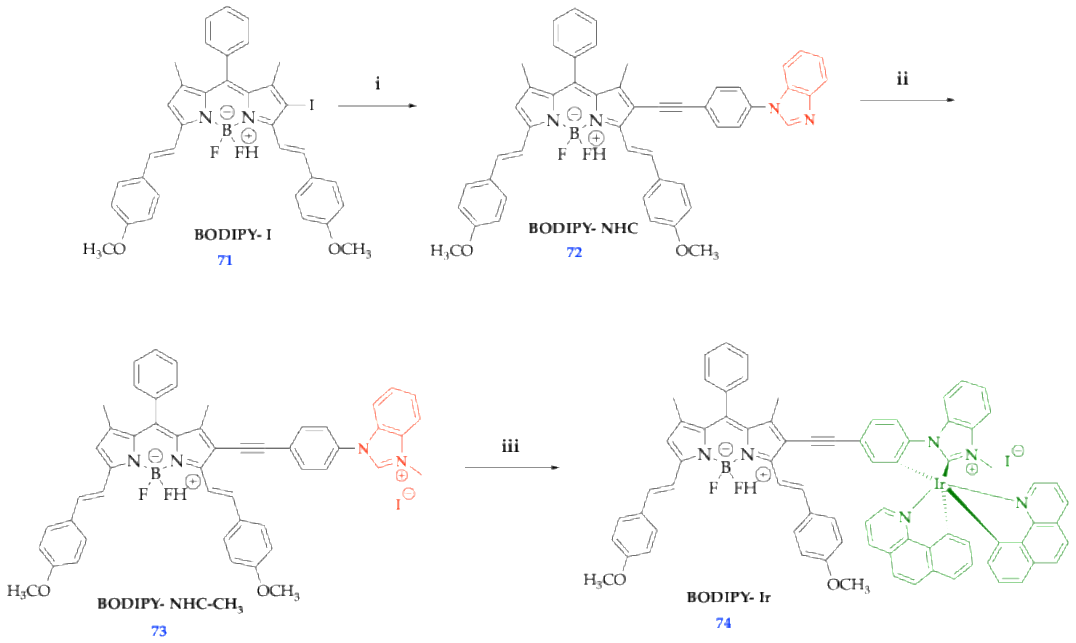


**Scheme 11.** Synthetic route for BODIPY-Ir, a BODIPY species used in forming J-type aggregates with self-assembling micelles to induce cellular apoptosis of tumor cells *via* reactive oxygen species (ROS) generation [67]. This figure was reproduced with permission from Liu *et al*. (2021), copyright 2021 [67].

 doi:10.20944/preprints202511.1766.v1



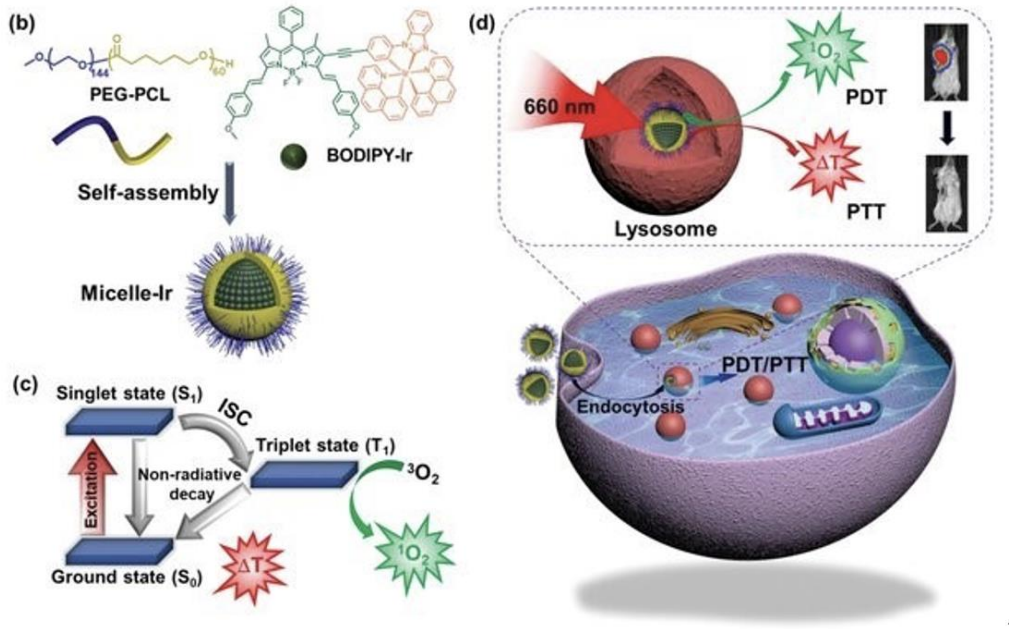


**Figure 21.** Left to Right: b) Visual depiction of encapsulation of BODIPY-Ir into micelles for constructing Micelle-Ir; c) Jablonski diagram depicting the photophysical processes leading to singlet oxygen ($^1O_2$) generation and photothermal effect (ΔT); d) Intracellular PDT/PTT effects. This figure was reproduced with permission from Liu *et al*. (2021), copyright 2021 [67].

*6.7. Advances in Cell Tracking and Cancer Detection Applications*

Advances in the development of photoactivable fluorophores have encompassed tracking cells through the visualization of labelled organelles with excellent localization precision [68, 69], especially in tumor detection. However, most synthetic dyes developed for subdiffraction visualization exist as cyanine and xanthene derivatives [70]. Thus, Zhang *et al* (2020) designed far-red photoactivable BODIPYs for the super-resolution imaging of live cells for photoactivated localization microscopy (PALM) [71]. In addition, asymmetric anthracene-fused BODIPY dyes synthesized by Yang *et al*. (2015) conferred a small energy gap (1.81 eV), large Stokes shift and high photostability, with extensive π conjugation attributed to red-shifted emission with a quantum yield of 40% and an enlarged Stokes shift of 1425 $cm^{-1}$ (53 nm) in $CHCl_3$ [23]. Moreover, cancer tumors are inherently hypoxic environments; thus, BODIPY-based probes leverage their relative insensitivity to pH to be applied to sense hypoxia *in vivo* and *in vitro* through fluorescence transformations and recognition mechanisms following interaction with targeted bio-reductive markers in hypoxic regions, as shown in Figures 22 and 23 [72]. In Figure 23, the installation of folate as a targeting moiety serves to advance the criteria outlined in Figure 22. In Normoxia (or normal $O_2$ levels), molecular oxygen can serve to quench triplet excited states of fluorophores, which decreases fluorescence. However, when less oxygen is present (hypoxia), the normoxia quenching pathway is suppressed, resulting in a greater proportion of the fluorophore excited state to undergo radiative relaxation, causing fluorescence to increase. With the specific conjugation to folate, folate receptors are overexpressed, and the folate-tagged fluorophore selectively internalizes in hypoxic tumor cells, allowing for accumulation of the dye where oxygen levels are low, improving bioimaging capabilities [72].

 doi:10.20944/preprints202511.1766.v1



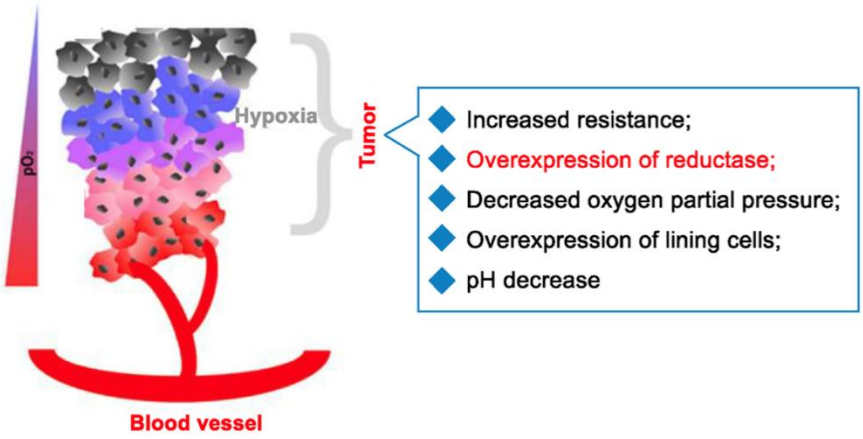


**Figure 22.** Characteristics of tumor hypoxia in which hypoxia typically accelerates bio-reductive reactions, causing the increased intracellular expression of reductases, which function as critical biomarkers for assessing the degree of tumor hypoxia. This figure was reproduced with permission from Gai *et al*. (2023), copyright 2023 [72]. .

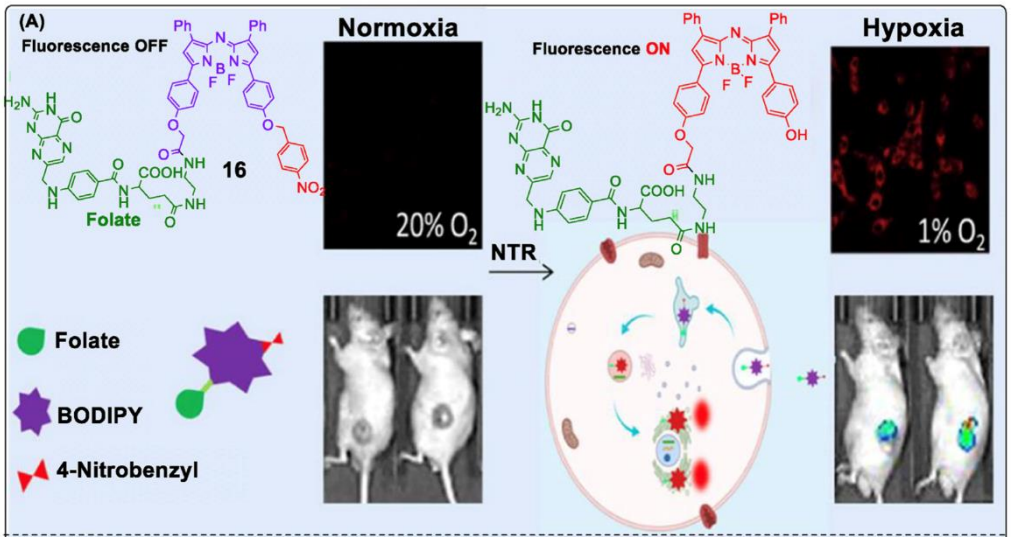


**Figure 23.** Example of BODIPY conjugation to folate as a means of creating a turn-on fluorophore. This figure was reproduced with permission from Gai *et al*. (2023), copyright 2023 [72]. .

In 2002, O'Shea and colleagues investigated where heavy-atom substituted fluorophores- Compounds 75 (PS1), 76 (PS2), and 77 (PS3), as shown in Figure 24- were synthesized to leverage heavy atom substitutions at the pyrrole ring rather than at the characteristic peripheral tetra (4) phenyl peripheral aryl rings as a means of improving fluorescence quantum yields. PS1 proved to be an exciting PS through Phase 1 clinical trials in tumor models- showed direct bromo substitution on the aza-BODIPY core results in efficient $^1O_2$ generation, whereas PS2 bearing a pH-responsive amine receptor proved to confer deleterious unwanted side effects as a non-selective PS due to accumulation in BOTH tumor and adjacent, healthy tissues [73].

Hlogyik *et.al* (2023) synthesized triazole-based Aza-BODIPY derivatives that were obtained *via* Cu(I)-catalyzed azide-alkyne cycloaddition (CuAAC) as the key step towards functionalization for *in vitro* photodynamic activity as photosensitizers. By leveraging the innate excellent photophysical properties conferred by the Aza-BODIPY scaffold, they sought exploit "click chemistry" to install (*N*-benzyltriazolyl) or azido (triethylene glycol) side chains to improve biological activity; thus, two novel derivatives (91 and 92) were synthesized and proved to be optically beneficial demonstrations

 doi:10.20944/preprints202511.1766.v1



of the well-established methodology of using copper (I) iodide (CuI) as a catalyst and triphenylphosphine ($PPh_3$) as an accelerating ligand, as shown in Scheme 12 [73].

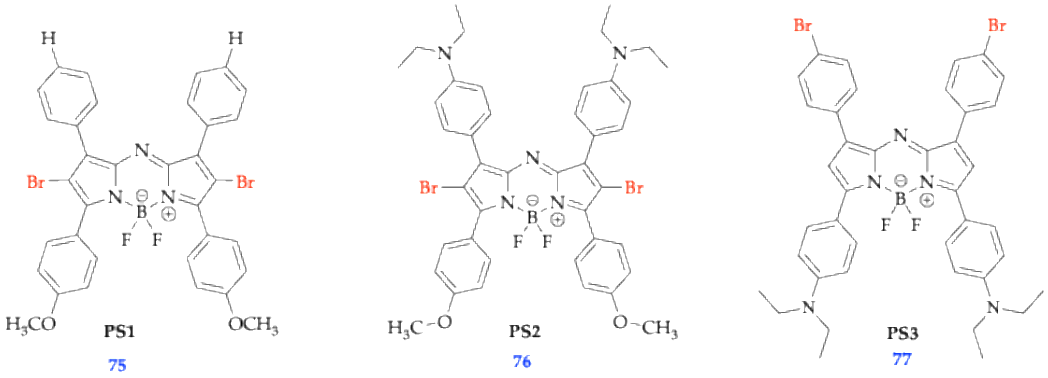


**Figure 24.** Structures of PS1, PS2, and PS3 synthesized as a rationale-based design to improve $^1O_2$ yields of photosensitizers through the introduction of bromine or iodine into the dye core [73].

Limitations of BODIPY dyes include a limited synthetic availability and scope, low fluorescence quantum yield, poor or little to no emission maxima, and optical instability in certain solvents, particularly aqueous media [73]. Through evaluation of the photophysical characterization, *in vitro* dark and light cytotoxicity studies, and evaluation of *in vitro* ROS generation of 91 and 92, their candidacy for being photosensitizers was evaluated [73]. However, Table 6 displays the photophysical properties of 91 and 92 in DMF, where all values are the same, except, 92 possessing a higher molar extinction coefficient.

**Table 6.** UV-Vis and fluorescence spectroscopic properties of compounds 87, 88, 91, and 92 with absorption and emission wavelength maximums, Stokes' Shift, and maximum molar absorptivity values displayed [73].

| **Compound** | **87** | **88** | **91** | **92** |
|---|---|---|---|---|
| Solvent | DMF | DMF | DMF | DMF |
| λabs [nm] **[73]** | 654 | 667 | 670 | 670 |
| λem [nm] **[73]** | 676 | 693 | 701 | 701 |
| Δ λ [nm] **[73]** | 22 | 26 | 31 | 31 |
| εmax [$M^{-1}$ $cm^{-1}$] **[73]** | 81,987 | 74,435 | 64,505 | 73,825 |
| (±) (SD) **[73]** | (± 7394) | (± 4023) | (± 5206) | (± 5586) |

Subsequent evaluation of *in vitro* dark- and light-induced toxicity of aza-BODIPY dye was conducted by subjecting fluorophores 87, 88, 91, and 92, as shown in Scheme 12, to the epidermoid carcinoma cell, A431. The two triazolyl aza-BODIPY derivatives, namely tetraphenyl compound 87 ($IC_{50}$: 0.96 μM) and its *bis*-triazolyl-TEG counterpart 91 ($IC_{50}$: 3.66 nM), resulted in efficient cell killing when irradiated, with the latter being 268-fold more active [73]. The introduction of the triazole moiety was added to increase anticancer potential and coupled with investigation of *in vitro* ROS generation, shown in Figure 25, the potential mechanism for light-induced toxicity is posited by the passive accumulation of molecular ROS indicator, 2′,7′-Dichlorofluorescin diacetate (DCFH-DA) within the cells. Upon illumination, DCF-DA is deacylated by cell esterases to form dichlorofluorescein (DCFH), and ROS, hydrogen peroxide, results in the formation of fluorescent product – 2′,7′-Dichlorofluorescin (DCF), as shown in Figure 25 [73, 74]. In conjunction with the reported phototoxicity levels of 87 and 91, a concomitant increase in ROS levels, was reported. However, the cells incubated with non-toxic 88 and 92, displayed a small increase in ROS levels compared to the cells illuminated in the absence of the dyes. Similarly, Figure 26 displays the advantage in improving the concentration-dependent light-induced toxicity through click chemistry to install triazole groups; compared to parent fluorophore 87, which possessed an $IC_{50}$ value of 0.96

 doi:10.20944/preprints202511.1766.v1



μM, the progeny fluorophore after CuACC, resulting in a nearly 262x increase in $IC_{50}$, with fluorophore 91 having an $IC_{50}$ value of 3.66 nM. As a result, compound 91, operating in the nanomolar range, serves as a promising candidate for the design of a new, selective, and heavy-atom-free scaffold for photosensitizers, as shown in Figure 25.

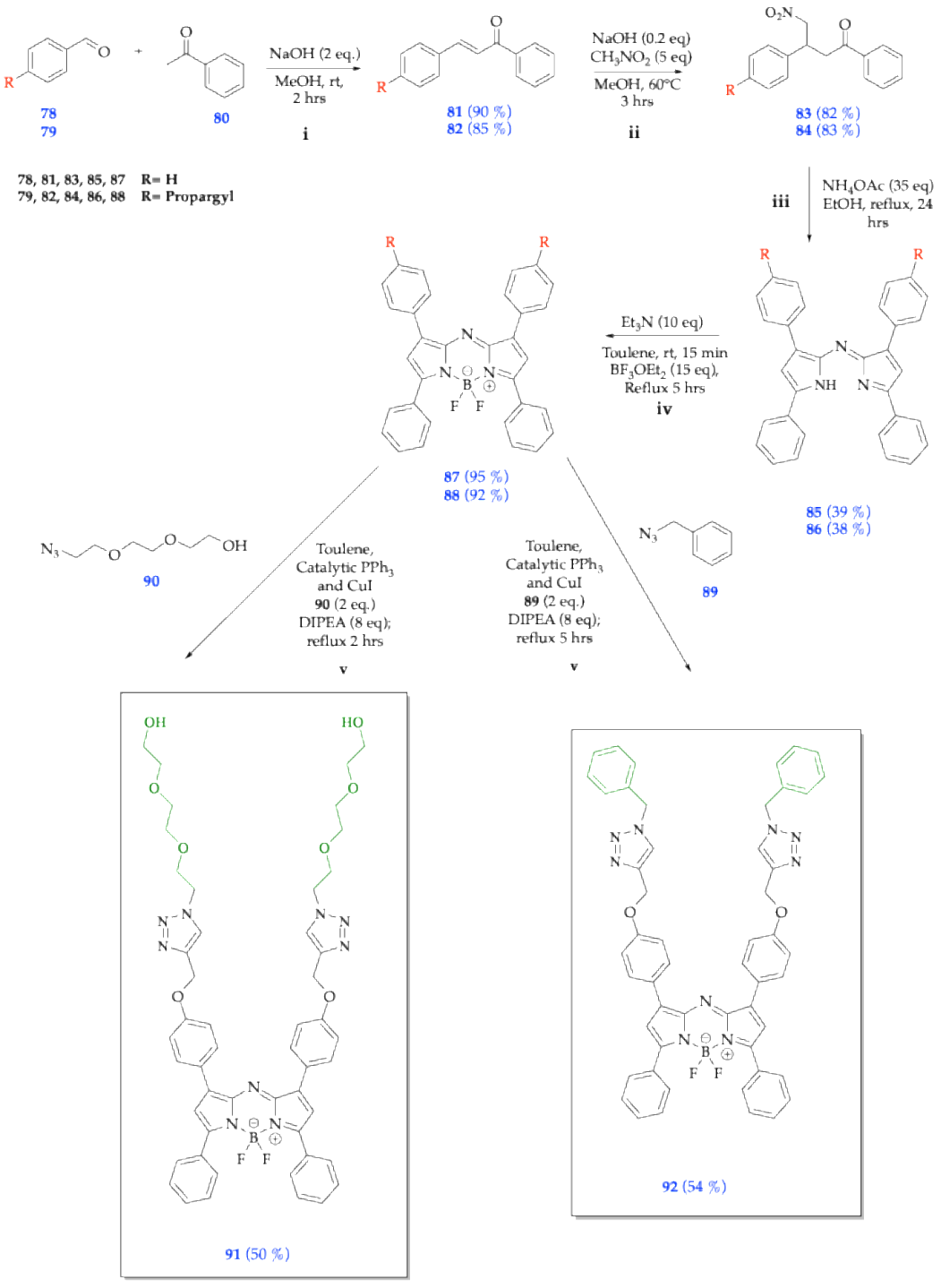


**Scheme 12.** Synthetic scheme for step-wise synthesis of triazole conjugated Aza-BODIPYs, resulting in fluorophores 91 and 92 [73].

 doi:10.20944/preprints202511.1766.v1



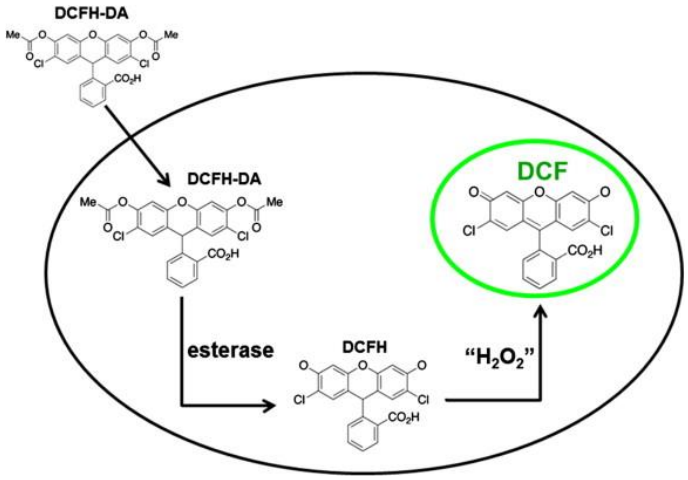


**Figure 25.** Mechanism of DCF-DA responding to oxidative stress analytes to form fluorescent 2′,7′-Dichlorofluorescin (DCF). This figure was reproduced with permission from Aranda *et al*. (2013), copyright 2013 [74].

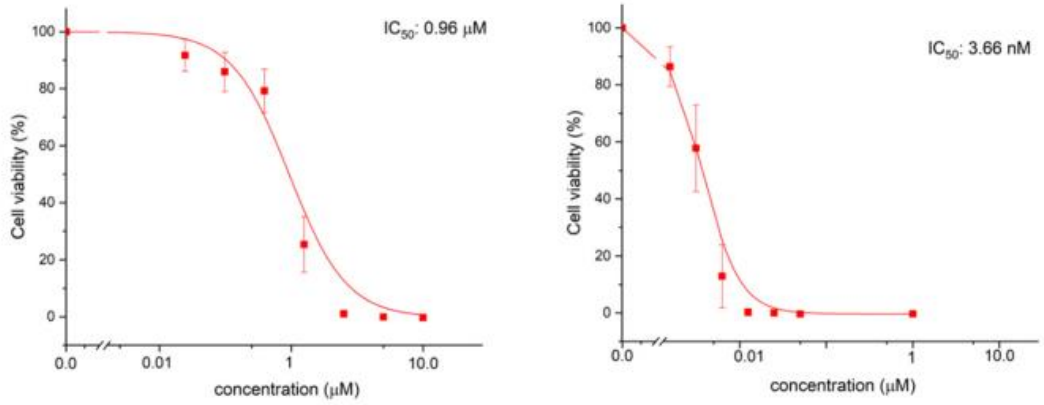


**Figure 26.** A) Left to Right: Concentration-dependent light-induced toxicity of compounds 87 and 91 with calculated $IC_{50}$ values shown. This figure was reproduced with permission from Hlogyik *et al*. (2023), copyright 2023 [73].

*6.8. Boron Functionalization: Forming Linker-Free NIR Aza-BODIPY Glutamine Conjugates*

Impinging on the advents of the introduction of heavy atoms at the 2 and 6 positions on the Aza-BODIPY core as a means of facilitating intersystem crossing and improving triplet state, Wang *et.al* (2020) deviated from the strategy of modifying the tetraphenyl core, and instead developed a one-pot reaction methodology for introducing amino acids onto the boron atom to produce linker-free BODIPY-glycine conjugates, as shown in Figure 26 [75]. L-glutamine is the most abundant naturally occurring amino acid in humans and plays an integral role *in vivo* as a nitrogen shuttle for circulating ammonia as well as for protein and glutathione synthesis, energy production, and is beneficial for minimizing infection in trauma and surgery patients [75].

Upon investigating optical spectroscopic and theoretical computational properties, compounds **93** and **94** exhibited increased cytotoxicity upon exposure to a low light dose of (≈ 1.5 J/cm$^2$), whereas the rest of the conjugate fluorophores did not show increased cytotoxicity in response to irradiation. Computational studies elucidated that the 2,6-dibrominated aza-BODIPYs **97, 99,** and **100** showed significantly higher comparative singlet oxygen quantum yields than the corresponding 2,6-unsubstituted aza-BODIPYs **93, 94,** and **96,** determined using 1,3-Diphenylisobenzofuran (DPBF) as an acceptor, as shown in Scheme 13 [75].

 doi:10.20944/preprints202511.1766.v1



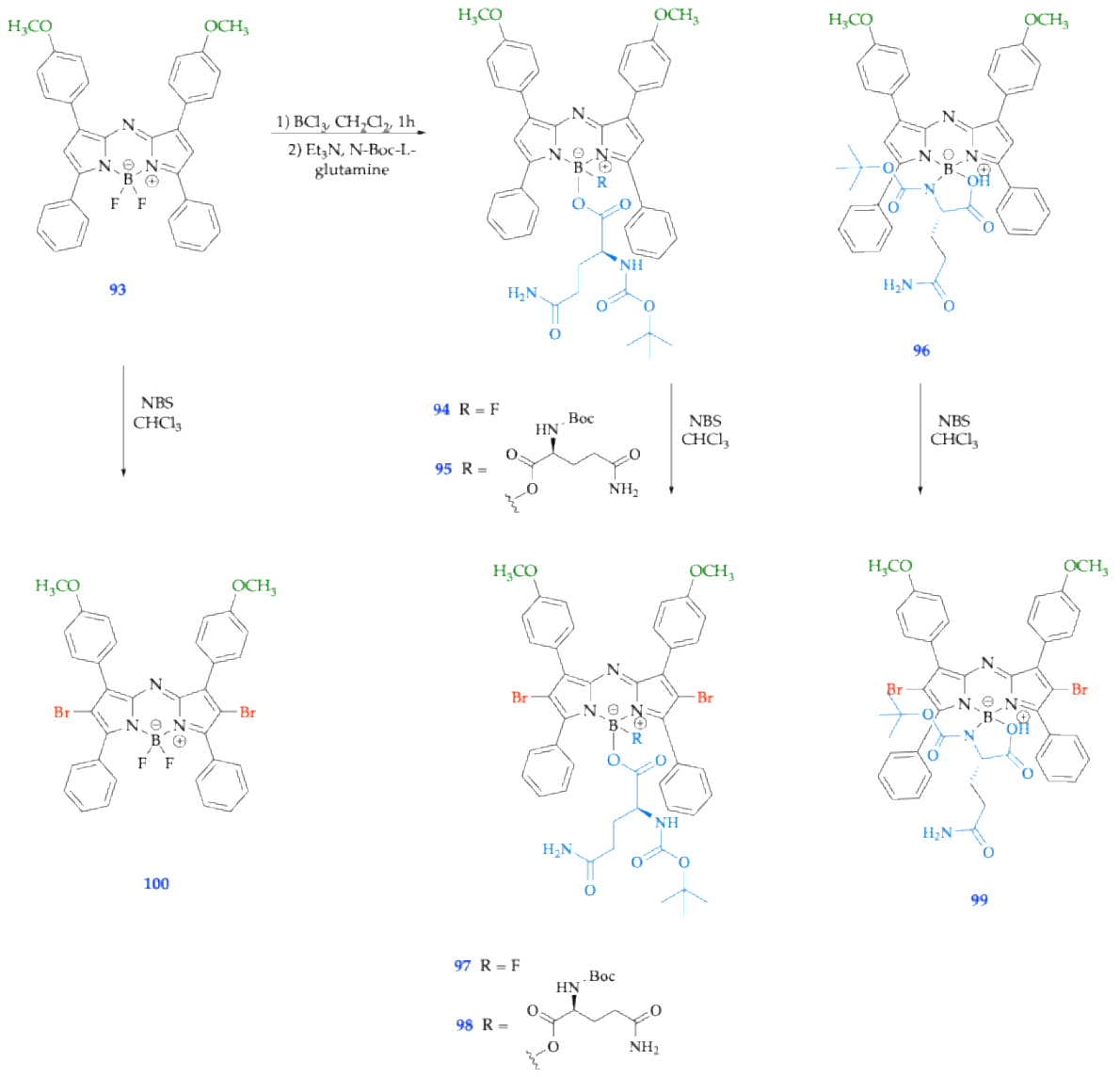


**Scheme 13.** Synthesis of Aza-BODIPY-Gln conjugates **94-99.** This scheme was redrawn but reproduced with permission from Wang *et al*. (2020), copyright 2020 [75].

As shown in Table 7, the results are also indicative that the cytotoxicity and the ability of aza-BODIPYs to produce singlet oxygen are not solely contingent upon the presence of bromine atoms at the 2,6-positions but also vary based on the number and substitution of the glutamine units attached to the boron atom. Notably, it is seen that the formation of a cyclic N, O-bidentate aza-BODIPY-Gln, as in compounds 96 and 99, induces the highest cytotoxicity, while substitution of the boron atom with two glutamine groups and the presence of 2,6-bromines leads to a significant decrease in singlet oxygen production [75]. As a result, Aza-BODIPYs with cyclic N, O- O-bidentate glutamine on boron displayed the highest cytotoxicity among all aza-BODIPY conjugates, making them promising bifunctional anticancer agents, while substitution of the boron atom with two glutamine groups and the presence of 2,6-bromines leads to a significant decrease in singlet oxygen production.

**Table 7.** Experimental and M06-2X/6-31 G(d,p) calculated spectroscopic properties of Aza-BODIPYs in $CHCl_3$ at room temperature [75].

| Compound | λabs [nm] Exp | λem [nm] Calc | Band Gap (eV) | ε [$M^{-1}$ $cm^{-1}$] | Oscillator Strength | λem [nm] | Φf [a] | Stoke's Shift [nm] |
|---|---|---|---|---|---|---|---|---|

 doi:10.20944/preprints202511.1766.v1



| | | | | | | | | |
|---|---|---|---|---|---|---|---|---|
| **93** [75] | 664 | 594 | 3.70 | 78,000 | 0.90 | 691 | 0.23 | 27 |
| **94** [75] | 664 | 612 | 3.64 | 53,300 | 0.79 | 697 | 0.32 | 33 |
| **96** [75] | 642 | 572 | 3.84 | 33,800 | 0.74 | 696 | 0.13 | 54 |
| **95** [75] | 667 | 593 | 3.72 | 47,300 | 0.74 | 703 | 0.23 | 36 |
| **100** [75] | 653 | 576 | 3.83 | 72,800 | 0.91 | 692 | < 0.01 | 39 |
| **97** [75] | 654 | 580 | 3.82 | 41,100 | 0.79 | 693 | < 0.01 | 39 |
| **99** [75] | 644 | 569 | 3.88 | 36,100 | 0.80 | 696 | < 0.01 | 52 |
| **98** [75] | 648 | 584 | 3.81 | 53,200 | 0.74 | 699 | < 0.01 | 51 |

## 7. Biosensing, Chemosensing, and pH Sensing Applications

As well as activation from environmental effects, enzymes, and nucleic acids and different prominent, widespread approaches are used to produce a PS. Photosensitizer-activation mechanisms include electrostatic assembly and bond formation that cleave, self-quenching, and numerous checkpoint-controlled activations that have been mentioned before. Control points in different locations are another approach to photosensitizer activation, successfully functioning as a photosensitizer activation logic controller [76, 77]. Luangphai *et al.* (2024) developed three aza-BODIPYs 101 (DA-Zn), 102 (DM-Zn), and 103 (DP-Zn), as shown in Figure 27, bearing dimethylaniline substituents that had $Zn^{2+}$ recognition ability and, upon binding to $Zn^{2+}$, exhibited the propensity for the fluorophore to be leveraged as a custom-built colorimeter for the detection of various environmental pollutants. For all three compounds, before the addition of $Zn^{2+}$, two strong absorption bands are observed at ~ 624 nm and ~ 760 nm, corresponding to the blue color appearance of them. These bands were attributed to the $S_0$–$S_1$ transition and therefore exhibited high intensity, while the significantly weaker band located at ~430 nm is attributed to the $S_0$–$S_2$ transition, as shown in Figure 28 [77, 78]. The multiple bands implied the presence of multiple closely lying electronic states led to these strong charge transfer (CT) transitions. CT involves the movement of an electron from a donor region (electron-rich area) to an acceptor region (electron-deficient area) [77, 78].

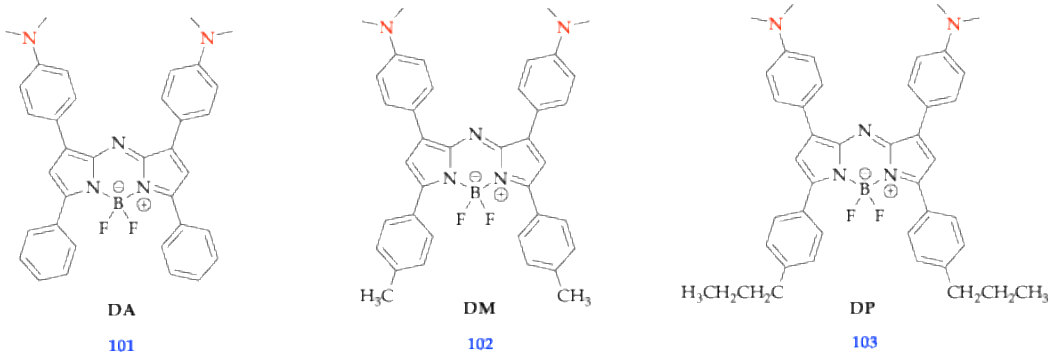


**Figure 27.** Synthetic route for aza-BODIPYs **101** DA (R=H), **102** DM (R=CH3), and **103** DP (R=$CH_2CH_2CH_3$) [77].

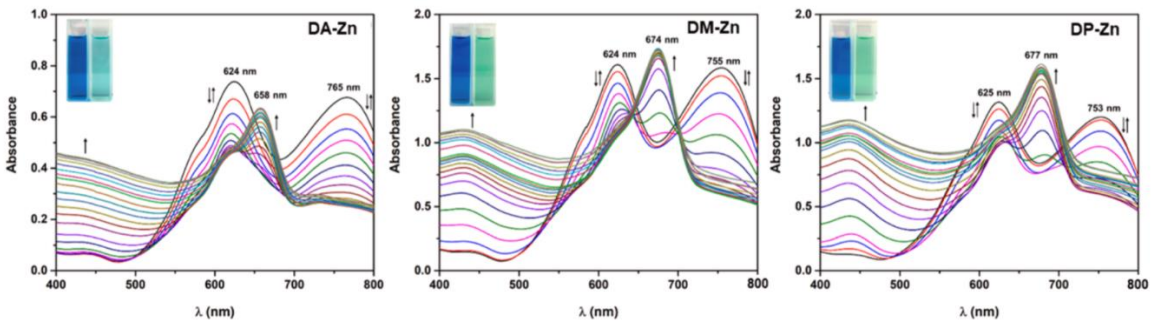

 doi:10.20944/preprints202511.1766.v1



**Figure 28.** UV–vis spectra of compounds 101 (DA), 102 (DM), and 103 (DP) (0.026 mM) titrated with $Zn^{2+}$at various equimolar ratios. The inset shows the color changes of the initial aza-BODIPY solution (blue) and the final color of the aza-BODIPY-Zn mixture (light emerald-green) [77]. This figure was reproduced with permission from Luangphai *et al*. (2024), copyright 2024 [77].

*7.1. Metal-Sensing, pH Sensing, and Detection of Reactive Oxygen Species (ROS)*

For instance, thienyl- containing aza-BODIPY dyes have been successfully synthesized use sensors for heavy metal detection of mercury, as shown in Figure 29, by utilizing the innate electronic configuration and lack of ligand field stabilization conferred by $Hg^{2+}$ to leverage it as a soft acid to accommodate a host of coordination numbers and geometries [79]. Mercury pollution is prominent in contaminated water, and its toxicity stems from the high affinity of thiol groups in proteins and enzymes. Industrial sources of mercury are attributed to coal mining, gold mining, solid waste incineration, fossil fuel consumption, and chemical manufacturing, resulting in the release of inorganic mercury Hg (0) and Hg (II) into the environment. Mercury poisoning has been connected to severe sensory, motor, and cognitive disorders [79].

Thus, the detection of mercury ions was of interest using aza-BODIPY dyes. The novel synthesis of this aza-BODIPY dye was obtained by utilizing the starting material of 2-vinylthiophene to obtain 3-(thiophene-2-yl)-2H-azirine required in the synthesis of a pyrrole. As displayed in Scheme 14, once the pyrrole was obtained, it was treated under HOAc, $Ac_2O$, and $NaNO_2$, followed by the traditional BODIPY synthesis using the complex of $BF_3$•$EtO_2$-$Et_3N$ to yield fluorophore 112 [79]. The thienyl-containing aza-BODIPY dye demonstrated optical properties of absorbance ($\lambda_{abs}$ = 760 nm) and emission ($\lambda_{em}$ = 782 nm) in the NIR region, and with high extinction coefficients of (136,000 $M^{-1}$ $cm^{-1}$) in fluorescence.[11] However, under physiological conditions of 10 μM of HEPE buffer at pH 7.3, the aza-BODIPY dye was found to be turned off with the binding of mercury ions. This observation is due to electron-withdrawing groups, which are part of the fluorophore π-system and involved in cation binding; the charge separation in the excited state is more stabilized than in the ground state, which results in the reduction of the $S_0$-$S_1$ gap. As a result, fluorescence quenching of the electrons from the electron-rich thienyl group to the BODIPY core is transferred after binding with the mercury ions, known as an intramolecular charge transfer (ICT). Thus, this water-soluble aza-BODIPY dye was tested in the presence of other metal ions such as $Na^+$, $K^+$, $Mg^{2+}$, $Ag^{2+}$, $Co^{2+}$, and others to see the effects on fluorescence intensity, which resulted in no significant difference in energy. Compared with compound 111, which binds to mercury and exhibits two analyte absorption bands upon binding to the heavy metal, compound 112 is a turn-off chemo sensor which results in a reduced fluorescence signal upon binding, as shown in Figure 29.

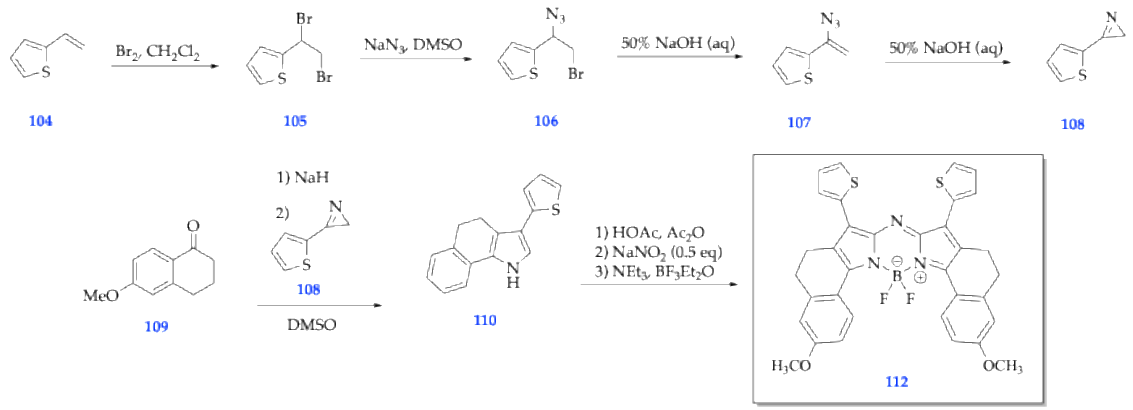


**Scheme 14.** Synthetic development of NIR fluorescent aza-BODIPY 112, which was found to be a turn-off fluorescent chemosensor [79]. .

 doi:10.20944/preprints202511.1766.v1



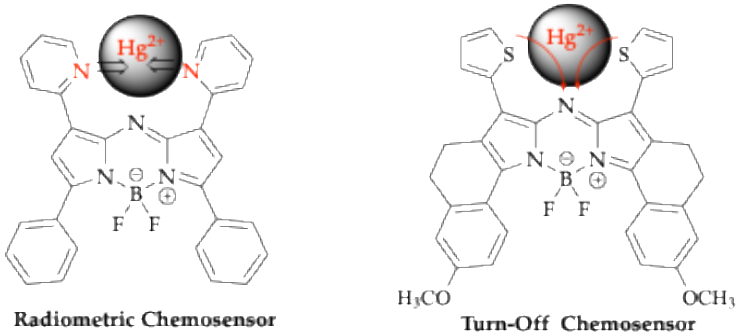


**Figure 29.** The electron-rich thienyl groups attached to the BODIPY core in compound 111 cause fluorescent quenching because the binding to $Hg^{2+}$ results in an intramolecular charge transfer (ICT) process [79]. .

Among the myriad biomedical applications of Aza-BODIPY dyes, they are widely employed as biosensors for the detection of hydrogen sulfide ($H_2S$), nitric oxide (NO), and even in pH sensing, specifically in mitochondria targeting, [80]. Adarsh *et al*. (2014) successfully reacted hydrogen sulfide with three new aza-BODIPY derivatives containing azido ($N_3$), amino ($NH_2$), and dimethylamino ($NMe_2$) groups to detect hydrogen sulfide *via* color change. Researchers elucidated the detection of $H_2S$ *via* color change when the aza-BODIPY probe containing the azido ($N_3$) group, changed color from bright blue to purple at a sensitivity threshold of 0.5 ppm of $H_2S$, as shown in Figure 30a. This color change was discovered to have been caused by the reduction of the azido group substituent on the Aza-BODIPY probe to an amino group *via* nitric oxide. Similarly, the colorimetric change is marked by the appearance of an isosbestic point at 740 nm in the absorption spectrum and the decrease in fluorescence emission intensity, respectively, as displayed in Figure 30b [81]. In addition, Merkushev *et al.*(2022) discovered that the primary reason for the solvatochromic effect surpassing the expected value of 5-8 nm for classic BODIPY dyes, and presenting as 15-20 nm, was due to solvent-induced stabilization due to the van der Waals interactions, the formation of hydrogen bonds, and/or th zation of the excited states of a solute by the solvent [82].

**(a)**

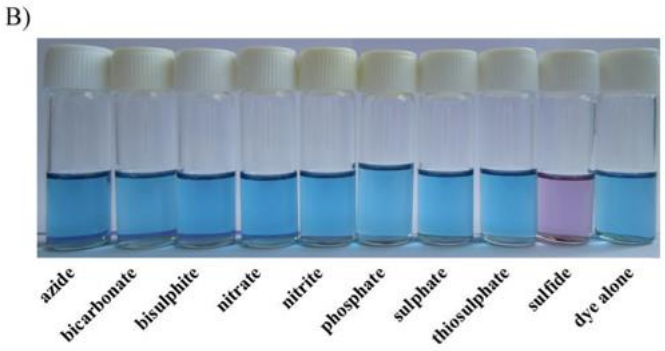


**(b)**

 doi:10.20944/preprints202511.1766.v1



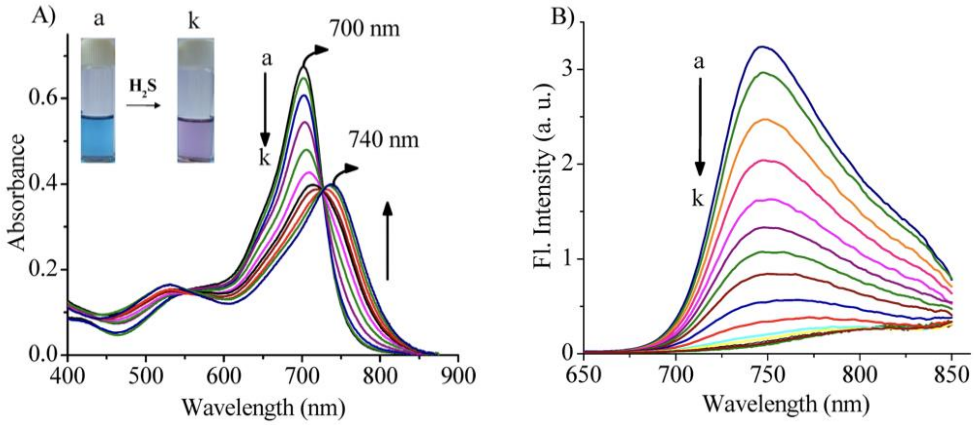


**Figure 30.** Left: a) Colorimetric response of the azido-containing probe towards various analytes; Right: b) changes in absorption and emission spectrum of azido-containing probe. These figures were reproduced with permission from Adarsh *et al*. (2014) copyright 2014 [81].

With regards to pH-sensing capabilities, Henary *et al.* (2014) devised hydroxylated NIR-BODIPY fluorophores and discovered that the pKa of the aza-BODIPY derivatives can be tuned from 9.10 to 10.85 by changing the position of the hydroxyl groups, as displayed in Figure 31, and exhibited a bathochromic shift of the absorbance maximum wavelength upon deprotonation of the hydroxyl substituent [83]. However, fluorophore 113 was discovered to be a lead compound for further optimization of developing pH-sensitive fluorophores. Through pKa analysis of plotting the first derivative with respect to change in *fluorescence intensity* and subsequ ıge in pH, an inflection point was computed, as shown in Figure 32a. The significance of this ınflection point indicates that at a pH of 10.1, there was no observed change in fluorescence intensity upon inducing a change in pH. As a result, it was logically surmised that this phenomenon must be due to the deprotonation of the phenol group, with the pKa value corresponding to 10.1 [83]. To validate this deductive premise, the pH titration was also performed with computing the change in *absorbance intensity* with respect to changing pH, where a similar pKa value of 10.6 was obtained, as displayed in Figure 32b [83].

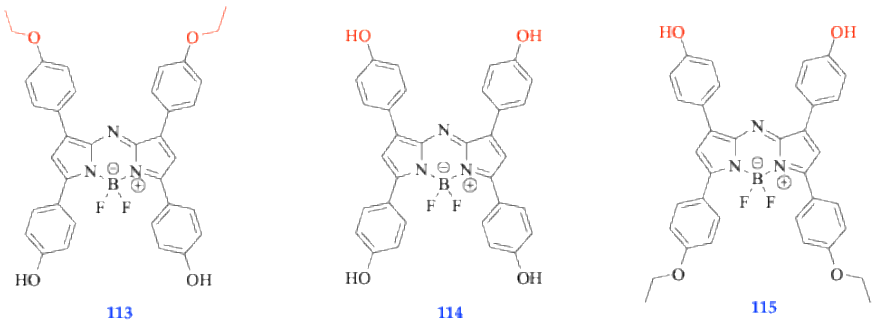


**Figure 31.** Hydroxylated Aza-BODIPY fluorophores 113, 114, and 115 [83].

 doi:10.20944/preprints202511.1766.v1



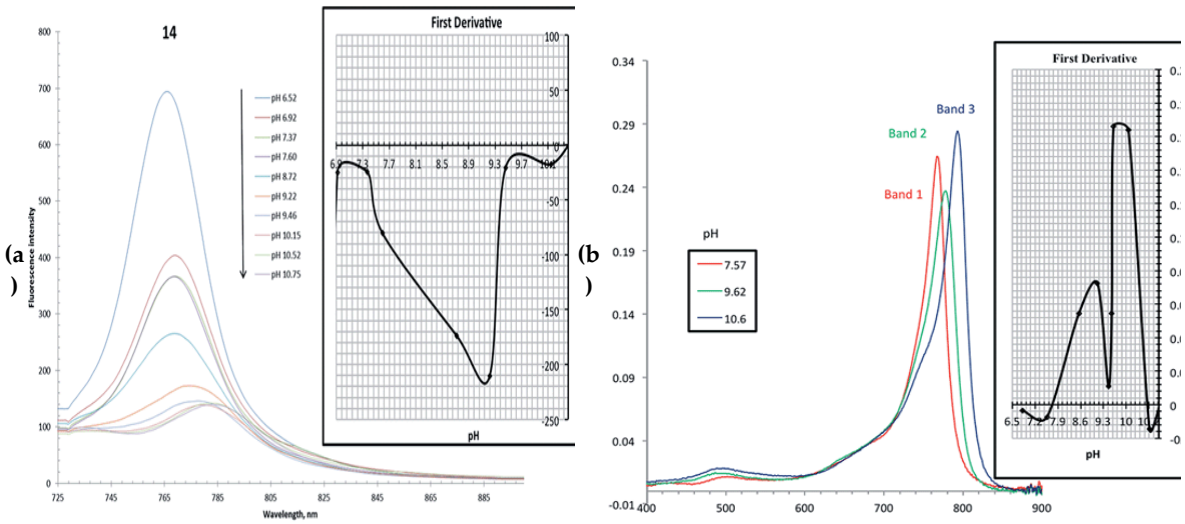


**Figure 32.** Left: a) pKa analysis of phenolic fluorophore **113 (**14**)** as exhibited by decreasing fluorescence intensity as pH increases and subsequent computation of pKa through the 1st derivative method to determine the inflection point to yield a determined pKa of 10.1 [83]. Right: b) Repeated pH titration of fluorophore **113** computed to yield 1st derivative of change of absorbance with respect to change in pH to yield pKa value of 10.6. Th**ese** figures were reproduced with permission from Henary *et al*. (2014) copyright 2014 [83].

Finally, to determine the true pKa of fluorophore **113**, a radiometric profile was computed by overlaying the increase in absorbance at 796 nm and the decrease of fluorescence emission at 765 nm, leading to an intersection at pH 9.20, which was deemed the true pKa of the compound as shown in Figure 33.

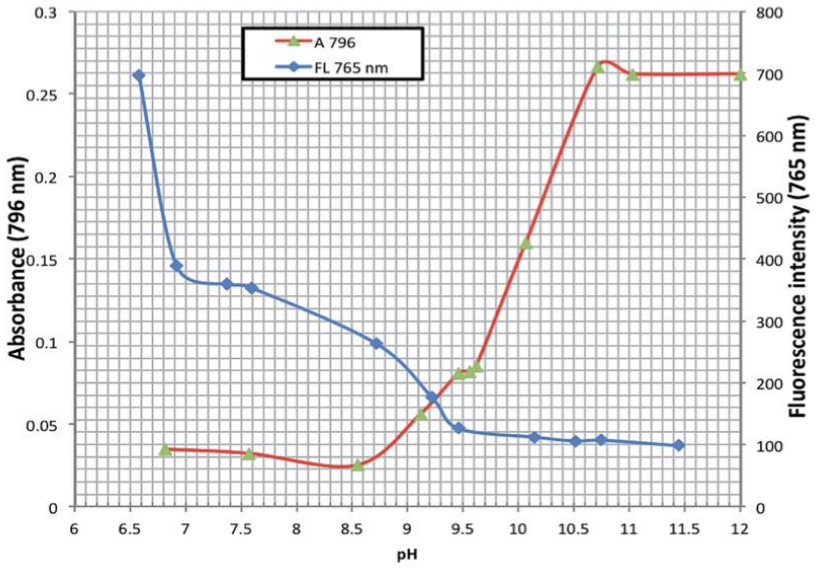


**Figure 33.** Radiometric pH profile of fluorophore **113**. Th**is** figure w**as** reproduced with permission from Henary *et al*. (2014) copyright 2014 [83].

In continuation, pH-sensitive probes with hydroxyl groups in the meta-position of a phenyl substituents can be used for facilitating "on-off" fluorescence responses by eliminating the conjugation to the chromophore [59, 84]; Liu *et al.* (2015) developed an application of the Boronic Acid Functionalized Aza-Bodipy (aza-BDPBA) dye for developing a glucose assay to be responsive for hydrogen peroxide [85]. ROSs are the major source of oxidative stress in cells, alongside RNSs

 doi:10.20944/preprints202511.1766.v1



(reactive nitrogen species). Both are highly reactive, but RNSs tend to be less damaging to cellular components than ROSs [86, 87, 88]. Advancements in using BODIPY for tracking mitochondria have entailed conjugating cations to the molecules, with cationic triphenylphosphine ($TPP^+$) and pyridinium used commonly because $TPP^+$ enhances lipid solubility. When attached with $TPP^+$ and ethylene glycol, it enhanced photothermal and photoacoustic effects to target mitochondria more precisely and efficiently. Also, $TPP^+$ exhibited high stability and low cytotoxicity [86, 87, 88].

Notably, Zhang *et.al* (2025) devised a portable sensing platform using a novel dipyrrolopyrazinedione-based Aza-BODIPY dimer (PzDP-PPAB, compound **117)** to be highly efficient at detecting hypochlorite ($ClO^-$) and hydrazine ($N_2H_4$). Due to limitations in current fluorescence detection of these 2 analytes, current methods exhibit slower and minor spectral changes, require high detection limits, and confer poor selectivity. As a result, the newly developed pyrrolopyrrole *aza*-BODIPY (DPP-PPAB) control compound **116** was synthesized from heteroaromatic amines and diketopyrrolopyrrole (DPP) to form a precursor intermediate compound, PzDP, which is not displayed. Then, through an imination reaction of electron-deficient PzDP precursor, activated by $TiCl_4$ with heteroaromatic amine for the first time, as shown in Figure 34, an additional 1,4 pyrazine ring is added to yield fluorophore **117**, as shown in Figure 34 [89]. When comparing the spectral response of PzDP-PPAB, compound **117,** and DPP-PPAB, compound **116,** to $N_2H_4$ and $ClO^-$, as shown in Figure 35. PzDP-PPAB **117** was exhibited to have the potential to be utilized as an efficient fluorescent probe for simultaneous detection of $N_2H_4$ and $ClO^-$ with distinguishable color change and a remarkable fluorescence "ON" behavior by introducing electron electron-deficient 1,4-pyrazine ring enhanced chromophore reaction strategy. In the case of $N_2H_4$, the slow decay of shoulder absorption at 588/628 nm in the NIR region and the appearance of a new band at 378 nm were shown with the increase of reaction time. The spectra remained invariant after 30 min [89]. On the contrary, the presence of $ClO^-$ induced the shoulder absorption band decay quickly, and the new band at 351 nm gradually strengthened [89].

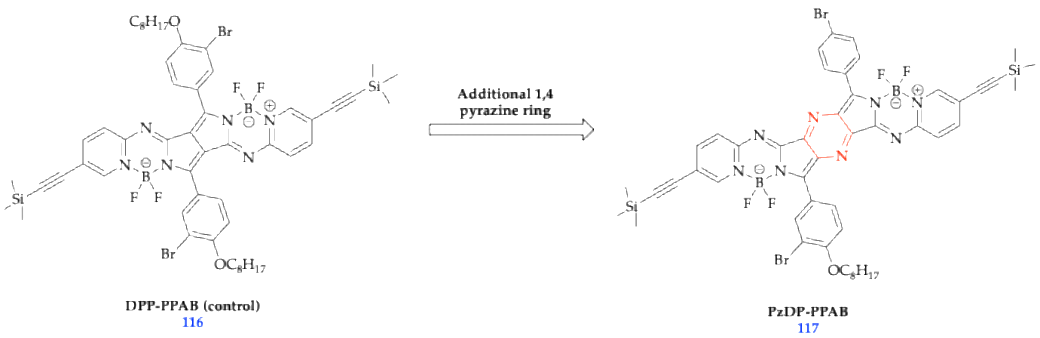


**Figure 34.** Compounds **116** (control) and compound **117,** which displayed $NH_2NH_2$ and $ClO^-$ induced distinct chromophore reaction to break the fluorophore upon binding to $N_2H_4$ and $ClO^-$ [89].

Similar efforts to advance environmental detection of $Fe^{3+}$ were conducted by Azizi-Khereshi *et.al* (2025), where colorimetric olive oil (OL)-Ag nanoparticles exhibited excellent selectivity for $Fe^{3+}$, displaying a low detection limit (LOD) of 0.81 μM and limit of quantification (LOQ) of 2.7 μM [90]. Ahmed and Henary (2025) also advanced the inception of metal sensing among dimeric fluorophores through the dimerization of heptamethine monomeric dyes to detect $Cu^{2+}$, where it was reported that a survey of eight dimeric heptamethine fluorophores did not exhibit any spectral changes in response to $Ag^+$, $Li^+$, $Na^+$, $K^+$, $Cr^{3+}$, $Ni^{2+}$, $Co^{2+}$, $Zn^{2+}$, $Hg^{2+}$, and $Ca^{2+}$, but did towards $Cu^{2+}$, rendering the fluorophores selective for $Cu^{2+}$ detection. [91]

Alongside the advances in pH sensor development, researchers have sought to leverage new heterocycles to design probes that simultaneously exhibit detection modalities through pH-sensitive responses, while also displaying therapeutic modalities through the tuning of photoacoustic/fluorescence imaging properties and shifting into the NIR-II window. For instance, Yong *et.al* (2023) developed near-infrared bithiophene Aza-BODIPY probes, compounds **118** and **119**,

 doi:10.20944/preprints202511.1766.v1



which differ in the installation of the bithiophene moiety at the 2 and 3 position, respectively as shown in Figure 36. Compounds **118** and **119** exhibited the ability to produce singlet oxygen ($^1O_2$) at pH = 5, but this was significantly enhanced at pH = 7, while maintaining excellent photoacoustic properties, as shown in Figure 34a and 34b, with fluorophores **118** (denoted as B5) and **119** (denoted as B6) alone versus encapsulation with Pluronic F127 to develop nanoparticles [92]. Preliminary pH studies showed fluorophore **118** had better photodynamic performance at pH = 5, whereas the photodynamic performance of **119** was improved under acidic conditions [92].

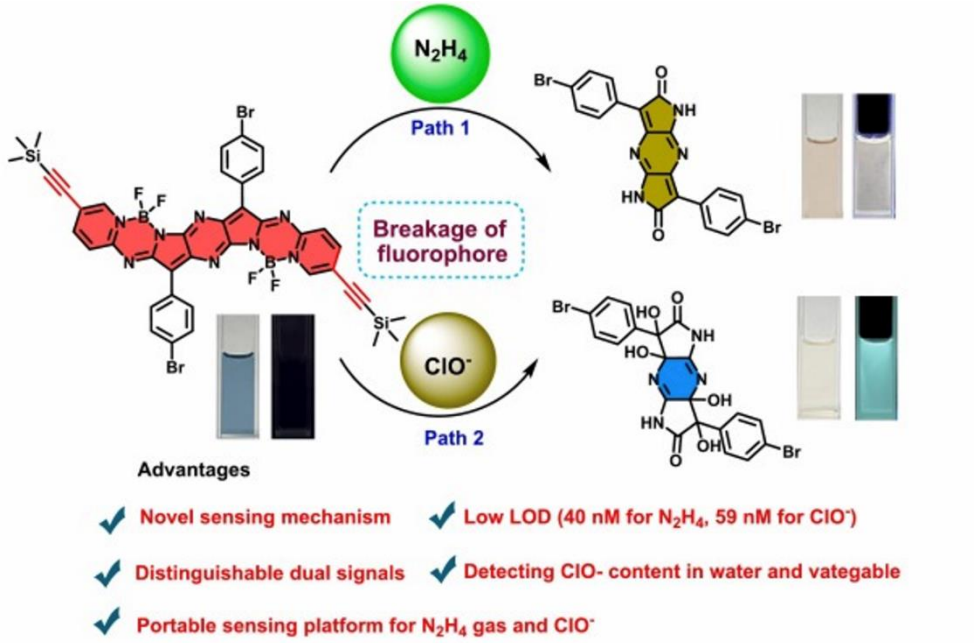


**Figure 35.** Depictions of colorimetric responses of DPP-PPAB **(116)** and PzDP-PPAB **(117)** and to $N_2H_4$ and $ClO^-$ [89]. Th**is** figure w**as** reproduced with permission from Zhang *et al*. (2025) copyright 2015 [89].

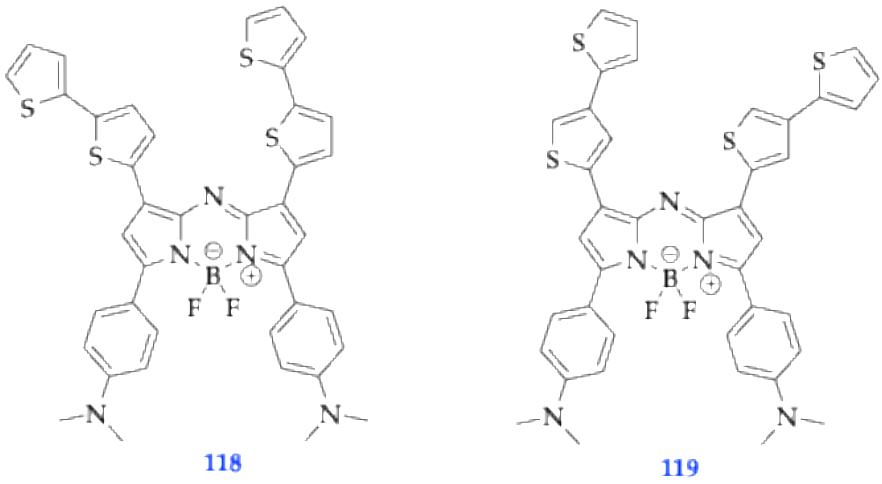


**Figure 36.** Bithiophene fluorophores **118** and **119** synthesized through O'Shea's route [92].

 doi:10.20944/preprints202511.1766.v1



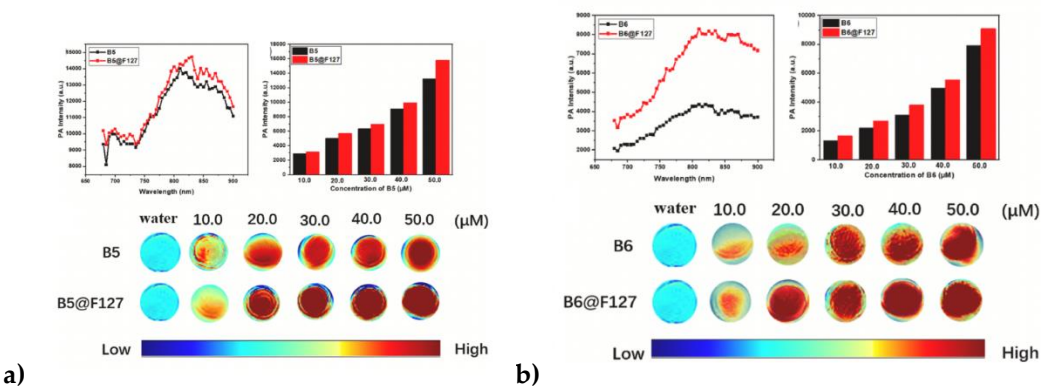


**Figure 37.** Comparison of photoacoustic signals for fluorophores **118** (B5) and **119** (B6) in both water and encapsulated in Pluronic F127 to create nanoparticle micelle structures. This figure was reproduced with permission from Yong *et al*., 2023, copyright 2023 [92].

Additional advances made in developing fluorescence pH sensors based on BODIPY structure sensitive in acidic media were conducted by Glavaš *et.al* (2023) who synthesized two BODIPY phenolic esters, compounds **120** and **121**, as shown in Scheme 14, which exhibited pH-responsive fluorescence with quenching of fluorescence by protonation due to photoinduced electron transfer (PET) from the BODIPY core to the phenol substituent. Electrochemical measurements and computational studies validated the feasibility of the PET mechanism in the protonated form of sensor **120** [93].

Conversely, in the alkaline pH range, Chen *et al.* (2025) devised a novel pH-responsive asymmetric aza-BODIPY probe *via* Schiff base formation, which exhibited turn-off fluorescence response between pH 9.6 to 12.4, with a computed pKa of 11.65. As shown in Scheme 15, the synthesis begins with a condensation reaction between a dione and aminobenzothiazole unit to reflux in dry dichlorobenzene for 10 minutes, then $TiCl_4$ and TEA are added to form the precursor aza-dipyrromethene intermediate, as evidenced by imine formation product completed *via* TLC. Finally, the resulting substrate is subjected to boron complexation [94]. Mechanistically, it was discovered that the probe relies on the deprotonation of the imine group within the aza-BODIPY core to confer an enhanced π-electron conjugation, in which the results of the pH-dependent fluorescence study revealed fluorescence decreasing with increasing pH until pH 12.4, in which the fluorescence was fully quenched [94], as shown in Figure 38. Figure 38 also demonstrates how the pH-response of fluorophore **122** is contingent upon the deprotonation of the imide group, as it significantly affects the absorption spectrum, in regions where the pH increases from 9.6 to 12.4, the intensities of the bands at 425 and 450 nm decrease, while the intensities around 381 nm and 397 nm increase, and a new absorption band emerges at 506 nm, as shown in Figure 39 [94].

 doi:10.20944/preprints202511.1766.v1



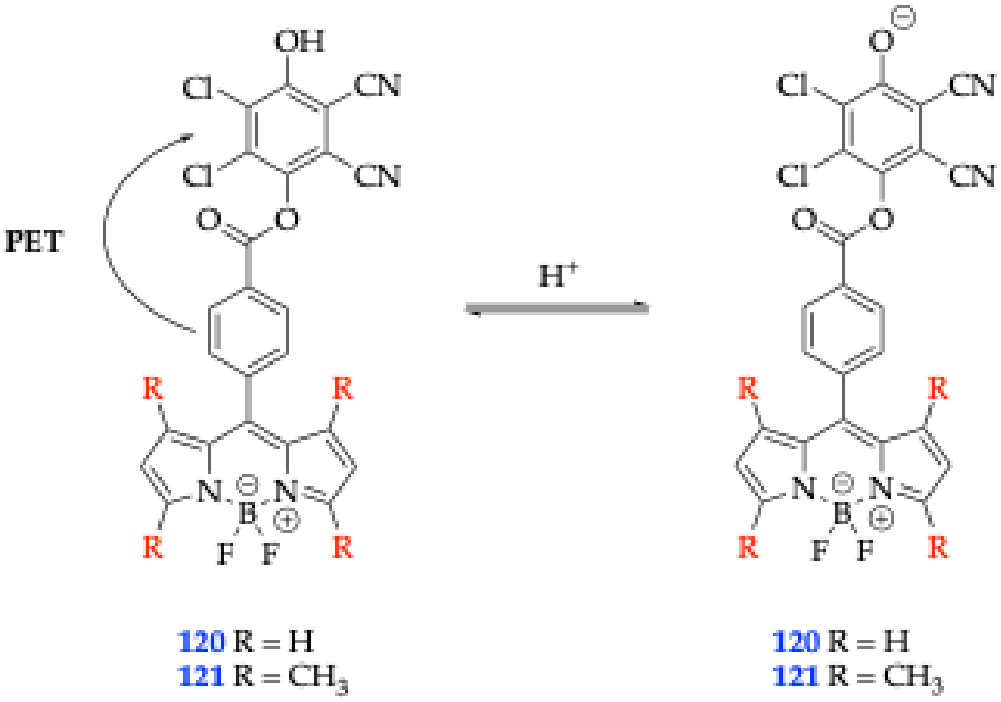


**Figure 38.** Protonation equilibrium of **120** and **121** resulting in the fluorescence in acidic media by PET mechanism [93].

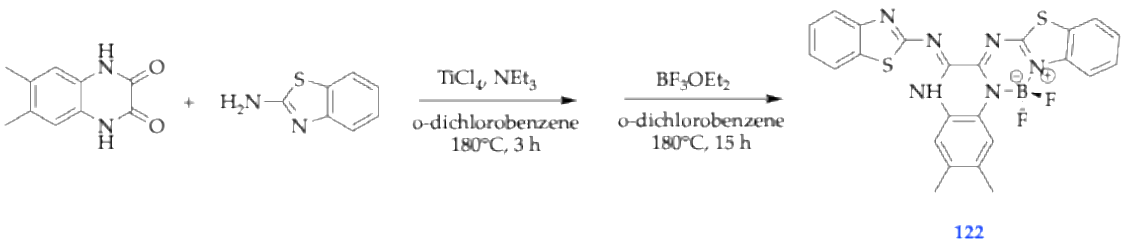


**Scheme 15.** Synthesis of fluorophore **122** [94].

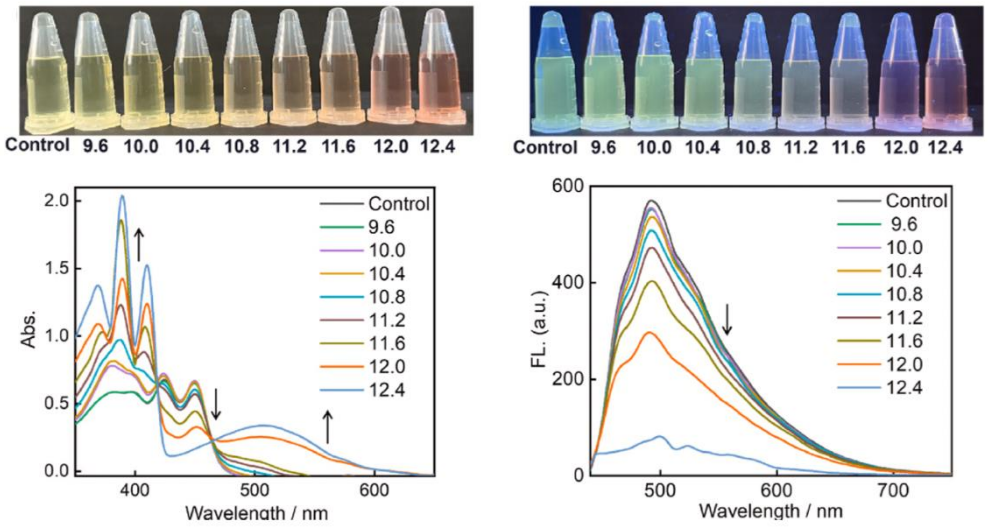


**Figure 39. Photographs of probe 122 under daylight top: (left) and UV light top: (right) at varying pH from 9.6** to 12.4. Bottom: (Left)- Absorption and bottom(right)- fluorescence spectra of probe **122** (40 μM) in

 doi:10.20944/preprints202511.1766.v1



DMSO/$H_2O$ solution (9:1, *v*/*v*) with varying pH from 9.6 to 12.4 ($\lambda_{ex}$: 425 nm, Excitation/Emission slit: 10/10 nm) This figure was reproduced with permission from Chen *et al*., 2025, copyright 2025 [94].

## 8. Conclusions

Thus, the BODIPY class of NIR dyes has gained momentum in advancing the inception of biomedical imaging and cell imaging/tracking. As evidenced by the chemistry and synthetic pathways outlined in this updated review, the synthesis of the BODIPY fluorophores has become increasingly versatile through the years 2014 – 2025, to the advent of creating novel dimeric BODIPY fluorophores and through the C-H arylation of *meso*-substituted BODIPYs with various bromoarenes. Also, through the 3 synthetic routes to developing Aza-BODIPY fluorophores, derivatives have been fine-tuned in their photophysical properties, tumor targeting through active targeting with biomolecules such as biotin and folate, and metal-sensing capabilities to detect various heavy-metal and anionic analytes; this presents a finite biomedical translational value towards developing therapeutics such as potentially chelation therapy. The limitations of venturing deeper into the NIR-II region have begun to be circumvented by C-C coupling and the incorporation of synthetically diverse heterocycles to increase conjugation and planar rigidity. In addition, *in vivo* stability has been advanced by the addition of cationic and anionic groups to facilitate solubility in aqueous regions (blood, plasma, and urine) while maintaining renal clearance, especially through the continued advancement of probing the NIR-II window further with nanoparticles, to leverage both photodynamic, photoacoustic, and photothermal pathways. Future work entails elucidating information to bridge the gaps of understanding how to achieve desirable optical properties while avoiding hydrophobicity and leveraging the advances in rationale-based design for selective analyte detection and pH sensitivity.

**Author Contributions:** O.B. (Olivia Basant), writing—reviewing, and editing; G.P. (Gyliann Peña) and E.L. (Edgardo Lobo), writing—reviewing, and editing; M.H., supervising, reviewing, editing, and proofreading the manuscript. All authors have read and agreed to the published version of the manuscript.

**Funding:** M.H. and O.B. (Olivia Basant) wish to thank the **Center for Diagnostics and Therapeutics** at Georgia State University for providing O.B. (Olivia Basant) with the CDT fellowship. We acknowledge funding from the **National Institutes of Health**, under grant **#R01EB034731** and **R01CA205941**. In addition, M.H. thanks the **Brains and Behavior Seed Grant**, the **Atlanta Clinical and Translational Science Institute for the Healthcare Innovation Program** Grant, as well as the **Georgia Research Alliance** for the Ventures Phase 1 grant.

**Institutional Review Board Statement:** Not applicable.

**Informed Consent Statement:** Not applicable.

**Data Availability Statement:** Data sharing is not applicable.

**Acknowledgments:** The authors wish to thank the Department of Chemistry at Georgia State University and the Brains and Behavior Grant, the Health Innovation Grant, the Center for Diagnostics and Therapeutics, and the Georgia Research Alliance for their financial support. The authors would like to thank the previous efforts of the draft provided by G.P. (Gyliann Peña) and E.L. (Edgardo Lobo) from 2019 as a foundation for O.B. (Olivia Basant) writing this updated review.

**Conflicts of Interest:** The authors declare no conflicts of interest.

## Abbreviations

$AC_2O$: Acetic Anhydride
a-TOH: a-Tocopherol
AIE: Aggregation-Induced Emission
aPS: Activatable photosensitizers
Aza-BDPBA: Aza-Boronic Acid Functionalized

 doi:10.20944/preprints202511.1766.v1



BODIPY: Boron-dipyrromethene
BuOH: Butanol
CT: Charge Transfer
CuAAC: Cu(I)-catalyzed azide-alkyne Cycloaddition
Cys: Cysteine
DABCO: Triazabicyclo [2.2.2] octane
DCFH-DA: 2′,7′-Dichlorofluorescin Diacetate
DFT: Density-Functional Theory
DDQ: (2,3-Dichloro-5,6-dicyano-1,4-benzoquinone)
DPBF: 1,3-Diphenylisobenzofuran
DPP: Diketopyrrolopyrrole
ECL: Electrochemiluminescence
EDG: Electron Donating Group
EWG: Electron Withdrawing Group
FE: Fluorescent Enhancement
FRET: Förster Resonance Energy Transfer
GSH: Glutathione
ISC: Intersystem Crossing
HOMO: Highest Unoccupied Molecular Orbital
Hcy: Homocysteine
ICT: Intramolecular Charge Transfer
LCMS: Laser Confocal Microscopy Scanning
LOD: Limit of Detection
LOQ: Limit of Quantification
LUMO: Lowest Unoccupied Molecular Orbital
MO: Molecular Orbital
MCR: Multicomponent Reactions
NAC: N-acetylcysteine
NIR: Near Infrared Region
NIR-II: Near-Infrared Region Window II
NP: Nanoparticles
OL: Olive Oil
PA: Picric Acid
PAI: Photoacoustic Imaging
PALM: Photoactivated Localization Microscopy
PBA: Phenyl Boronic Acid
PEG-3: Polyethylene Glycol
PDT: Photodynamic Therapy
PET: Positron Emission Tomography
PET: Photoinduced Electron Transfer
PM: Plasma Membrane
PPAB: Pyrrolopyrrole Aza-BODIPY
PS: Photosensitizers
$PTPE_3$ NPs: Pyrrolopyrrole aza-BODIPY nanoparticles
RDX: Hexahydro-1,3,5-trinitro-1,3,5-triazine
RNS: Reactive Nitrogen Species
ROSs: Reactive Oxygen Species
RNSs: Reactive Nitrogen Species
SNR: Signal-to-Noise Ratio
TPP: Triphenylphosphonium
TPE: Tetraphenylethylene
TOH: Tocopherol

 doi:10.20944/preprints202511.1766.v1



V-PDT: Vascular Photodynamic Therapy
UV: Ultraviolet

## References


1. Zhu, S.; Hu, Z.; Tian, R.; Yung, B. C.; Yang, Q.; Zhao, S.; Kiesewetter, D. O.; Niu, G.; Sun, H.; Antaris, A. L.; *et al*. Repurposing Cyanine NIR-I Dyes Accelerates Clinical Translation of Near-Infrared-II (NIR-II) Bioimaging. *Adv Mater* 2018, e1802546. DOI: 10.1002/adma.201802546 PubMed.
2. Shukla, V. K.; Chakraborty, G.; Ray, A. K.; Nagaiyan, S. Red and NIR emitting ring-fused BODIPY/aza-BODIPY dyes. *Dyes and Pigments* 2023, *215*, 111245. DOI: https://doi.org/10.1016/j.dyepig.2023.111245.
3. Yuan, A.; Wu, J.; Tang, X.; Zhao, L.; Xu, F.; Hu, Y. Application of near-infrared dyes for tumor imaging, photothermal, and photodynamic therapies. *Journal of Pharmaceutical Sciences* 2013, *102* (1), 6-28. DOI: https://doi.org/10.1002/jps.23356.
4. Felbeck, T.; Hoffmann, K.; Lezhnina, M. M.; Kynast, U. H.; Resch-Genger, U. Fluorescent Nanoclays: Covalent Functionalization with Amine Reactive Dyes from Different Fluorophore Classes and Surface Group Quantification. *The Journal of Physical Chemistry C* 2015, *119* (23), 12978-12987. DOI: 10.1021/acs.jpcc.5b01482.
5. Kuronuma, Y., Watanabe, R., & Hiruta, Y. (2025). The latest developments of near-infrared fluorescent probes from NIR-I to NIR-II for bioimaging. *Analytical Sciences*, 41(6), 737-757. https://doi.org/10.1007/s44211-025-00735-7
6. Ersoy, G.; Henary, M. Roadmap for Designing Donor-π-Acceptor Fluorophores in UV-Vis and NIR Regions: Synthesis, Optical Properties and Applications. *Biomolecules* 2025, *15* (1), 119.
7. Sarasiya, S.; Sarasiya, S.; Henary, M. Exploration of NIR Squaraine Contrast Agents Containing Various Heterocycles: Synthesis, Optical Properties and Applications. *Pharmaceuticals* 2023, *16* (9), 1299.
8. Rana, P.; Singh, N.; Majumdar, P.; Prakash Singh, S. Evolution of BODIPY/aza-BODIPY dyes for organic photoredox/energy transfer catalysis. *Coordination Chemistry Reviews* **2022**, *470*, 214698. DOI: https://doi.org/10.1016/j.ccr.2022.214698.
9. Wang, H.; Fronczek, F. R.; Vicente, M. G. H.; Smith, K. M. Functionalization of 3,5,8-Trichlorinated BODIPY Dyes. *The Journal of Organic Chemistry* **2014**, *79* (21), 10342-10352. DOI: 10.1021/jo501969z.
10. Bañuelos-Prieto, J.; Sola-Llano, R. Introductory Chapter: BODIPY Dye, an All-in-One Molecular Scaffold for (Bio)Photonics. In *BODIPY Dyes - A Privilege Molecular Scaffold with Tunable Properties*, Bañuelos-Prieto, J., Sola-Llano, R. Eds.; IntechOpen, **2018**.
11. Cao, J.; Zhu, B.; Zheng, K.; He, S.; Meng, L.; Song, J.; Yang, H. Recent Progress in NIR-II Contrast Agent for Biological Imaging. *Frontiers in Bioengineering and Biotechnology* **2020**, *Volume 7 - 2019*, Review. DOI: 10.3389/fbioe 2019.00487.
12. Zhang, Y.; Song, K.-H.; Tang, S.; Ravelo, L.; Cusido, J.; Sun, C.; Zhang, H. F.; Raymo, F. M. Far-Red Photoactivatable BODIPYs for the Super-Resolution Imaging of Live Cells. *Journal of the American Chemical Society* **2018**, 140 (40), 12741-12745. DOI: 10.1021/jacs 8b09099.
13. Zhou, Y.; Ji, P.; Sun, Q.; Gao, H.; Liu, Z. BODIPY-based small molecular probes for fluorescence and photoacoustic dual-modality imaging of superoxide anion in vivo. *Talanta* **2025**, *294*, 128269. DOI: https://doi.org/10.1016/j.talanta.2025.128269.
14. Kye, H.; Jo, D.; Jeong, S.; Kim, C.; Kim, J. Photoacoustic Imaging of pH-Sensitive Optical Sensors in Biological Tissues. *Chemosensors* **2024**, *12* (12), 257.
15. Li, A.; Wang, F.; Li, Y.; Peng, X.; Liu, Y.; Zhu, L.; He, P.; Yu, T.; Chen, D.; Duan, M.; *et al*. Fluorination of Aza-BODIPY for Cancer Cell Plasma Membrane-Targeted Imaging and Therapy. *ACS Applied Materials & Interfaces* **2025,** 17 (2), 3013-3025. DOI: 10.1021/acsami.4c17943.
16. Zhang, X.; Wu, Y.; Chen, L.; Song, J.; Yang, H. Optical and Photoacoustic Imaging In Vivo: Opportunities and Challenges. *Chemical & Biomedical Imaging* **2023**, *1* (2), 99-109. DOI: 10.1021/cbmi.3c00009.
17. Bodio, E.; Goze, C. Investigation of B-F substitution on BODIPY and aza-BODIPY dyes: Development of B-O and B-C BODIPYs. *Dyes and Pigments* **2019**, *160*, 700-710. DOI: https://doi.org/10.1016/j.dyepig.2018.08.062.

 doi:10.20944/preprints202511.1766.v1




18. Chauhan, P.; Chu, K.; Yan, N.; Ding, Z. Comparison study of electrochemiluminescence of boron-dipyrromethene (BODIPY) dyes in aprotic and aqueous solutions. *Journal of Electroanalytical Chemistry* **2016**, 781, 181-189. DOI: https://doi.org/10.1016/j.jelechem.2016.06.022.
19. Mao, W.-J.; Wang, T.-T.; Chen, L.; Zhang, L.; Li, S. Synthesis and optical properties of tyramine-functionalized boron dipyrromethene dyes for cell bioimaging. *Spectrochimica Acta Part A: Molecular and Biomolecular Spectroscopy* **2025**, *324*, 124980. DOI: https://doi.org/10.1016/j.saa.2024.124980.
20. Jiang, X.-D.; Xi, D.; Zhao, J.; Yu, H.; Sun, G.-T.; Xiao, L.-J. A styryl-containing aza-BODIPY as a near-infrared dye. *RSC Advances* **2014**, *4* (105), 60970-60973, 10.1039/C4RA10188J. DOI: 10.1039/C4RA10188J.
21. Boens, N.; Verbelen, B.; Ortiz, M. J.; Jiao, L.; Dehaen, W. Synthesis of BODIPY dyes through postfunctionalization of the boron dipyrromethene core. *Coordination Chemistry Reviews* **2019**, 399, 213024. DOI: https://doi.org/10.1016/j.ccr.2019.213024.
22. Loudet, A.; Burgess, K. BODIPY Dyes and Their Derivatives: Syntheses and Spectroscopic Properties. *Chemical Reviews* **2007**, *107* (11), 4891-4932. DOI: 10.1021/cr078381n.
23. Yang, L.; Liu, Y.; Zhou, X.; Wu, Y.; Ma, C.; Liu, W.; Zhang, C. Asymmetric anthracene-fused BODIPY dye with large Stokes shift: Synthesis, photophysical properties and bioimaging. *Dyes and Pigments* **2016**, *126*, 232-238. DOI: https://doi.org/10.1016/j.dyepig.2015.11.028.
24. Killoran, J.; McDonnell, S. O.; Gallagher, J. F.; O'Shea, D. F. A substituted BF2-chelated tetraarylazadipyrromethene as an intrinsic dual chemosensor in the 650–850 nm spectral range. *New Journal of Chemistry* **2008**, 32 (3), 483-489, 10.1039/B713020A. DOI: 10.1039/B713020A.
25. Sørensen, M. L. H.; Vosch, T.; Laursen, B. W.; Hansen, T. Spectral shifts of BODIPY derivatives: a simple continuous model. *Photochemical & Photobiological Sciences* 2019, 18 (6), 1315-1323, 10.1039/C8PP00430G. DOI: 10.1039/C8PP00430G.
26. Wang, M.; Vicente, M. G. H.; Mason, D.; Bobadova-Parvanova, P. Stability of a Series of BODIPYs in Acidic Conditions: An Experimental and Computational Study into the Role of the Substituents at Boron. *ACS Omega* **2018**, *3* (5), 5502-5510. DOI: 10.1021/acsomega.8b00404.
27. Rybczynski, P.; Smolarkiewicz-Wyczachowski, A.; Piskorz, J.; Bocian, S.; Ziegler-Borowska, M.; Kędziera, D.; Kaczmarek-Kędziera, A. Photochemical Properties and Stability of BODIPY Dyes. *International Journal of Molecular Sciences* **2021**, *22* (13), 6735.
28. Greene, L. E.; Lincoln, R.; Krumova, K.; Cosa, G. Development of a Fluorogenic Reactivity Palette for the Study of Nucleophilic Addition Reactions Based on meso-Formyl BODIPY Dyes. *ACS Omega* **2017**, 2 (12), 8618-8624. DOI: 10.1021/acsomega.7b01795.
29. Lu, H.; Mack, J.; Yang, Y.; Shen, Z. Structural modification strategies for the rational design of red/NIR region BODIPYs. *Chemical Society Reviews* **2014**, *43* (13), 4778-4823, 10.1039/C4CS00030G. DOI: 10.1039/C4CS00030G.
30. Jiao, L.; Wu, Y.; Wang, S.; Hu, X.; Zhang, P.; Yu, C.; Cong, K.; Meng, Q.; Hao, E.; Vicente, M. G. Accessing near-infrared-absorbing BF2-azadipyrromethenes via a push-pull effect. *J Org Chem* **2014**, 79 (4), 1830-1835. DOI: 10.1021/jo402160b From NLM.
31. Porolnik, W.; Koczorowski, T.; Wieczorek-Szweda, E.; Szczolko, W.; Falkowski, M.; Piskorz, J. Microwave-assisted synthesis, photochemical and electrochemical studies of long-wavelength BODIPY dyes. *Spectrochimica Acta Part A: Molecular and Biomolecular Spectroscopy* **2024**, *314*, 124188. DOI: https://doi.org/10.1016/j.saa.2024.124188.
32. Shi, Z.; Han, X.; Hu, W.; Bai, H.; Peng, B.; Ji, L.; Fan, Q.; Li, L.; Huang, W. Bioapplications of small molecule Aza-BODIPY: from rational structural design to in vivo investigations. *Chemical Society Reviews* **2020**, *49* (21), 7533-7567, 10.1039/D0CS00234H. DOI: 10.1039/D0CS00234H.
33. Grover, V.; Ravikanth, M. Synthesis of novel fluorescent 3-pyrrolyl BODIPYs and their derivatives. *Tetrahedron Chem* **2025**, *13*, 100121. DOI: https://doi.org/10.1016/j.tchem.2025.100121.
34. Wang, J.; Yu, C.; Hao, E.; Jiao, L. Conformationally restricted and ring-fused aza-BODIPYs as promising near infrared absorbing and emitting dyes. *Coordination Chemistry Reviews* **2022**, *470*, 214709. DOI: https://doi.org/10.1016/j.ccr.2022.214709.

35. Donyagina, V. F.; Shimizu, S.; Kobayashi, N.; Lukyanets, E. A. Synthesis of N, N-difluoroboryl complexes of 3,3′-diarylazadiisoindolylmethenes. *Tetrahedron Letters* **2008**, *49* (42), 6152-6154. DOI: https://doi.org/10.1016/j.tetlet.2008.08.026.
36. Wang, Y.; Zhang, D.; Xiong, K.; Shang, R.; Jiang, X.-D. Near-infrared absorbing (>700 nm) aza-BODIPYs by freezing the rotation of the aryl groups. *Chinese Chemical Letters* **2022**, *33* (1), 115-122. DOI: https://doi.org/10.1016/j.cclet.2021.06.083.
37. Roohi, H.; Mohtamadifar, N. The role of the donor group and electron-accepting substitutions inserted in π-linkers in tuning the optoelectronic properties of D-π-A dye-sensitized solar cells: a DFT/TDDFT study. *RSC Adv* **2022**, *12* (18), 11557-11573. DOI: 10.1039/d2ra00906d From NLM.
38. Fron, E.; Coutiño-Gonzalez, E.; Pandey, L.; Sliwa, M.; Van der Auweraer, M.; De Schryver, F. C.; Thomas, J.; Dong, Z.; Leen, V.; Smet, M.; *et al*. Synthesis and photophysical characterization of chalcogen-substituted BODIPY dyes. *New Journal of Chemistry* **2009**, *33* (7), 1490-1496, 10.1039/B900786E. DOI: 10.1039/B900786E.
39. Giacomazzo, G. E.; Palladino, P.; Gellini, C.; Salerno, G.; Baldoneschi, V.; Feis, A.; Scarano, S.; Minunni, M.; Richichi, B. A straightforward synthesis of phenyl boronic acid (PBA) containing BODIPY dyes: new functional and modular fluorescent tools for the tethering of the glycan domain of antibodies. *RSC Adv* **2019**, *9* (53), 30773-30777. DOI: 10.1039/c9ra07608e From NLM.
40. Bardon, K. M.; Selfridge, S.; Adams, D. S.; Minns, R. A.; Pawle, R.; Adams, T. C.; Takiff, L. Synthesis of Water-Soluble Far-Red-Emitting Amphiphilic BODIPY Dyes. *ACS Omega* **2018**, *3* (10), 13195-13199. DOI: 10.1021/acsomega.8b01487.
41. Tonnelé, C. Chemical Sensors: Modelling the Photophysics of Cation Detection by Organic Dyes. **2013**.
42. Nguyen, Y. T.; Shin, S.; Kwon, K.; Kim, N.; Bae, S. W. BODIPY-based fluorescent sensors for detection of explosives. *Journal of Chemical Research* **2023**, *47* (2), 17475198231168961. DOI: 10.1177/17475198231168961.
43. Sprenger, T.; Schwarze, T.; Müller, H.; Sperlich, E.; Kelling, A.; Holdt, H.-J.; Paul, J.; Martos Riaño, V.; Nazaré, M. BODIPY-Equipped Benzo-Crown-Ethers as Fluorescent Sensors for pH Independent Detection of Sodium and Potassium Ions. *ChemPhotoChem* **2023**, *7* (2), e202200270. DOI: https://doi.org/10.1002/cptc.202200270.
44. Cugnasca, B. S.; Junior, T. C. T.; Penna, T. C.; Zuluaga, N. L. B.; Bustos, S. O.; Chammas, R.; Cuccovia, I. M.; Correra, T. C.; Dos Santos, A. A. Seleno-BODIPY as a fluorescent sensor for differential and highly selective detection of Cysteine and Glutathione for bioimaging in HeLa cells. *Dyes and Pigments* **2025**, *236*, 112658. DOI: https://doi.org/10.1016/j.dyepig.2025.112658.
45. Karatay, A.; Miser, M. C.; Cui, X.; Küçüköz, B.; Yılmaz, H.; Sevinç, G.; Akhüseyin, E.; Wu, X.; Hayvali, M.; Yaglioglu, H. G.; *et al.* The effect of heavy atoms on two-photon absorption properties and intersystem crossing mechanism in aza-boron-dipyrromethene compounds. *Dyes and Pigments* **2015**, *122*, 286-294. DOI: https://doi.org/10.1016/j.dyepig.2015.07.002.
46. Liu, Y.-c.; Zhang, Y.; Liu, G.-j.; Xing, G.-w. J- and H-aggregates of heavy-atom-free Aza-BODIPY dyes with high 1O2 generation efficiency and photodynamic therapy potential. *Dyes and Pigments* **2023**, *208*, 110813. DOI: https://doi.org/10.1016/j.dyepig.2022.110813.
47. Klymchenko, A. Emerging field of self-assembled fluorescent organic dye nanoparticles. *Journal of Nanoscience Letters* **2013**, *3*, 21.
48. Choi, H. S.; Gibbs, S. L.; Lee, J. H.; Kim, S. H.; Ashitate, Y.; Liu, F.; Hyun, H.; Park, G.; Xie, Y.; Bae, S.; et al. Targeted zwitterionic near-infrared fluorophores for improved optical imaging. *Nat Biotechnol* **2013**, *31* (2), 148-153. DOI: 10.1038/nbt.2468 From NLM.
49. Choi, H. S.; Nasr, K.; Alyabyev, S.; Feith, D.; Lee, J. H.; Kim, S. H.; Ashitate, Y.; Hyun, H.; Patonay, G.; Strekowski, L.; et al. Synthesis and in vivo fate of zwitterionic near-infrared fluorophores. *Angew Chem Int Ed Engl* **2011**, *50* (28), 6258-6263. DOI: 10.1002/anie.201102459 .From NLM.
50. Adarsh, N.; Babu, P. S. S.; Avirah, R. R.; Viji, M.; Nair, S. A.; Ramaiah, D. Aza-BODIPY nanomicelles as versatile agents for the in vitro and in vivo singlet oxygen-triggered apoptosis of human breast cancer cells. *Journal of Materials Chemistry B* **2019**, *7* (14), 2372-2377, 10.1039/C9TB00124G. DOI: 10.1039/C9TB00124G.
51. Glavaš, M.; Zlatić, K.; Jadreško, D.; Ljubić, I.; Basarić, N. Fluorescent pH sensors based on BODIPY structure sensitive in acidic media. *Dyes and Pigments* **2023**, *220*, 111660. DOI: https://doi.org/10.1016/j.dyepig.2023.111660.

 doi:10.20944/preprints202511.1766.v1




52. Killoran, J.; Allen, L.; Gallagher, J. F.; Gallagher, W. M.; O'Shea, D. F. Synthesis of BF2 chelates of tetraarylazadipyrromethenes and evidence for their photodynamic therapeutic behaviour. *Chem Commun (Camb)* **2002**, (17), 1862-1863. DOI: 10.1039/b204317c. From NLM.
53. Verbelen, B.; Leen, V.; Wang, L.; Boens, N.; Dehaen, W. Direct palladium-catalysed C–H arylation of BODIPY dyes at the 3- and 3,5-positions. *Chemical Communications* **2012**, *48* (73), 9129-9131, 10.1039/C2CC34549H. DOI: 10.1039/C2CC34549H.
54. Kwan, H. Y.; Fu, X.; Liu, B.; Chao, X.; Chan, C. L.; Cao, H.; Su, T.; Tse, A. K. W.; Fong, W. F.; Yu, Z. L. Subcutaneous adipocytes promote melanoma cell growth by activating the Akt signaling pathway: role of palmitic acid. *J Biol Chem* **2014**, *289* (44), 30525-30537. DOI: 10.1074/jbc.M114.593210.From NLM.
55. Nishikata, T.; Abela, A. R.; Huang, S.; Lipshutz, B. H. Cationic Pd(II)-catalyzed C-H activation/cross-coupling reactions at room temperature: synthetic and mechanistic studies. *Beilstein J Org Chem* **2016**, *12*, 1040-1064. DOI: 10.3762/bjoc.12.99 .From NLM.
56. Mendive-Tapia, L.; Zhao, C.; Akram, A.; Preciado, S.; Albericio, F.; Lee, M.; Kielland, N.; Read, N.; Lavilla, R.; Vendrell, M. Spacer-free BODIPY fluorogens in antimicrobial peptides for direct imaging of fungal infection in human tissue. *Nature Communications* **2016**, *7*, 10940. DOI: 10.1038/ncomms10940.
57. De Moliner, F.; Kielland, N.; Lavilla, R.; Vendrell, M. Modern Synthetic Avenues for the Preparation of Functional Fluorophores. *Angewandte Chemie International Edition* **2017**, *56* (14), 3758-3769. DOI: https://doi.org/10.1002/anie.201609394.
58. Jiang, X.; Zhang, T.; Sun, C.; Meng, Y.; Xiao, L. Synthesis of aza-BODIPY dyes bearing the naphthyl groups at 1,7-positions and application for singlet oxygen generation. *Chinese Chemical Letters* **2019**, *30* (5), 1055-1058. DOI: https://doi.org/10.1016/j.cclet.2019.02.016.
59. Staudinger, C.; Breininger, J.; Klimant, I.; Borisov, S. M. Near-infrared fluorescent aza-BODIPY dyes for sensing and imaging of pH from the neutral to highly alkaline range. *Analyst* **2019**, *144* (7), 2393-2402, 10.1039/C9AN00118B. DOI: 10.1039/C9AN00118B.
60. Dutta, D.; Nair, R. R.; Mangalath, S.; Nair, S. A.; Joseph, J.; Gogoi, P.; Ramaiah, D. Biocompatible Aza-BODIPY-Biotin Conjugates for Photodynamic Therapy of Cancer. *ACS Omega* **2023**, *8* (29), 26180-26190. DOI: 10.1021/acsomega.3c02416.
61. Wang, C.; Daddario, C.; Pejić, S.; Sauvé, G. Synthesis and Properties of Azadipyrromethene-Based Complexes with Nitrile Substitution. *European Journal of Organic Chemistry* **2020**, *2020* (6), 714-722. DOI: https://doi.org/10.1002/ejoc.201901736.
62. Li, J.-Z.; Lin, H.-L.; Li, H.-Y.; Cao, H.-W.; Lang, X.-X.; Chen, Y.-S.; Chen, H.-W.; Wang, M.-Q. Red-emitting Styryl-BODIPY dye with donor-π-acceptor architecture: Selective interaction with serum albumin via disaggregation-induced emission. *Dyes and Pigments* **2023**, *216*, 111357. DOI: https://doi.org/10.1016/j.dyepig.2023.111357.
63. Dong, L.; Li, H.; Tian, Y.; Niu, L.-Y. Novel phenothiazine-based amphiphilic Aza-BODIPYs for highly efficient photothermal therapy. *Dyes and Pigments* **2023**, *217*, 111369. DOI: https://doi.org/10.1016/j.dyepig.2023.111369.
64. Bian, S.; Zheng, X.; Liu, W.; Li, J.; Gao, Z.; Ren, H.; Zhang, W.; Lee, C. S.; Wang, P. Pyrrolopyrrole aza-BODIPY-based NIR-II fluorophores for in vivo dynamic vascular dysfunction visualization of vascular-targeted photodynamic therapy. *Biomaterials* **2023**, *298*, 122130. DOI: 10.1016/j.biomaterials.2023.122130 From NLM.
65. Tian, Y.; Zhou, H.; Cheng, Q.; Dang, H.; Qian, H.; Teng, C.; Xie, K.; Yan, L. Stable twisted conformation aza-BODIPY NIR-II fluorescent nanoparticles with ultra-large Stokes shift for imaging-guided phototherapy. *Journal of Materials Chemistry B* **2022**, *10* (5), 707-716, 10.1039/D1TB02066H. DOI: 10.1039/D1TB02066H.
66. Wu, P.; Zhu, Y.; Liu, S.; Xiong, H. Modular Design of High-Brightness pH-Activatable Near-Infrared BODIPY Probes for Noninvasive Fluorescence Detection of Deep-Seated Early Breast Cancer Bone Metastasis: Remarkable Axial Substituent Effect on Performance. *ACS Central Science* **2021**, *7* (12), 2039-2048. DOI: 10.1021/acscentsci 1c01066.

67. Liu, B.; Jiao, J.; Xu, W.; Zhang, M.; Cui, P.; Guo, Z.; Deng, Y.; Chen, H.; Sun, W. Highly Efficient Far-Red/NIR-Absorbing Neutral Ir (III) Complex Micelles for Potent Photodynamic/Photothermal Therapy. *Adv Mater* **2021**, *33* (32), e2100795. DOI: 10.1002/adma.202100795 From NLM.
68. Elgun, T.; Yurttas, A. G.; Cinar, K.; Ozcelik, S.; Gul, A. Effect of aza-BODIPY-photodynamic therapy on the expression of carcinoma-associated genes and cell death mode. *Photodiagnosis Photodyn Ther* **2023**, *44*, 103849. DOI: 10.1016/j.pdpdt.2023.103849 From NLM.
69. Hlogyik, T.; Laczkó-Rigó, R.; Bakos, É.; Poór, M.; Kele, Z.; Özvegy-Laczka, C.; Mernyák, E. Synthesis and in vitro photodynamic activity of aza-BODIPY-based photosensitizers. *Organic & Biomolecular Chemistry* **2023**, *21* (29), 6018-6027, 10.1039/D3OB00699A. DOI: 10.1039/D3OB00699A.
70. Samanta, S.; Lai, K.; Wu, F.; Liu, Y.; Cai, S.; Yang, X.; Qu, J.; Yang, Z. Xanthene, cyanine, oxazine and BODIPY: the four pillars of the fluorophore empire for super-resolution bioimaging. *Chemical Society Reviews* **2023**, *52* (20), 7197-7261, 10.1039/D2CS00905F. DOI: 10.1039/D2CS00905F.
71. Zhang, Y.; Tang, S.; Ravelo, L.; Cusido, J.; Raymo, F. M. Chapter Six - Far-red photoactivatable BODIPYs for the super-resolution imaging of live cells. In *Methods in Enzymology*, Chenoweth, D. M. Ed.; Vol. 640; Academic Press, 2020; pp 131-147.
72. Gai, L.; Liu, Y.; Zhou, Z.; Lu, H.; Guo, Z. BODIPY-based probes for hypoxic environments. *Coordination Chemistry Reviews* **2023**, *481*, 215041. DOI: https://doi.org/10.1016/j.ccr.2023.215041.
73. Hlogyik, T.; Laczkó-Rigó, R.; Bakos, É.; Poór, M.; Kele, Z.; Özvegy-Laczka, C.; Mernyák, E. Synthesis and in vitro photodynamic activity of aza-BODIPY-based photosensitizers. *Organic & Biomolecular Chemistry* **2023**, *21* (29), 6018-6027, 10.1039/D3OB00699A. DOI: 10.1039/D3OB00699A.
74. Aranda, A.; Sequedo, L.; Tolosa, L.; Quintas, G.; Burello, E.; Castell, J. V.; Gombau, L. Dichloro-dihydro-fluorescein diacetate (DCFH-DA) assay: a quantitative method for oxidative stress assessment of nanoparticle-treated cells. *Toxicol In Vitro* **2013**, *27* (2), 954-963. DOI: 10.1016/j.tiv.2013.01.016 From NLM.
75. Wang, M.; Zhang, G.; Kaufman, N.; Bobadova-Parvanova, P.; Fronczek, F.; Smith, K.; Vicente, M. Linker-Free Near-IR Aza-BODIPY-Glutamine Conjugates Through Boron Functionalization. *European Journal of Organic Chemistry* **2020**, *2020*. DOI: 10.1002/ejoc.201901772.
76. Lovell, J. F.; Liu, T. W. B.; Chen, J.; Zheng, G. Activatable Photosensitizers for Imaging and Therapy. *Chemical Reviews* **2010**, *110* (5), 2839-2857. DOI: 10.1021/cr900236h.
77. Luangphai, S.; Thuptimdang, P.; Buddhiranon, S.; Chanawanno, K. Aza-BODIPY-based logic gate chemosensors and their applications. *Spectrochimica Acta Part A: Molecular and Biomolecular Spectroscopy* **2024**, *322*, 124806. DOI: https://doi.org/10.1016/j.saa.2024.124806.
78. Pascal, S.; Bellier, Q.; David, S.; Bouit, P.-A.; Chi, S.-H.; Makarov, N. S.; Le Guennic, B.; Chibani, S.; Berginc, G.; Feneyrou, P.; et al. Unraveling the Two-Photon and Excited-State Absorptions of Aza-BODIPY Dyes for Optical Power Limiting in the SWIR Band. *The Journal of Physical Chemistry C* **2019**, *123* (38), 23661-23673. DOI: 10.1021/acs.jpcc.9b08376.
79. Jiang, X.-D.; Zhao, J.; Li, Q.; Sun, C.-L.; Guan, J.; Sun, G.-T.; Xiao, L.-J. Synthesis of NIR fluorescent thienyl-containing aza-BODIPY and its application for detection of $Hg^{2+}$: Electron transfer by bonding with $Hg^{2+}$. *Dyes and Pigments* **2015**, *125*. DOI: 10.1016/j.dyepig.2015.09.023.
80. Ye, Y.; Sun, J.; Tang, F.; Xie, R.; Wang, H.; Ding, A.; Pan, S.; Li, L. Mitochondria-Targeting BODIPY Probes for Imaging of Reactive Oxygen Species. *Advanced Sensor Research* **2023**, *2* (9), 2300057. DOI: https://doi.org/10.1002/adsr.202300057.
81. Adarsh, N.; Krishnan, M. S.; Ramaiah, D. Sensitive Naked Eye Detection of Hydrogen Sulfide and Nitric Oxide by Aza-BODIPY Dyes in Aqueous Medium. *Analytical Chemistry* **2014**, *86* (18), 9335-9342. DOI: 10.1021/ac502849d.
82. Merkushev, D.; Vodyanova, O.; Telegin, F.; Melnikov, P.; Yashtulov, N.; Marfin, Y. Design of Promising aza-BODIPYs for Bioimaging and Sensing. *Designs* **2022**, *6* (2), 21.
83. Salim MM, Owens EA, Gao T, Lee JH, Hyun H, Choi HS, Henary M. Hydroxylated near-infrared BODIPY fluorophores as intracellular pH sensors. *Analyst*. **2014** Oct 7;139(19):4862-73. doi: 10.1039/c4an01104j. PMID: 25105177; PMCID: PMC4386627.

84. Yadav AK, Tapia Hernandez R, Chan J. A general strategy to optimize the performance of aza-BODIPY-based probes for enhanced photoacoustic properties. Methods Enzymol. 2021;657:415-441. doi: 10.1016/bs.mie.2021.06.022. Epub **2021** Jul 21. PMID: 34353497.
85. Liu, Y.; Zhu, J.; Xu, Y.; Qin, Y.; Jiang, D. Boronic Acid Functionalized Aza-Bodipy (azaBDPBA) based Fluorescence Optodes for the Analysis of Glucose in Whole Blood. *ACS Appl Mater Interfaces* **2015**, *7* (21), 11141-11145. DOI: 10.1021/acsami.5b00265 From NLM.
86. Ma, D.; Hou, S.; Bae, C.; Pham, T. C.; Lee, S.; Zhou, X. Aza-BODIPY-based probe for photoacoustic imaging of ONOO− in vivo. *Chinese Chemical Letters* **2021**, *32* (12), 3886-3889. DOI: https://doi.org/10.1016/j.cclet.2021.05.048.
87. Walter, E. R. H.; Lee, L. C.-C.; Leung, P. K.-K.; Lo, K. K.-W.; Long, N. J. Mitochondria-targeting biocompatible fluorescent BODIPY probes. *Chemical Science* **2024**, *15* (13), 4846-4852, 10.1039/D3SC06445J. DOI: 10.1039/D3SC06445J.
88. Shamim, M.; Dinh, J.; Yang, C.; Nomura, S.; Kashiwagi, S.; Kang, H.; Choi, H. S.; Henary, M. Synthesis, Optical Properties, and In Vivo Biodistribution Performance of Polymethine Cyanine Fluorophores. *ACS Pharmacology & Translational Science* **2023**, *6* (8), 1192-1206. DOI: 10.1021/acsptsci 3c00101.
89. Zhang, Y.; Gan, Y.; Lai, B.; Ran, X.; Cao, D.; Wang, L. A portable sensing platform using a novel dipyrrolopyrazinedione-based aza-BODIPY dimer for highly efficient detection of hypochlorite and hydrazine. *Spectrochim Acta A Mol Biomol Spectrosc* **2025**, *341*, 126415. DOI: 10.1016/j.saa.2025.126415 From NLM.
90. Azizi-Khereshki, N.; Zavvar Mousavi, H.; Farsadrooh, M.; Evazalipour, M.; Feizi-Dehnayebi, M.; Mohammadi Ziarani, G.; Henary, M.; Rtimi, S.; Aminabhavi, T. M. Biogenic synthesis of silver nanoparticles for colorimetric detection of Fe3+ in environmental samples: DFT calculations and molecular docking studies. *Journal of Environmental Management* **2025**, *387*, 125880. DOI: https://doi.org/10.1016/j.jenvman.2025.125880.
91. Ahmed, T. E.; Henary, M. Dimerizing Heptamethine Cyanine Fluorophores from the Meso Position: Synthesis, Optical Properties, and Metal Sensing Studies. *Organic Letters* **2025**, *27* (25), 6623-6629. DOI: 10.1021/acs.orglett.5c01620.
92. Yong, Z.; Wen, B.; Dou, Q.; Guo, H.; Hu, C.; Bi, J.; Zhang, M.; Zhao, J.; Lin, Y.; Wang, J.; et al. Design, synthesis, and characterization of pH-responsive near-infrared bithiophene Aza-BODIPY. *Dyes and Pigments* **2023**, *219*, 111614. DOI: https://doi.org/10.1016/j.dyepig.2023.111614.
93. Glavaš, M.; Zlatić, K.; Jadreško, D.; Ljubić, I.; Basarić, N. Fluorescent pH sensors based on BODIPY structure sensitive in acidic media. *Dyes and Pigments* **2023**, *220*, 111660. DOI: https://doi.org/10.1016/j.dyepig.2023.111660.
94. Chen, Z.; Shimizu, S.; Ji, S.; Pan, J.; Wang, Y.; Feng, R. A novel BODIPY-based fluorescent probe for naked-eye detection of the highly alkaline pH. *Spectrochimica Acta Part A: Molecular and Biomolecular Spectroscopy* **2025**, *325*, 125083. DOI: https://doi.org/10.1016/j.saa.2024.125083.